UNIVERSITÀ DEGLI STUDI DI NAPOLI FEDERICO II

DIPARTIMENTO DI FARMACIA

DOTTORATO DI RICERCA IN SCIENZA DEL FARMACO

XXIX CICLO 2014/2017

From bioactive natural products to drug-like small molecules

Dott.ssa Maria Senese

Tutor

Prof.ssa Anna Aiello

Coordinatore

Prof. ssa M.V. D'Auria

INDEX

ABSTRACT

Natural products have historically been the most productive source of leads for the development of drugs. Thanks to the chemical methodologies of natural products, a vast array of bioactive secondary metabolites from terrestrial and marine sources has been discovered. Many of these natural products became current drug candidates. Therefore, the research of new biologically active compounds through structure elucidation and biological tests is the central issue of these studies. My research is placed in this field and it has been mainly devoted to the discovery and to the chemical and pharmacological investigation of new bioactive natural products as "lead compounds" in the antitumor and antimalarial activities area. My work, described in this PhD thesis, was organized in two different topics: i) isolation and structural characterization of bioactive secondary metabolites from marine invertebrates, ii) synthesis of thiazinoquinones derivatives endowed with cytotoxic and antiplasmodial activities from marine natural metabolites. The achievement of my research project required isolation and extraction procedures. The chemical characterization of the isolated compounds has been performed through an extensive spectroscopic analysis (UV, IR, ECD, 1D and 2D NMR) together with mass spectrometry, computational and electrochemistry methods. I have also used synthetic methods both for the chemical derivatization of the isolated molecules and for the preparation of analogues on the simplified model of natural molecules.

During the course of my PhD research, whose results are reported in the following thesis, I have been dealing with the extraction and the chemical re-investigation of a new collection of the Mediterranean ascidian *Phallusia fumigata.* This analysis led to the isolation of one sulfated sterol, phallusiasterol C, which is a possible modulator of the PXR nuclear receptor. Morover, I have been strongly involved in completing the stereochemistry assignment of phosphoeleganin, a complex acyclic marine natural product, isolated previously from the Mediterranean ascidian *Sidnyum elegans.*

In addition, the electrochemical response of four natural cytotoxic thiazinoquinones, beforehand isolated and characterized from *Aplidium* species, has been investigated, in order to clarify the mechanism of action which is the basis of their cytotoxicity. The research for new antiplasmodial hits is another main topic of my PhD activity discussed in this thesis. Previously, having identified the thiazinoquinone nucleus as new active chemiotype against *P. falciparum*, my research started from the development of two new series of methoxy and amide derivatives inspired by two marine metabolites isolated from the Mediterranean ascidian *Aplidium conicum.* Recently, in order to refine this pharmacophore model and improve the pharmacokinetic and pharmacodynamic properties, I have performed a rational design and synthesis of new modified analogues with simplified side chains and different substituents. In collaboration with the Department of Biomedical, Surgical and Dental sciences (University of Milan), the synthetic analogues of natural quinones have been tested for their in vitro antiplasmodial activity against both chloroquine (CQ)-sensitive (D10) and -resistant (W2) strains of *P. falciparum*, although some of them were strongly cytotoxic. Some of the synthetic derivatives showed significant antiplasmodial activity together with some important structural requirements. Additionally, in order to rationalize the structure-activity relationships (SARs), an integrated approach based on computational and electrochemistry studies was performed. These studies were carried out by a further collaborating external research group. The above results clearly evidence that quinone natural products represent an excellent source of novel "drug-like" small molecules for drug discovery in antimalarial research.

ITALIAN ABSTRACT

Le sostanze naturali sono da sempre una delle più ricche fonti di composti guida per la scoperta di farmaci. Grazie agli studi chimichi sui prodotti naturali, è stata scoperta una vasta gamma di metaboliti secondari bioattivi da fonti terrestri e marine. Molti di questi prodotti naturali sono divenuti attualmente *drug candidates*. Pertanto, il problema centrale di questi studi resta la ricerca di nuovi composti biologicamente attivi attraverso la determinazione stereostrutturale e i test biologici.

La mia ricerca si colloca in questo ambito e si è incentrata sulla scoperta e sullo studio chimico e farmacologico di nuovi prodotti naturali bioattivi, come nuovi potenziali "*leads"* per la terapia antitumorale e antimalarica.

Il mio lavoro, descritto in questa tesi di Dottorato, è stato organizzato in due differenti argomenti: i) isolamento e caratterizzazione strutturale di metaboliti secondari bioattivi da invertebrati marini, ii) sintesi di derivati tiazinochinonici con attività citotossica ed antiplasmodio a partire da lead compounds di origine naturale.

La realizzazione del mio progetto di ricerca ha richiesto l'utilizzo di diverse metodiche di estrazione e di isolamento. La caratterizzazione chimica dei composti isolati è stata effettuata attraverso un'ampia analisi spettroscopica (UV, IR, ECD e NMR mono- e bi-dimensionale) insieme a metodi spettrometria di massa, studi computazionali ed elettrochimici. Sono state utilizzate anche metodiche sintetiche sia per la derivatizzazione chimica delle molecole isolate che per la preparazione di analoghi semplificati sul modello di molecole naturali.

Nel corso dell'attività di ricerca svolta durante il corso di Dottorato, i cui risultati sono riportati nella seguente tesi, mi sono occupata dell'estrazione e dell'analisi chimica *ex novo* dell'ascidia del Mar Mediteranneo *Phallusia fumigata.* Questa analisi ha portato all'isolamento di uno sterolo solfatato, phallusiasterolo C, un possibile modulatore del recettore nucleare PXR.

La mia attività di ricerca si è incentrata anche sul completamento della determinazione della configurazione assoluta della fosfoeleganina, un prodotto

naturale aciclico complesso, isolato in precedenza dall'ascidia del Mar Mediteranneo *Sidnyum elegans*.

Inoltre, sono stati eseguiti studi elettrochimici e computazionali su quattro tiazinochinoni citotossici naturali, precedentemente isolati e caratterizzati dall'ascidia *Aplidium conicum,* con l'intento di chiarire il meccanismo d'azione che è alla base della loro citotossicità.

La ricerca di nuovi hits antimalarici è un altro tema principale della mia attività di dottorato, discussa in questa tesi. Precedentemente, avendo individuato il nucleo tiazinochinonico come nuovo chemiotipo attivo contro il *Plasmodium falciparum*, il punto di partenza della mia ricerca è stato lo sviluppo di due nuove serie di metossi e ammido derivati, progettati sul modello di due metaboliti marini isolati dall'ascidia *Aplidium conicum.* Recentemente, al fine di perfezionare questo modello farmacoforico e di migliorarne le proprietà farmacocinetiche e farmacodinamiche, ho effettuato la sintesi di nuovi analoghi modificati con catene laterali semplificate e diversi sostituenti.

In collaborazione con il Dipartimento di Scienze Biomediche Chirurgiche e Odontoiatriche dell'Università di Milano, gli analoghi sintetici sono stati testati per valutare la loro attività antiplasmodio, *in vitro*, sui ceppi di *Plasmodium falciparum* D10 (clorochina-sensibile) e W2 (clorochina-resistente). Alcuni di questi composti sono risultati fortemente citotossici, mente altri hanno esibito una significativa attività antiplasmodio insieme ad alcuni requisiti strutturali importanti.

Inoltre, per comprendere le relazioni struttura-attività (SAR), questi composti sono stati sottoposti a studi computazionali ed elettrochimici, effettuati avvalendoci della collaborazione di gruppi di ricerca esterni.

L'insieme dei risultati ottenuti evidenziano chiaramente che i chinoni naturali rappresentano un'ottima fonte di nuove "drug-like" small molecules per lo sviluppo di nuovi farmaci antimalarici.

PUBLICATIONS OF THE CANDIDATE DURING THE PH.D. PERIOD

1. Imperatore, C.; Aiello, A.; D'Aniello, F.; Senese, M.; Menna, M. Alkaloids from marine invertebrates as important leads for anticancer drugs discovery and development. *Molecules* **2014,** *19,* 20391-20423
2. Imperatore, C.; Senese, M.; Aiello, A.; Luciano, P.; Fiorucci, S.; D'Amore, C.; Carino, A.; Menna, M. Phallusiasterol C, a new disulfated steroid from the Mediterranean tunicate *Phallusia fumigata. Mar. Drugs,* **2016,** *14,* 117.
3. Imperatore, C.; Persico, M.; Cimino, P.; Aiello, A.; Senese, M.; Cebrián-Torrejón, G.; Fattorusso, C.; Menna, M.; Doménech-Carbó, A. Correlation between electrochemistry, DFT calculations and cytotoxic activity of marine thiazinoquinones. **2017**. (submitted)
4. Luciano, P.; Senese, M.; Imperatore, C.; Aiello, A.; Menna, M. Assignment of the Complete Stereochemistry of Phosphoeleganin via organic synthesis, chiral derivatization, and UDB concept application. **2017**. (submitted).
5. Imperatore, C.; Senese, M.; Aiello, A.; Fattorusso, C.; Luciano, P.; Persico, M.; Basilico, N.; Parapini, S.; Taramelli, D.; Menna, M. Development of nature inspired antimalarial leads possessing the thiazinoquinone pharmacophore. **2017**. (in elaboration)

INTRODUCTION

The constant need for the discovery of more effective and less expensive drugs is legitimated by several crucial factors, such as exisisting diseases without cure, drug resistance, emergence of new or mutated viruses, and very expensive drugs.[1] Nature represents a fascinating resource of new bioactive molecules and the study of these metabolites has been up to now the most successful way to the drug discovery. The discovery of natural products helped numerous life saving medicines and medical breakthroughs, particularly in the treatment of cancer, infectious diseases, hypercholesterolemia and immunological disorders.

Well-known examples of widely used natural products are lovastatin (anticholesterolemic agent), erythromycin (antibiotic), cyclosporine A, amphotericin B (fungicidal agent), and FK506 (immunosuppressive agents).[2,3] In addition, according to an article written by the National Cancer Institute (NCI) scientists, the new molecules, recently introduced as anticancer drugs, were completely inspired by natural products and their derivatives.[4] The largely unexplored marine world, which probably harbors the greatest biodiversity, may be the biggest resource to discover novel structures with new mechanisms of action that cover biologically relevant activities. However, it issues several challenges, including the access to the marine environment and the chemical and biological characterizations of the promising natural products, which are often collected in a very minute amount. Consequently, updates in technologies, also in sampling methods, new synthetic approaches, biotechnology, and nanoscale NMR for structure determination are all crucial to the success of marine natural products as drug leads. Until a few years ago, more than a micromole of a compound was essential to assign completely its

---

[1] Strobel, G. D. *Mol. Biol. Rev.*, **2003**, 67, 491.
[2] O'Neill, M.; J.A. Lewis in *Human Medicinal agents from Plant.* Kinghorn, A. D., Balandrin, M. F., Eds.; ACS Symposium Series 534; American Chemical Society: Washington, D. C., **1993**, 48.
[3] Cragg, G.M.; Newmann, D. J.; Snader K.M. *J. Nat. Prod.*, **1997**, 60, 52.
[4] Newman, D. J. C., G. M.; Snader, K. M. *J. Nat. Prod.*, **2003**, 66, 1022.

structure. Recent advances, expecially in NMR structure determination methodologies, have changed this obligation and now it is possible to analise the product on a nanomole or even picomole scale.[5]

In this thesis, the results obtained during my PhD research program, are illustrated. My research was indeed grounded in the field of natural products chemistry and mainly aimed to the discovery of new bioactive natural compounds, useful as models for the development of new medicinal drugs. The research work was divided into two different parts, the isolation and pharmacological characterization of new bioactive molecules from terrestrial and marine organisms and the optimization of the studied natural leads through de novo synthesis and/or structural modifications. Our efforts were directed towards the design and the synthesis of simplified analogues of the natural products. Through active collaborations with selected national and foreign research groups, both natural and synthetic compounds selected collections have been submitted to pharmacological tests plus an original combination of electrochemical and computational studies in order to analise the structure-activity relationships. The whole of my studies led to the isolation and identification of several bioactive molecules, with different structures, ranging from simple linear polyfunctionalized alkyl chains to complex polycyclic frameworks, and contributed to enlarge the chemical diversity generated into natural products of marine origin.

On the other hand, the synthetic studies performed using already known marine natural compounds led to the identification of derivatives with significant antiplasmodial activity and also highlighted some structural requirements critical for both the antiplasmodial and the cytotoxic activities. My research strongly highlighted the potential of natural products to qualify as lead structures for medicinal chemistry, affording analogues easier to synthesize and with better bioactivity.

---

[5] Montaser, R; Luesch H. *Future Med Chem*., **2011**, 12,1475-89

CHAPTER 1

THE NATURAL PRODUCTS IN DRUG DISCOVERY

1.1. The natural products as a source of therapeutic agents and of structural diversity

Natural products remain a foundamental component in the search and development for innovative, safe and less expensive medicaments. Actually, in developed nations, the majority of all prescribed drugs derive from natural products, whose only available sources are animals, marine, plants, and microorganisms. The utility of natural products in the prevention and treatment of human diseases follows three criteria: I) the introduction of new natural chemical molecules of a wide structural diversity, used as templates for semi synthetic and total synthetic modification; II) the number of diseases prevented or treated by them; and III) their frequency of use in the treatment and prevention of human diseases. Natural products are rich sources of lead compounds suitable for further modifications during drug development. A potential explanation of the natural products success is their classification as so-called privileged structures. This concept is based on the fact that these chemical entities are produced by living organisms (in particular the secondary metabolites) and they have evolved throughout millenniums, getting a specific biological activity in comparison to the "randomly" developed synthetic chemicals. In spite of the great potential, only a small part of globe's living species has ever been tested for any activity.[6]

One key point of natural products is, thus, their great structural and chemical diversity. The idea of creating drug leads embraces the concept of achieving high molecular diversity within the boundaries of reasonable DRUG-LIKE properties.[7,8] They provided, also, design principles for the development of combinatorial library. In chemical genetics/genomics, the access to collections

---

[6] Chin, Y. W., Balunas, M. J., Chai, H. B., King- horn, A. D. *The American Association of Pharmaceutical Scientists Journal.,* **2006**, 8, 239-242.
[7] Ajay, W. P. W., Murcko, M. *J. Med. Chem*., **1998**, 41, 3314–3324.
[8] Sadowski, J., Kubinyi, H. *J. Med. Chem*., **1998**, 41, 3325–3329.

of structurally diverse and complex small molecules is extremely important. Regarding the chemical genetics/genomics, two are the major compounds sources: natural products (including their derivatives) and combinatorial chemistry libraries. Due to the developing of combinatorial chemistry, nowadays preparing a large number of small molecules is relatively easy. Additionally, because of their important biological processes, new chemical modulators have been identified from the screening of small molecules originating from combinatorial chemistry library. [9,10]

However, the traditional combinatorial libraries process, 'one-synthesis/one-scaffold', generally shows limited structural diversity.

On the other hand, natural products are known to possess an even greater diversity in chemical space hence producing a deep-routed impact on chemical biology and drug development.[11,12,13] Most of the natural products produced by plants or microorganisms are not meant to bind to human proteins. However, for many years, microorganisms and plants have evolved leading to the production of small ligands (or natural products) for their macromolecular targets inside the living organisms.[14] Furthermore, several human proteins targets contain structural domains that are similar to those which small ligands (or natural products) have coevolved with.[15]

By means of the natural selection process, natural products possess a vast and unique chemical diversity and have evolved for optimal interactions with biological macromolecules.

---

[9] Wurdak H., Zhu S., Min KH., Aimone L., Lairson LL., Watson J., Chopiuk G., Demas J., Charette B., Weerapana E., Cravatt BF., Cline HT., Peters EC., Zhang J., Walker JR., Wu C., Chang J., Tuntland T., Cho CY., Schultz PG. *Proc Natl Acad Sci USA*., **2010**, 107, 16542–16547.

[10] Bradner J.E., Mak R., Tanguturi S.K., Mazitschek R., Haggarty S.J., Ross K., Chang C.Y., Bosco J., West N., Morse E., Lin K., Shen J.P., Kwiatkowski N.P., Gheldof N., Dekker J., DeAngelo D.J, Carr S.A., Schreiber S.L., Golub T.R., Ebert B.L. *Proc Natl Acad Sci USA.,* **2010**, 107, 12617–12622.

[11] Clardy J., Walsh C. *Nature*., **2004**, 432, 829–837.

[12] Feher M., Schmidt J.M. *J Chem Inf Comput Sci*., **2003**, 43, 218–227.

[13] Rosén J., Gottfries J., Muresan S., Backlund A., Oprea T.I. *J Med Chem*., **2009**, 52, 1953–1962.

[14] Firn R.D., Jones C.G. *Nat Prod Rep*., **2003**, 20, 382–391.

[15] Bon R.S, Waldmann H. *Acc Chem Res*., **2010**, 43, 1103–1114.

Indeed, another important advantage of natural products is their biological background. Biosynthesis of natural products includes interactions with modulating enzymes, and binding to other proteins, which stands for their actual biological function. Thus, in order to develop an effective drug, the ability of natural products to interact with other molecules is necessary. Most probably, this is a consequence of their sterically more complex structure.[16] In addition, natural products have higher molecular weights; fewer halogen, nitrogen, or sulfur atoms but more oxygen atoms; and more bridgehead tetrahedral carbon atoms, rings, and chiral centers.

In the past, most drugs have been discovered by identifying the active ingredient from traditional remedies.[6] Nowadays, instead, the new approach includes the control of diseases and infections at the molecular and physiological level and to target specific entities. The drug discovery process is long and it involves the identification of candidates, characterization, synthesis, screening, and assays for therapeutic efficacy. Once a compound has shown its potential in these tests, the process of drug development prior to clinical trials begins.[17]

The success of natural products is related to several disciplines such as: molecular and cellular biology, synthetic and analytical chemistry, biochemistry, and pharmacology.[18] Pharmaceutical industry, in this prospect, should change its mindset and address itself to natural product based drug discovery programs.[19] Infact, an integrated approach, combining different discovery tools and disciplines, will provide for sure the key for success in natural product drug discovery and development.

1.2. The marine environment as a prolific source of bioactive compounds and chemical diversity

Because of the structural and biological diversity of their constituents, marine enviroment is a unique and renewable resource for the discovering and

---

[16] Lutz, M. K. *Nature Biotechnology*., **2003**, 21, 602-604.
[17] Lahlou, M. *Expert Opinion on Drug Discovery*., **2007**, 2, 697-705.
[18] Nisbet, L. J., Moore, M., Soejarto, D. D. *Current Opinion in Biotechnology*., **1997**, 8, 708-712.
[19] Mouhssen, L. *Pharmacology & Pharmacy*., **2013**, 4, 17-31

development of potential new drugs and bioactive entities. The study of marine natural products is more complex than that of terrestrial origin compounds due to their difficulty in collection and identification. However, despite these difficulties, the marine environment is a very rich source of powerful compounds that have shown significant activities in anti-inflammatory, antitumor, allergy, analgesia, immuno-modulation, and anti-viral assays.[20]

The oceans cover more than 70% of the earth's surface and contain more than 300,000 described species of plants and animals.[21,22]

Macroscopic plants and animals have adapted to all regions of the oceans, including temperate, polar, and tropical areas. The activity and the number of natural products is directly related to the huge biodiversity of life that the marine environment has. The most promising marine natural products are small to medium molecular weight compounds produced principally by marine invertebrates (sponges, soft corals, tunicates) and microbes. These organisms live in a highly competitive and complex environment and produce a vast variety of toxic chemicals in order to prevent parasitism and predation. All marine organisms have provided a parade of very unusual novel structures; biogenetically, they can be included in the biosynthetic pathways used for terrestrial secondary metabolites, whereas, structurally, they often posses predominantly marine functional groups. In Particular, ascidians' chemistry is characterised by the presence of nitrogenous metabolites. Thanks to the combined efforts of marine natural product pharmacologists and chemists, several promising compounds have been identified; some of them have been already selected as promising candidates for extended pre-clinical evaluation, whereas others are already at advanced stages of clinical trials. Most of these products are used for cancer therapy; for example, the marine alkaloid ecteinascidin 743 (ET-743), which is an anti-tumour compound particularly effective against solid tumours.[19]

---

[20] Pomponi, SA. *J Biotechnol*.,**1999**, 70, 5–13.
[21] Newman, D.J. Cragg, G. M.; *J. Nat. Prod*., **2004**, 67 (8), 1216–1238.
[22] Jimeno, J.M. *Anticancer Drugs*., **2002**, 13 ,15–19.

On the other hand, the search of marine origin molecules has evolved relatively slowly, mainly because of the small available quantities of the living material. It is very common to isolate less than one milligram of a bioactive substance from one kilogram of the marine organism. However, more sensitive methods of NMR spectroscopy and mass spectrometry combined with advanced liquid chromatography techniques are currently used for identification and characterization of natural products. So, complex molecular structures can be now solved using less than one milligram of compound. Chemical identification of the molecules present in biological extracts is just one step of their full investigation; a particularly interesting aspect is the individuation of their real producers. The incredible potential of even a single marine organism to produce secondary metabolites is due to the peculiar features of the marine environment. The highly rich secondary metabolism of some marine invertebrates can be explained by the evidence that marine invertebrates harbour microorganisms in their tissues (in particular in the extra- and intra-cellular spaces), such as bacteria, cyanobacteria and fungi. In some cases, associated microorganisms may constitute up to a 40% of the biomass. The possible microbial origin of bioactive molecules from marine invertebrates, recently highlighted new and interesting perspectives for their synthesis at commercial level. Isolation and cultivation of the suspected microbial producers either from the tissues of invertebrates or from the surrounding seawater could provide a more satisfying answer to the supply problem. If bacteria are actually the producers of bioactive metabolites of interest, transferring the gene clusters, responsible for the biosynthesis of the respective natural products, to a vector suitable for large-scale fermentation could provide an alternative strategy thereby avoiding the difficulties in culturing symbiotic bacteria.

A fascinating example of the great variety of secondary metabolites, from marine sponges, can be represented by bromopyrrole alkaloids. These natural products, whose architectural complexity ranges from simple, achiral, monomeric oroidin (**1**, **Figure 1.1**) to 16-stereocenter-containing tetrameric stylissadines (**4-5, Figure 1.2**), have been isolated from different species of

Agelasidae, *Axinellidae*, *Dyctionellidae* and *Hymeniacidonidae* sponges families.[23] These alkaloids, belonging to the outlined above sponges families, show a systematic recurrence which allowed to speculate their taxon-specificity and, later on, to consider them as chemical markers for phylogenetically related sponges.[24] The majority of these alkaloids share the key building block pyrrole-imidazole; oroidin (**1**) was the first member isolated from this group and it is the underlying structural motif of this alkaloids family.[25]

On this subject, we can mention the oroidin-like linear monomers (**1-3**) and tetramers (**4-5**). These structures contain the skeleton of oroidin without any further C-C or C-N bond formation. Hymenidin (**2**, **Figure 1.1**), isolated from the Okinawan sponge *Hymeniacidon sp.*[26] is the 2-debromo derivative of oroidin, whereas clathrodin (**3**), isolated from the Caribbean Sea sponge *Agelas clathrodes*[27] is its 2,3-debromo derivative.

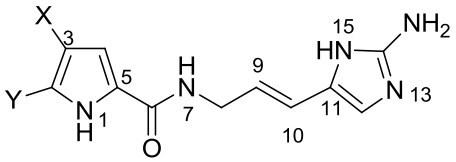

1 X = Y = Br
2 X = Br Y = H
3 X = Y = H

Figure 1.1. Structures of oroidin (**1**), hymenidin (**2**), and clathrodin (**3**).

The degree of bromination of the pyrrole moiety has been shown to affect the biological properties of these compounds. Both oroidin and hymenidin have exhibited to reduce the voltage dependent calcium elevation in PC12 cells. Furthermore, the potency of the tested alkaloids increases together with the number of bromine atoms associated to the pyrrole ring. Analogously, the bromination degree also affects the feeding deterrent properties, hymenidin

---

[23] Forte, B., Malgesini, B., Piutti, C., Quartieri, F., Scolaro, A., Papeo, G. *Mar. Drugs*., **2009**, 7, 705-753.
[24] Braekman, J.C., Daloze, D., Stoller, C., Van Soest, R.W.M. *Biochem. Syst. Ecol*., **1992**, 20, 417-431.
[25] Garcia, E. E., Benjamin, L. E., Fryer, R. I. *J. Chem. Soc. D. Chem. Commun*., **1973**, 78-79.
[26] Kobayashi, J., Ohizumi, Y., Nnakamura, H., Hirata, Y. *Experientia.,* **1986**, 42, 1176-1177.
[27] Morales, J. J., Rodriguez, A. D. *J. Nat. Prod*., **1991**, 54, 629-631.

being less potent than oroidin.[28] Oroidin, hymenidin and clathrodin showed marked antiserotonergic and anticholinergic activities.[29,29,] Clathrodin is a sodium channel neurotoxin, which acts by influencing the channel ionic conductance.[30] Adversely, stylissadines (**4**-**5**) are tetrameric molecules. Structurally speaking, they are ether-linked dimers of massadine, they are the largest ones and, with their 16 stereogenic centers, they represent the most complex structures within the oroidin family of alkaloids so far discovered. They both have biological activity as antagonists of the P2X7 receptor involved in inflammatory diseases, however, their high molecular weight together with their structural complexity make them hard to develop as drugs.[31]

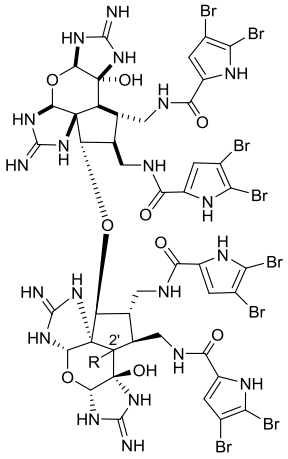

Figure 1.2. Oroidin-like tetramers: stylissadines A and B (**4-5**).

In conclusion, it is evident that marine environment will continue to be a major source of new drug leads, however, the effective utilization of these resources will require advances in technologies together with the opening of new frontiers in science.

---

[28] Assmann, M., Zea, S., Koeck, M. *J. Nat. Prod*., **2001**, 64, 1593-1595.23.
[29] Rosa, R. Silva, W., Escalona de Motta, G., Rodriguez, A. D., Morales, J. J., Ortiz, M. *Experientia.,* **1992**, 48, 885-887.
[30] Rivera Rentas, A.L., Rosa, R., Rodriguez, A. D., Escalona de Motta, G. *Toxicon*.,**1995**, 33, 491-497.
[31] Grube, A., Köck, M. *Org. Lett*., **2006**, 8, 4675-4678

CHAPTER 2

METHODOLOGY IN ISOLATING AND CHARACTERIZING MARINE NATURAL PRODUCTS

The collection of biological material in the marine environment as well as its identification involves a great number of restrictions that lead to the necessity of separating small quantities of mixture and of characterizing them in a non-destructive way.

The study of marine natural products follows different steps such as the isolation, purification and the structural determination of the isolated new compounds.

2.1. Isolation procedures

The isolation of natural products from natural sources exhibits numerous problems, because they may only exist in infinitesimal quantities. Therefore, a good selection of different techniques and approaches is required to solve this issue. The problem of separation and isolation of new metabolites was overcome with the introduction of sophisticated techniques, such as the various analytical and preparative chromatographic methods, enabling a successful procedure of purification. Normally, after biomass extraction with adequate solvents (like acetone, ethanol, and/or chloroform), the first step of natural compounds isolation, from the main extract, consists of a sequential gradient partition with solvents. The so gained fractions contain compounds distributed according to their polarity. In particular, in the case of bioactive extract, this process can be guided by the appropriate assay in order to localize the active component. Subsequently, different purification procedures can be performed, taking in consideration the various properties of the components of these fractions. Specifically, the fractions of low or medium polarity, usually monitored, enclose lipophilic organic compounds that can be usually separated by standard normal or reverse phase column chromatography and/or MPLC and finally HPLC to obtain the individual components.

Medium Pressure Liquid Chromatography (MPLC) is a liquid-solid chromatography, in which the liquid mobile phase is forced through the solid stationary phase at medium pressure. MPLC is more efficient, regarding the resolution, in comparison to the open-column and the flash chromatography methods and, in addition, the separation involves a significant gain in time. The solid stationary phase can be a normal phase, like silica gel, or bonded phase (RP-8, RP-18). The technique uses a pressure of *ca.* 5-40 bar and can readily accommodate much larger sample loads (100 mg-100 g) that are generally applied in other separations. Concerning the separating power, MPLC lies between flash chromatography and semi-preparative HPLC.

High Performance (or High Pressure) Liquid Chromatography (HPLC) is the most widely used chromatographic method, employing both the normal- and reverse-phase. It is used in the preparative separation of samples, to "optimize" the isolation of natural products (optimization of the experimental conditions, checking of the different fractions all over the separation). However, HPLC is usually applied as the last step in purification processes providing pure compounds in high yields, and, in this regard, the quantities involved have the tendency to be at the lower end of the scale.

Finally, the isolated compounds are structurally characterized and are subjected to pharmacological assays.

2.2. Structural determination methods

Recently, natural products chemistry has seen an exponential growth due to advances in isolation techniques, as well as in the synthetic and biosynthetic approaches and spectroscopic and chromatographic methods.

The structural determination described in my thesis is considerably based on spectroscopic techniques, in particular mass spectrometry (MS) and nuclear magnetic resonance (NMR), and sometimes degradation methods too, coupled with circular dichroism (ECD) and computational methods.

2.2.1. Mass Spectrometry

Mass Spectrometry is a destructive analytical technique, utilized to define the elementary formula of unknown compounds through the measurement of their molecular masses. Firstly, a molecule is ionized and transferred to gas phase in the ionisation source and then it is transported to the mass analyzer to measure its mass properties. In order to obtain a mass spectrum, in the ion source, must be generated ions in a gas-phase. They are consequently accelerated, by an electric field, up to they get to a particular speed and they are transferred to the mass analyzer, which separate different ions on the base of their mass/charge (*m/z*) ratio. The separated ions are after that measured on the detector and the results showed.

Most of compounds reported in the following chapters have been analyzed by Electrospray Ionisation (ESI) mass spectrometry through an Orbitrap system.

This type of technique is used to identify non-volatile molecules, directly from the liquid phase (**Figure 2.1**). The start and the end of this process can be verified by an electrical circuit through which the spray of liquid-charged droplets is driven.

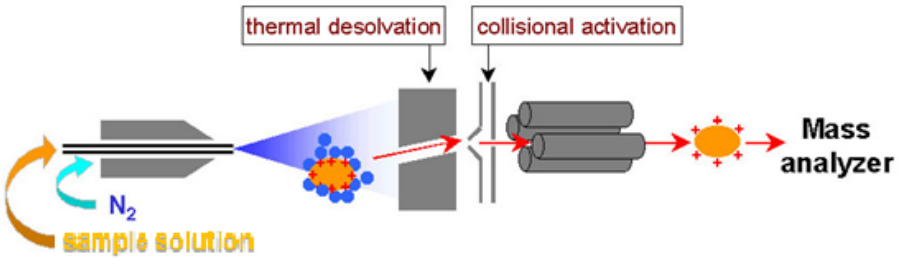

Figure 2.1 ESI mass spectrometry.

At the beginning of this process, a molecule presents as an entity or complex charged and dissolved in a water-rich environment while at the end of it, the same molecule is displayed by a mass analyser as a series of multicharged ions. In vacuum, the biomolecular ions are then selectively examined according to their mass/charge ratio. Due to the electric potential of the capillary, each droplet of the spray carries an excess of positive or negative charge, and this causes wide protonation or deprotonation of the molecules of the sample,

developing ions. An uncharged carrier gas for example nitrogen is utilized to help the liquid to be nebulized and the neutral solvent in the droplets to evaporate.

Orbitrap is an innovative kind of mass analyzer introduced by Makarov.[32] The LTQ-Orbitrap combines the most advanced Ion Trap and Fourier Transform technologies into a single instrument with unique analytical power and adaptability. The instrument affords a high mass resolution, accurate mass determinations, and MS for routine high-throughput analysis.

In an orbitrap, ions are injected tangentially into the electric field between the electrodes and captured because their electrostatic attraction to the inner electrode is in equilibrium with centrifugal forces. Therefore, ions cycle around the central electrode in rings. Additionally, the ions also move back and forth along the axis of the central electrode. Therefore, ions of a specific mass-to-charge ratio move in rings that oscillate along the central spindle (**Figure 2.2**). The occurrence of these harmonic oscillations is independent of the ion velocity and is inversely proportional to the square root of the mass-to-charge ratio (*m/z*).

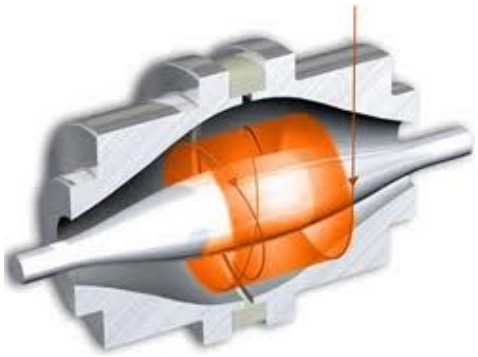

Figure 2.2. Ion trajectories in an Orbitrap mass spectrometer.

By sensing the ion oscillation similar as in the FT-MS (Fourier transform mass spectrometry), the trap can be utilized as a mass analyzer. Orbitraps have a high mass accuracy (1-2 ppm), a high resolving power (up to 200,000). Now,

[32] Hu, Q.; Noll, R. J.; Li, H.; Makarov, A.; Hardmanand, M.; Cooks, R. G.; *J. Mass Spectrom.*, **2005**, 40, 430–443.

there are two commercial LTQ-Orbitrap instruments, the Discovery and XL models. One of the principal differences is that the XL has a linear octopole collision cell (absent in the Discovery model), in which collisional activation and fragmentation can be achieved. Even if this feature affords additional versatility to MS/MS experiments, the analytical performance and fundamental principles of operation of the Orbitrap analyzers in both instruments are identical.[33]

2.2.2. Nuclear Magnetic Resonance

The structural determination of the isolated compounds can be carried out through the Nuclear Magnetic Resonance[34,35,36] spectroscopy which is based on the reorientations of nuclear spins with respect to an applied static magnetic field. Furthermore, to standard ^{1}H and ^{13}C NMR spectra, a large use of 2D NMR experiments has been made during my research activity. They are superior to their 1D NMR counterparts both for the information on the connection between nuclei and for the easier assignment of nuclei resonating in crowded regions of the spectra (signal overlapping is much less likely in two dimensions than in one).

For example, in order to establish the connectivity of the molecule through the identification of spins which are coupled to each other, the COSY (COrrelation SpectroscopY) experiments are widely used.

Another type of the 2D NMR experiment is the HSQC (Heteronuclear Single Quantum Correlation) that permits to obtain a chemical shift correlation between directly bonded ^{1}H-^{13}C.

The HMBC (Heteronuclear Multiple Bond Correlation) experiment is a heteronuclear two-and three-bond ^{1}H-^{13}C correlation experiment; its sequence is less efficient than HSQC because the involved $^{2,3}J_{CH}$ couplings are smaller (3-10Hz). Moreover, while $^{1}J_{CH}$ are all quite close to each other, $^{2,3}J_{CH}$ can be

---

[33] Perry, R. H.; Cooks, R. G.; Noll, R. J.; *Mass Spectrometry Reviews.*, **2008**, 27, 661– 69.
[34] Bax, A.; Two-Dimensional Nuclear Magnetic Resonance in Liquids, Delft University Press, Dordrecht, **1982**.
[35] Palmer III, A. G.; Cavanagh, J.; Wright, P. E.; Rance, M.; *J. Magn. Reson.*, **1991**, 151-170.
[36] Bax, A.; Summers, M. F.; *J. Am. Chem. Soc.*, **1986**, 2093-94.

very dissimilar, making necessary the optimization of the experiment for each kind of coupling. Consequently, in many HMBC spectra not all of the correlation peaks which could be expected from the structure of the molecule are existent. Cross peaks are between protons and carbons that are two or three bonds away while direct one-bond cross-peaks are suppressed. In conclusion, this experiment allows the connection of the fragments and the assembling of the structure of the molecules.

CHAPTER 3

DISCOVERY OF NEW MARINE NATURAL PRODUCTS FROM INVERTEBRATES

3.1. Introduction

For the research of new active metabolites, the natural world offers an endless number of amazing matters. However, many of the most intriguing problems concern compounds only available in definitely minute quantities. Through the bioassay-guided separations, original compounds with different activities can be isolated from various invertebrates. In addition, update spectroscopic and mass spectrometry techniques provide an improvement of the study of the compounds that exsist in nature in infinitesimal amounts. The researcher, in the discovery of new bioactive compounds follows different steps such as the isolation of major quantities of compound, the defining of its structure and the attempt to use it in the pharmaceutical field.

Since the marine organisms rapresent a reach source of bioactive metabolites, I have partly focused my attention on the investigation of the marine invertebrates, such as sponges and tunicates.

Sponges, lacking any digestive, nervous, muscular, circulatory systems or any physical defence from their predators, just produce secondary metabolites, which are involved in their chemical defence, and are essential for their survival. In fact, many species are composed of toxic substances, probably to intimidate predators and also to defend their place in the marine ecosystem.

Several promising compounds have been identified from marine sponges. They possess pronounced biological activity and they already reached advanced stages of clinical trials, mostly for the treatment of cancer, and some of them have been selected as candidates for extended preclinical evaluation.

Lately, ascidians have increasingly become the target of natural products research and as result many new ascidian metabolites have been obtained, raising the interest of both pharmacologists and synthetic chemists.

Ascidians belong to the *phylum* Chordata, which comprises all vertebrate animals, including mammals. Therefore, they represent the most evolved group

of animals commonly investigated by marine natural products chemists. These species belong to the class of tunicates because the covering of their body looks like a tunic.

While adult ascidians are exclusively marine invertebrates and resemble to the other chordates, their larvae look like amphibian tadpoles and contain notochorods, pharyngeal slits, dorsal hollow nerve cords, all of which are lost during development. There are approximately 2000 living species of tunicates, and ascidians are the most abundant among them. As regard the morphology of adult ascidians, the ones which live solitary have a length ranged from 1 cm up to 15cm while those that live in colonies don't exceed the length of 5 cm. Some of them are of undefined shape, resembling sponges or fleshy coelenterates. The contractions causing sea squirt to spray water stream allow inexperienced observers to distinguish tunicates from other marine invertebrates.

3.2. Phallusiasterol C, a new disulfated steroid from the Mediterranean Tunicate *Phallusia fumigata*

The chemical diversity shown by marine steroids depend on the basic carbon skeleton extensive oxygenation, cleavage and/or re-arrangement on the rings of tetracyclic nucleus, and alteration of the side chain.[37,38,39,40,41]

In fact, "usual" sterols generally present a 3-hydroxycholestane or 3-hydroxy-Δ^5-cholestane nucleus and a C8–C10 side chain[42], whereas marine sterols show one or both the distinctive features of carbon side chains in the C10 to C12 range, involving loss of carbon atoms or their addition at other positions than C-24, and multiple oxygenation of the side chain and/or the nucleus.[43] The new steroidal structures, isolated from sea organisms, are more than 1600. In

---

[37] Lakshmi, V.; Kumar, R. *Nat. Prod. Res*. **2009**, 23, 801–850.
[38] Sarma, N.S.; Krishna, M.S.; Pasha, S.G.; Rao, T.S.P.; Venkateswarlu, Y.; Parameswaran, P.S. *Chem. Rev*. **2009**, 109, 2803–2828.
[39] Zhang, W.; Guo, Y.W.; Gu, Y.C. *Curr. Med. Chem*. **2006**, 13, 2041–2090.
[40]Sica, D.; Musumeci, D. **2004**, 69, 743–756.
[41] Sun, P.; Meng, L.Y.; Tang, H.; Liu, B.S.; Li, L.; Yi, Y.; Zhang, W. *J. Nat. Prod*. **2012**, 75, 1656–1659.
[42] Goad, L.J.; Scheuer, P.J., Ed.; Academic Press: New York, NY, USA, **1978**; Volume 2, pp. 76–172.
[43] Schmitz, F.J.; Scheuer, P.J., Ed.; Academic Press: New York, NY, USA, **1978**; Volume 1, pp. 241–297.

particular, they have been isolated mainly from marine invertebrates, including algae, porifera, and tunicates.[42,43] The structural diversity of these metabolites, especially the polar sterols, is reflected in a variety of different pharmacological properties, including cytotoxic[44], antifeedant[45], spermatostatic[46], anti-inflammatory[47] and anti-human cytomegalovirus[48] (HCMV) activities. Particularly, the role of marine steroids, as nuclear receptor ligands, has been recently highlighted.[49] Sulfated steroids endowed with dual farnesoid X receptor (FXR) and pregnane X receptor agonism–antagonism have been recognized like solomonsterols A (**9**) and B (**10**), isolated from the sponge *Theonella swinhoei*,[50,51] and phallusiasterol A (**7**), previously isolated from the Mediterranean ascidian *Phallusia fumigata*, together with its C-6 epimer phallusiasterol B[52] (**8**, **Figure 3.1**).

Specifically, investigation of phallusiasterols effects on the activity of pregnane-X-receptor (PXR) has shown that phallusiasterol A induces PXR transactivation in HepG2 cells and stimulates the expression of the PXR target genes CYP3A4 and MDR1 in the same cell line, whereas phallusiasterol B was inactive. This study confirmed the role of steroids in regulating the nuclear receptors (NR) activity, and highlighted a crucial reliance on some structural features, like the configuration at C-6, of the ligand-receptor binding.

Particularly, during my research I have been dealing with the re-investigation of a new collection of *P. fumigata.* This study led to the isolation, from the

---

[44] Yan, X.H.; Lin, L.P.; Ding, J.; Guo, Y.W. *Bioorg. Med. Chem. Lett.* **2007**, 17, 2661–2663.
[45] Li, R.; Shao, C.L.; Qi, X.; Li, X.B.; Li, J.; Sun, L.L.; Wang, C.Y. *Mar. Drugs*. **2012**, 10, 1422–1432.
[46] Tillekeratne, L.M.V.; Liyanage, G.K.; Ratnasooriya, W.D.; Ksebati, M.B.; Schmitz, F.J. *J. Nat. Prod*. **1989**, 52, 1143–1145.
[47] Cheng, S.Y.; Huang, Y.C.; Wen, Z.H.; Hsu, C.H.; Wang, S.K.; Dai, C.F.; Duh, C.Y. *Steroids.* **2009**, 74, 543–547.
[48] Chen, W.H.; Wang, S.K.; Duh, C.Y. *Mar. Drugs.* **2011**, 9, 1829–1839.
[49] Blumberg, B.; Sabbagh, W., Jr.; Juguilon, H.; Bolado, J., Jr.; van Meter, C.M.; Ong, E.S.; Evans, R.M. *Genes Dev*. **1998**, 12, 3195–3205.

[50] Festa, C.; de Marino, S.; D'Auria, M.V.; Bifulco, G.; Renga, B.; Fiorucci, S.; Petek, S.; Zampella. *J. Med. Chem*. **2011**, 54, 401–405.
[51] Mencarelli, A.; D'Amore, C.; Renga, B.; Cipriani, S.; Carino, A.; Sepe, V.; Perissutti, E.; D'Auria, M.V.; Zampella, A.; Distrutti, E.; Fiorucci, S. *Mar. Drugs.* **2013**, 12, 36–53.
[52] Imperatore, C.; D'Aniello, F.; Aiello, A.; Menna, M.; Fiorucci, S.; D'Amore, C.; Sepe, V. *Mar. Drugs.* **2014**, 12, 2066–2078.

more polar fraction of the butanol extract, of a new disulfated sterol, which has been named phallusiasterol C (**6**, **Figure 3.1**), whose structure was elucidated by spectroscopic means. Several subsequent normal-phase chromatographies of the ethyl acetate extract of the ascidian *P. fumigata,* collected from the bay of Pozzuoli (Napoli, Italy), provided the isolation of the compound **6** in its pure form.

A pseudomolecular ion at *m/z* 567.2054 $[M–Na^+]^-$ was seen in the high-resolution ESI mass spectrum (negative ion mode), suggesting for compound **6** a molecular formula of $C_{26}H_{40}NaO_8S_2^-$ (calcd. 567.2057), which indicated six unsaturation degrees.

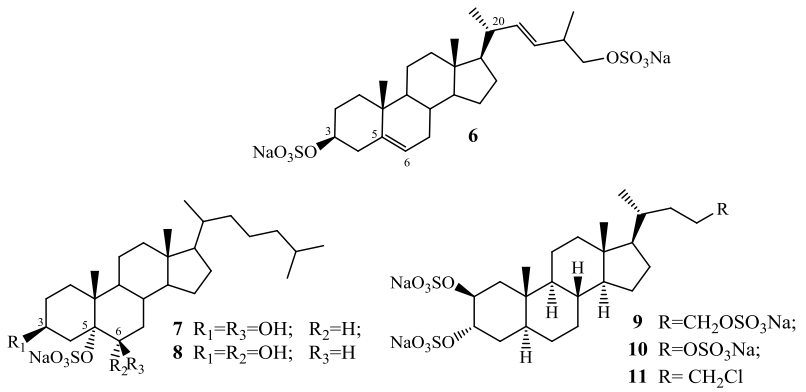

Figure 3.1. Structures of phallusiasterol C **(6)**, phallusiasterols A **(7)** and B **(8)**, solomonsterols A **(9**) and B **(10)**, and chalinulasterol **(11).**

The ESI and MS/fragmentation pattern of **6** revealed the presence of two sulfate groups from the peaks 545 (M in hydrogen form), 272 (double charged species), and 447 [M $NaHSO_4$ Na^+]. The ^1H NMR spectrum (CD_3OD) of **6** suggested its steroidal structure, with two up-field methyl singlets at δ 0.72 (H_3-18) and 1.03 (H_3-19) and one methyl doublet at δ 1.03 (*J*=6.4 Hz, H_3-21). Other proton resonances, combined with ^{13}C NMR and mass data, highlighted the presence of one secondary (δ_H 4.14, dddd, *J*=11.4, 11.4, 4.8, 4.8 Hz, δ_C 80.0, CH) and one primary (δ_H 3.88, dd, *J*=9.3, 6.0 Hz; δ_H 3.74, dd, *J*=9.3, 7.8 Hz, δ_C 73.8, CH_2) sulfoxy groups in the molecule. Furthermore, three olefin signals, resonating in the proton spectrum at δ 5.38 (dd, *J*=6.9, 3.3 Hz, 1H, H-

6), 5.35 (dd, *J*=15.3, 8.5 Hz, 1H, H-22), and 5.28 (dd, *J*=15.3, 7.0 Hz, 1H, H-23), were assigned to two double bonds, one trisubstituted and one disubstituted, based on the four down-field resonances present in the ^{13}C NMR spectrum at δ_C 141.5 (C), 123.4 (CH), 138.5 (CH) and 130.2 (CH).

The interpretation of COSY, HSQC and HMBC 2D NMR experiments permitted the assembly of the steroidal backbone and the assignment of all the protons and carbons of the tetracyclic system to the relevant resonances. (**Table 3.1**). The location of the secondary sulfoxy group at C-3 and the $\Delta^{5(6)}$ position of the endocyclic double bond were so deduced. The HMBC correlation peaks of the methyl protons H_3-19 with C-1, C-5, C-9, and C-10 and of H_3-18 with C-12, C-13, C-14, and C-17 located the A/B and C/D ring junctions and completed the planar structure determination of the steroid ring system. The nature of the side chain was readily deduced by COSY map analysis. A single ^1H-^1H spin system was delineated, starting at the methyl doublet at δ 1.03 (H_3-21) which was correlated to the proton at δ 2.06 (H-20). The latter was coupled with both the H-17 methine proton (δ 1.67) and the olefinic proton at δ 5.35 (H-22), then, in turn coupled with the other olefin proton at δ 5.28 (H-23). This showed the Δ^{22} position of the remaining double bond, whose *E*-configuration was suggested by the *J* value (15.3 Hz) of H-22 and H-23. The coupling of H-23 to the multiplet at δ 2.44 (H-24), which was in turn coupled both to the methyl protons at δ 1.02 (H_3-26) and the sulfoxy methylene protons at δ 3.74 (H-25a) and δ 3.88 (H-25b), completed the assignment, indicating a 24-methyl-25-sulfoxy C26 side chain for **6** (**Figure 3.2**). The relative stereochemistry of phallusiasterol C (**6**) with the B/C and C/D t*rans* ring junctions, was established through the analysis of ROESY data and coupling constant analysis. The axial orientation of H-8, H-9 and H-14 was apparent from their respective coupling constants, as well as the orientation of the angular methyl groups from the ROESY correlations of both H_3-18 and H_3-19 with H-8 and the axial H-11β.

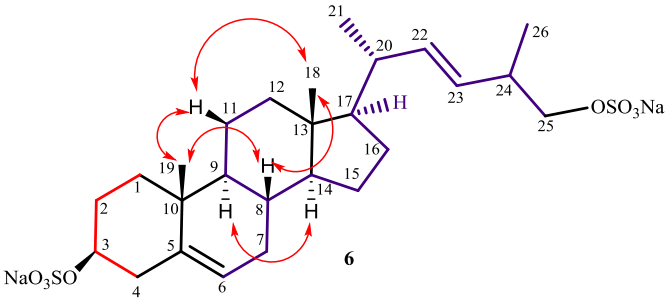

Figure 3.2. COSY segments (represented as colored bonds) and key ROESY correlations (arrows) for the phallusiasterol C (**6**).

Table 3.1. ^{1}H (700 MHz) and ^{13}C (125 MHz) NMR data for phallusiasterol C (**6**) in CD_3OD.

Position	δ_H (mult., *J* in Hz)	δ_C	HMBC	Pos.	δ_H (mult., *J* in Hz)	δ_C	HMBC
1β	1.90, dt, (13.5, 3.6)	38.4	2, 5, 10, 19	**-**	-	-	-
1α	1.10, m		2, 3, 10, 19	**13**	-	43.4	-
2β	1.63, m [a]	29.9	1, 3, 10	**14α**	1.02 [b]	58.2	8, 13, 15, 16, 18
2α	2.07, m [a]		1, 3, 10	**15β**	1.07, m [a]	25.3	13, 14, 16, 17
3α	4.14, dddd, (11.4, 11.4, 4.8, 4.8)	80.0	1, 2, 4	**15α**	1.58 [a,b]		8, 14, 16
4β	2.34, dd, (13.2, 11.4)	40.3	2, 3, 5, 6, 10	**16β**	1.28, m [a]	29.7	13, 15, 17
4α	2.53, ddd, (13.2, 4.8, 2.2)		2, 3, 5	**16α**	1.71, m [a]		13, 17, 20
5	-	141.5	-	**17**	1.17, m	57.2	13, 15, 16, 20, 22
6	5.38, dd, (6.9, 3.3)	123.4	4, 7, 8, 10	**18**	0.72, s	12.5	12, 13, 14, 17
7β	1.98, dt, (13.4, 6.9, 3.3)	33.0	5, 6, 8, 9	**19**	1.03, s	19.7	1, 5, 9, 10
7α	1.55 [b]		5, 8, 14	**20**	2.06, m	41.5	17, 21, 22, 23
8β	1.48, m (qd, 10.7, 4.3)	33.2	7, 9, 14	**21**	1.03, d, (6.4)	19.7	17, 20, 22
9α	0.96, ddd (13.2, 10.7, 4.3)	51.7	8, 10, 11, 19	**22**	5.35, dd, (15.3, 8.5)	138.5	20, 21, 23, 24
10	-	37.7	-	**23**	5.28, dd, (15.3, 7.0)	130.2	20, 21,22, 25, 26
11β	1.55 [b]	22.1	9, 10, 12	**24**	2.44, m	37.6	22, 23, 25,26
11α	1.51, m		9, 10, 12	**25a**	3.88, dd, (9.3, 6.0)	73.8	23, 24, 26
12β	2.01, dt, (12.9, 3.5)	41.0	11, 14	**25b**	3.74, dd, (9.3, 7.8)		23, 24, 26
12α	1.18, m		9, 13, 14	**26**	1.02, d, (6.2)	21.2	23, 24, 25

[a] Assignments may be interchanged. [b] Overlapped by other signals.

On this skeleton, the 3β-sulfoxy configuration was assigned on the basis of the coupling pattern of H-3 indicating its axial orientation.[53,54,55] Thanks to this

[53] Aiello, A.; Fattorusso, E.; Menna, M.; Carnuccio, R.; Iuvone, T. *Steroids* **1995**, 60, 660–673.
[54] Fujimoto, Y.; Yamada, T.; Ikekawa, N. *Chem. Pharm. Bull.* (Tokyo) **1985**, 33, 3129–3133.
[55] Notaro, G.; Piccialli, V.; Sica, D.; Corriero, G. *J. Nat. Prod.* **1991**, 54, 1570–1575.

information, the structure of phallusiasterol C (**6**) was established as (22*E*)-26,27-dinor-24ξ-methyl-cholesta-5,22-dyen-3β, 25-diyl-3,25-sodium disulfate. Based on the reported activity of phallusiasterols A and B, as nuclear receptor ligands, the effects of phallusiasterols C as modulators of PXR receptor have been also investigated. A transactivation assay on HepG2 cells, a human hepatocarcinoma cell line, has been performed. These studies displayed that, despite the structural similarity with solomonsterol A for the short and sulfated side chain, compound **6** was inactive as PXR agonist. Additionally, it also failed to reverse the induction of luciferase activity caused by rifaximin, indicating that it was not a PXR antagonist (**Figure 3.3**). Similar results have been obtained by analyzing the effect exerted by **6** in terms of regulation of PXR mediated induction of two PXR target genes, CYP3A4 and MDR1, in the same cell line. In this assay, compound **6** failed to induce the expression of both target genes (data not shown).

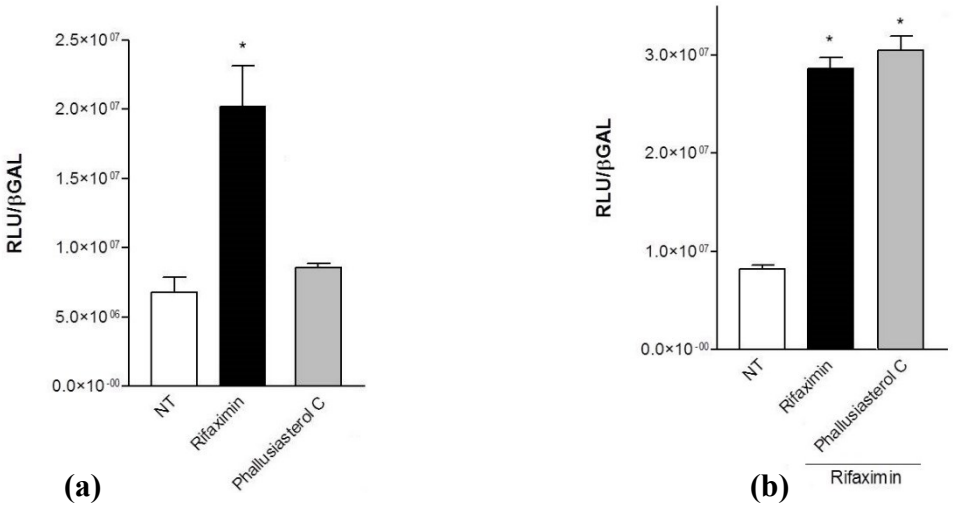

Figure 3.3. (a, b) Luciferase reporter assay. HepG2 cells were transiently transfected with pSG5-PXR, pSG5-RXR, pCMV-βgalactosidase and p(CYP3A4)-TK-Luc vectors and then stimulated with (a) 10 μM rifaximin or phallusiasterol C (**6**) for 18 h, or (b) 10 μM rifaximin alone or in combination with 50 μM of compound **6**. Relative Luciferase Units were normalized with β-galactosidase Units (RLU/βgal). All experiments were performed in triplicate.
NT, not treated cells. R, Rifaximin. *P < 0.05 versus NT cells. Data are mean ± SE.

These results, although negative, were important for the knowledge of the structure-PXR regulating activity relationship, concerning the sulfated steroids. In the binding model, proposed for solomonsterols to the PXR receptor, a clear stabilizing interaction between the side chain sulfate group and the positively charged Lys210 is observed.[49] This model was supported by many studies on chalinulasterol (**11**), which has a structural relationship with solomonsterols and differ from the latter in having a chlorine atom instead of a sulfate function at position C-24 of the side chain.[56] Chalinulasterol lacked any PXR modulating activity and, as a consequence, an essential role of the sulfate group present in the side chain has been proposed. However, the activity of phallusiasterol A **(7)** as PXR agonist, which can be compared to that of rifaximin, a well characterized ligand for the human PXR, opposes this assumption since it presents a "regular" sterol side chain (**Figure 3.1**). Instead, the feature and/or the shape of the region around the A/B ring junction seems to be crucial; in fact, both phallusiasterol B **(8)**, which differs from phallusiasterol A only for the configuration at C-6, and phallusiasterol C, showing the $\Delta^{5(6)}$ double bond, lacked any PXR modulating activity (**Figure 3.1**). In conclusion, the investigation of the possible role of phallusiasterol C as modulator of the PXR nuclear receptor revealed important structural requirements for the PXR nuclear receptor activity of sulfated steroidal structures.

3.3. Cytotoxic thiazinoquinones from the Mediterranean ascidian *Aplidium conicum.*

Ascidians of the genus *Aplidium*[57] are recognized as an important source of chemical diversity and bioactive natural products. Among the compounds isolated by this genus are present many meroterpenes. These compounds form a class of complex metabolites, which derive from a mixed terpenoid-

[56] Teta, R.; Della Sala, G.; Renga, B.; Mangoni, A.; Fiorucci, S.; Costantino, V. *Mar. Drugs.* **2012**, 10, 1383–1390.
[57] Fenical, W. in *Food-Drugs from the Sea Proceedings*. (Eds.: H. H. Webber, G. D. Ruggieri), Marine Technology Society, Washington DC, **1976,** *4,* 388-394.

polyketide biosynthetic pathway and display a structural diversity.[58] The quantity of meroterpenes in the species *Aplidium conicum* depends on the place where they are collected. For example, it has been found out that the specimens of *A. conicum* situated in Tarifa Island, in Spain, contained geranyl hydroquinone and its hydroxylated and/or cyclized analogues as well as various chromenols.[59]

From samples of the same ascidian, collected in Italy along Sardinia coasts, my research group have isolated a large group of new meroterpenes, with different polycyclic skeletons, but all show an unusual thiazinoquinone ring.

In the present thesis, the electrochemistry of four natural thiazinoquinones (**12-15**; **Figure 3.4**) from *Aplidium* species was reported in order to clarify the mechanism of action which is the basis of their cytotoxicity. The chemical and farmacological characterization of these compounds was previously discussed.[60,61,62] This work was already performed and completed for the compounds **12-15** that showed an interesting cytotoxic activity on different cell lines[60,61,62] (**Table 3.2**).

The electrochemical studies were elaborated together with the research group of Prof. Doménech-Carbò (University of Valencia, Spain) which, using an innovative technique, "the solid-state electrochemistry following the voltammetry of microparticles technique (VMP)", has provided information about the electrochemical response of the compounds, either alone or in presence of heme and O_2 in order to test the ability of the compounds to react with heme and the reactive oxygen species (ROS). It is known that because of their electrophilic properties some natural quinones can react directly with cellular nucleophiles, including soluble and protein thiol groups, and may

---

[58] Zubìa, E.; Ortega, M. J.; Salvà, J. *Mini-Rev. Org. Chem.* **2005**, 2, 389-399.
[59] Garrido, L.; Zubía, E.; Ortega, M. J.; Salvá, J. *J. Nat. Prod.* **2002**, 65, 1328-1331.
[60] Aiello, A.; Fattorusso, E.; Luciano, P.; Menna, M.; Esposito, G.; Iuvone, T.; Pala, D. *Eur. J. Org. Chem.* **2003**, 898-900.
[61] Aiello, A.; Fattorusso, E.; Luciano, P.; Mangoni, A.; Menna, M. *Eur. J. Org. Chem.* **2005**, 5024-5030.
[62] Aiello, A.; Fattorusso, E.; Luciano, P.; Macho, A.; Menna, M.; Muñoz, E. *J. Med. Chem.* **2005,** 48, 3410-3416.

inhibit critical processes in the cell.[63,64] Some quinones intercalate between the base pairs of DNA leading to blockage of DNA, RNA, and protein synthesis[65] while some others stabilize binding of nuclear topoisomerase II to DNA resulting in protein-associated DNA strand breaks.[66,67]

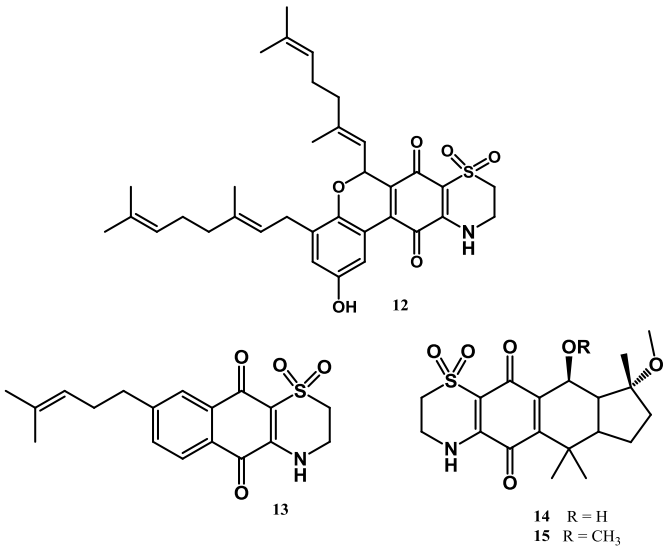

Figure 3.4. Structures of the studied compounds

In addition, cytotoxic quinones can exert their effects through the formation of redox-reactive species.[68,69,70] Single-electron reduction of quinones is catalyzed by flavoenzymes, resulting in the formation of semiquinone free radicals. These latter can then either bind directly to DNA, protein, and lipid, or undergo further redox reactions.[71,72,73,74] In recent years, particular interest has been paid

---

[63] Di Monte, D.; Ross, D.; Bellomo, G.; Eklow, L.; Orrenius, S. *Arch. Biochem. Biophys.* **198**4, 235, 334-342.
[64] Ross, D.; Thor, H.; Orrenius, S.; Moldeus, P. *Chem.-Biol. Interact.* **1985**, 55, 177-184.
[65] Pigram, W.J.; Fuller, W. L.; Hamilton, D. *Nature* **1972**, 235, 17-19.
[66] Tewey, K.M.; Rowe, T.C.; Yang, L.; Halligan, B.D.; Liu, L.F. *Science* **1984**, 226, 466-468.
[67] Pommier, Y.; Schwartz, R.E.; Zwelling, L.A.; Kohn, K.W. *Biochemistry* **1985**, 24, 6406-6410.
[68] Cohen, G.M.; Doherty, M. d'A.; Br. J. *Cancer Suppl*. **1987**, 8, 46-52.
[69] Samoilova, R. I.; Crofts, A. R.; Dikanov, S. A. *J. Phys. Chem*. **2011**, 115, 11589–11593.
[70] Verrax, J.; Beck, R.; Dejeans, N.; Glorieux, C.; Sid, R.C. Pedrosa, B.; Benites, J.; Vásquez, D.; Valderrama, J.A.; Calderon, P.B. *Anticancer Agents Med Chem*. **2011**, 11, 213-221.
[71] Sinha, B.; Gregory, J.L. *Biochem. Pharmacol*. **1981**, 30, 2626-2629.
[72] Goormaghtigh, E.; Pollakis, G.; Ruysschaert, J.M. *Biochem. Pharmacol.* **1983**, 32, 889-893.
[73] Bachur, N.R.; Gordon, S.L.; Gee, M.V.; Kohn, H. *Proc. Natl. Acad. Sci*. USA **1979**, 76, 954-957.
[74] Muller, F.; Crofts, A. R.; Kramer, D. M. *Biochemistry.* **2002**, 41, 7866–7874.

to quinone-based compounds forming reactive semiquinone radicals which can then reduce oxygen to form reactive oxygen species (ROS), such as superoxide radicals ($O_2 \cdot^-$), and regenerate the parent molecule.[68] This pathway has been considered as operative for some natural quinones[75,76,77] but it is not the sole leading to ROS generation. Semiquinone free radical species can indeed interfere with the whole electron transport chain in the mitochondria, being either oxidized or reduced.[74] In this scenario, thiaplidiaquinone B (**12, Figure 3.4**), a cytotoxic prenylated benzoquinone isolated from the marine ascidian *Aplidium conicum*, was proved[78] to induce apoptosis in Jurkat cells due to a rapid overproduction of intracellular ROS, which mediate the collapse of the mitochondrial transmembrane potential. Kinetic experiments showed that ROS production preceded the disruption of the mitochondrial potential, and the later one paralleled the appearance of apoptotic cells.[78]

Table 3.2. Source and cytotoxic activity against cancer cell lines of the studied compounds.

Cmp	Source	IC_{50} (μM)			
		MCF-7[a]	**C6[b]**	**RBL-2H3[c]**	**Jurkat[d]**
12	*A. conicum* Capo Caccia (Italy)	NT[e]	NT	NT	3
13	*A. conicum*	NT	20.3	231.6	NT
14	*A. conicum*, Tarifa Island (Spain)	44.5	NT	NT	NT
15	*A. conicum*, Tarifa Island (Spain)	125.0	NT	NT	NT

[a] Human breast adenocarcinoma cells
[b] Rat glioma cells
[c] Rat basophilic leukaemia cells
[d] Human leukemia T Jurkat
[e] NT: not tested

[75] Inbaraj, J. J.; Gandhisan, R.; Murugesan, R. *Free Radic. Biol. Med*. **1999**, 26, 1072-1078.
[76] Benchekroun, M. N.; Myers, C. E.; Sinha, B. K. *Free Radic. Biol. Med*. **1994**, 17, 191-200.
[77] Huang, P.; Feng, L.; Oldham, E. A.; Keating, M. J.; Plunkett, W. *Nature* (London) **2000**, 407, 390-395.
[78] Aiello, A.; Fattorusso, E.; Luciano, P.; Macho, A.; Menna, M.; Muñoz, E. *J. Med. Chem.* **2005**, 48, 3410–3416.

In the present work, VMP was applied to the study of the electrochemistry of thiaplidiaquinone B[78] (**12**) as well as other cytotoxic marine-derived meroterpenes, such as conicaquinone A (**13**), conithiaquinones A and B (**14**, **15**), also isolated from *A. conicum* (**Figure 3.4**).[79,80] The methodology previously used to study several synthetic quinone analogues[81] was expanded by combining conventional solution phase and VMP approaches incorporating electrochemically generated ROS[82,83,84] and by integrating computational studies performed on the starting quinone structures, as well as, on the reduced species. Interaction with dsDNA was also monitored in order to obtain further information to be correlated with the observed effects of these natural thiazinoquinones on cells growth and viability.

3.3.1. Electrochemical studies

The voltammetric response of the studied compounds in DMSO solution was a consequence of a mainly reversible one-electron redox couple, corresponding to the quinone to semiquinone reduction, thus coinciding to the typical electrochemistry of quinones in nonaqueous electrolytes.[85] In light of the low solubility in water of these compounds, solid state electrochemistry was performed on microparticulate films of them dipped into aqueous PBS at physiological pH. **Figure 3.5** displays the negative- and positive-going scan cyclic voltammograms of **12**. Reduction peaks occur, in the initial cathodic scan (**Figure 3.5 a**), at −0.65(C_1) and −1.03 V vs. Ag/AgCl (C_2).

---

[79] Aiello, A.; Fattorusso, E.; Luciano, Menna, M.; Esposito, G.; Iuvone, T.; Pala, D. *Eur. J. Org. Chem*. **2003**, 898-900.
[80] Menna, M.; Aiello, A.; D'Aniello, F.; Imperatore, C.; Luciano, P.; Vitalone, R.; Irace, C.; Santamaria, R. *Eur. J. Org. Chem*. **2013**, 3241-3246.
[81]Imperatore, C.; Persico, M.; Aiello, A.; Luciano, P.; Guiso, M.; Sanasi, M.F.; Taramelli, D.; Parapini, S.; Cebrián-Torrejón, G.; Doménech-Carbó, A.; Fattorusso, C.; Menna, M. *RSC Adv*. **2015**, 7, 70689-70702.
[82] Yano, T.; Tryk, D.A.; Hashimoto, K.; Fujishima, A. *J. Electrochem. Soc.* **1998**, 145, 1870-1876.
[83] Marselli, B.; Garcia-Gomez, J.; Michaud, P.-A.; Rodrigo, M.A.; Comninellis, C. *J. Electrochem. Soc*. **2003**, 150, D79–D83.
[84] Kapałka, A.; Foti, G.; Comninellis, C. *Electrochim. Acta.* **2009**, 54, 2018–2023.
[85] Zuman, P.; Perrin, C.L. *Organic Polarography*, John Wiley & Sons, New York, **1969.**

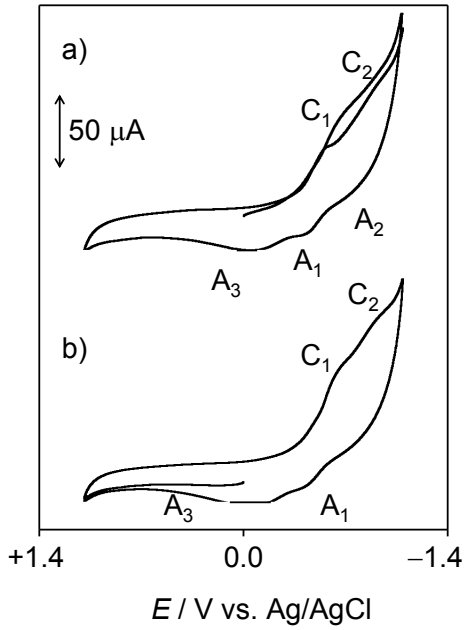

Figure 3.5. Cyclic voltammograms of **12** microparticulate films on glassy carbon electrode immersed into 0.10 M PBS at pH 7.4. Potential scan initiated at 0.0 V a) in the negative and b) in the positive directions; potential scan rate 50 mV s^{-1}.

These signals are coupled, in the consequent anodic scan, with a feeble shoulder at –0.80 (A_2) and a well-defined, although feeble, oxidation peak at –0.45 V (A_1) which goes before a wide oxidation signal at –0.04 V (A_3).This peak is not found in initial anodic scan voltammograms (**Figure 3.5 b**), thus proving that the process A_3 is due to the oxidation of any product generated in previous cathodic steps.

The voltammetry of all the studied quinones was analogous, but the potential separation and the relative height of peaks C_1 and C_2 differed considerably. This is shown in **Figure 3.6**, where semi-derivative deconvolution of the voltammetric curves was carried out in order to improve peak resolution. As can be seen in this figure, **13** and **14** exhibit peaks C_1 and C_2 of similar intensity and the peak A_1 remains well-defined. On the other hand, the peak C_1 is relatively weak in **12** and **15** and the former displays some weak signals A_1 and A_3, while the latter presents a relatively intense peak A_1 without showing peak A_3.

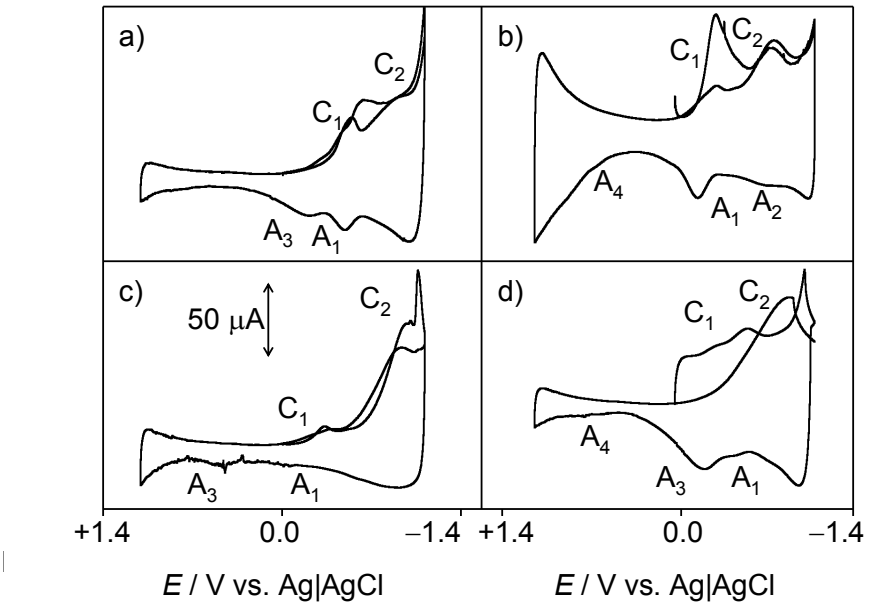

Figure 3.6. Cyclic voltammograms, after semi-derivative convolution, of a) **13;** b) **14**; c) **15**; d) **12**. microparticulate films on glassy carbon electrode immersed into 0.10 M PBS at pH 7.4. Potential scan initiated at 0.0 V a) in the negative and b) in the positive directions; potential scan rate 50 mV s^{-1}.

This voltammetry can be explaned on the basis of the precise knowledge of the electrochemistry of quinones in solution phase[86] and the Lovric and Scholz model on the electrochemistry of ion-insertion solids.[87,88,89,90,91] Considering the organic compounds in contact with aqueous electrolytes, solid state electrochemical reaction initially occurs at the solid particle/base electrode/electrolyte three-phase junction and spreads through the solid via proton insertion coupled with electron hopping between immobile redox centers in the solid.[87-91]

The reduction of quinones (Q) in aqueous solution takes place typically via two rounds of electron-transfer (E) coupled with proton acceptance (chemical reaction (C)) obtaining a quinone radical anion or semiquinone ($Q^{\bullet-}$) which is

[86] Chambers, J.Q. *Electrochemistry of quinones*. Wiley, New York, **1988.**
[87] Lovric, M.; Scholz, F. *J. Solid State Electrochem*. **1997**, 1, 108-113.
[88] Lovric, M., Hermes, M.; Scholz, F. *J. Solid State Electrochem*. **1998**, 2, 401-404.
[89] Oldham, K.B. *J. Solid State Electrochem.* **1998**, 2, 367-377.
[90] Lovric, M.; Scholz, F. *J. Solid State Electrochem*. **1999**, 3, 172-175.
[91] Schröder, U.; Oldham, K.B.; Myland, J.C.; Mahon, P.J.; Scholz, F. *J. Solid State Electrochem.* **2000**, 4, 314-324.

protonated producing a radical ($HQ^{\bullet}$) that is subsequently reduced to QH^{-}, and new protonation reaction generates the corresponding hydroquinone (QH_2) species (**Scheme 3.1**).

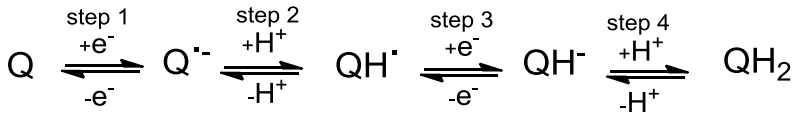

Scheme 3.1.. Reduction pathway of quinone to hydroquinone in aqueous environment.

The general reduction process can be described in terms of an ECEC mechanism which appears, depending on the pH and the buffering capacity of the electrolyte, as a unique voltammetric couple (C_1/A_1), where the cathodic wave often **(Figure 3.6 a, b)** looks like two superimposed signals.[85-86]

The comparison with the electrochemistry of synthetic thiazinoquinones[81] suggests that the above electrochemical process would be followed by the reduction of the SO_2 unit to SO at more negative potentials (C_2/A_2 couple). The peak A_3, which is depleted when the peak A_2 is well developed **(Figure 3.6 b)**, can be due to the oxidation of the reduced form resulting from the initial reduction C_1 through the NH motif. In some cases, **(Figure 3.6 b, d),** a not well defined anodic shoulder ca. +0.6 V (A_4) appears. This process can be attributed to the oxidation of the NH unit of the parent quinone.[81]

3.3.2. Interaction with ROS

In order to test the possible interaction of the studied compounds with ROS, the voltammetry of microparticulate films of the same samples in contact with air-saturated PBS was carried out. **Figure 3.7** compares the cathodic response of an unmodified glassy carbon electrode in contact with air-saturated PBS at physiological pH, with those of microparticulate films of the studied natural products on that electrode.

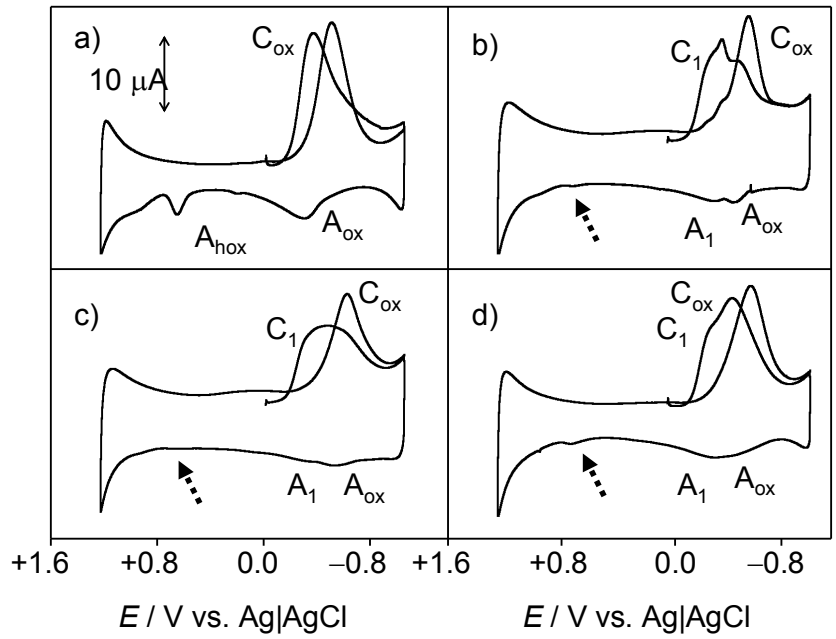

Figure 3.7. Cyclic voltammograms, after semi-derivative deconvolution, of a) unmodified glassy carbon electrode in contact with air-saturated PBS at pH 7.4 and b-d) electrode modified with b) **13**; c) **14**; d) **12**. Potential scan rate 50 mV s^{-1}.

At the unmodified glassy carbon electrode, dissolved oxygen yields a reduction wave at ca. –0.85 V (C_{ox}) which can be assigned, following literature, to the one-electron reduction of O_2 to the radical anion superoxide $O_2^{\cdot -}$ which is rapidly protonated and reduced to H_2O_2 **(Equations 3.1-3.6)**.[91,92,93,94]

Indeed, the electrochemical reduction at carbon electrodes of oxygen dissolved in aqueous electrolytes (C_{ox}) proceeds through a multistep pathway complicated by adsorption processes initiated by the one-electron reduction of O_2 to superoxide radical anion.

$$O_2 + e^- \rightarrow O_2^{\bullet -}(ads) \qquad \textbf{(3.1)}$$

[92] Nagaoka, T.; Sakai, T.; Ogura, K.; Yoshino, T. *Anal. Chem*. **1986**, 58, 1953-1955.
[93] Xu, J.; Huang, W.; McCreery, R.L. *J. Electroanal. Chem*. **1996**, 410, 235-242.
[94] Ratsgar, S.; Deng, H.; Cortés-Salazar, F.; Scanlon, M.D.; Pribil, M.; Amstutz, V.; Karyakin, A.A.; Shahrokhian, S.; Girault, H.H. *ChemElectroChem*. **2014**, 1, 59-63.

The generated radical anion undergoes protonation **(3.2)** followed by electrochemical reduction **(3.3):**

$$O_2^{\bullet -}(ads) + H_2O \rightarrow HO_2^{\bullet}(ads) + OH^- \quad \textbf{(3.2)}$$

:

$$HO_2^{\bullet}(ads) + e^- \rightarrow HO_2^- \quad \textbf{(3.3)}$$

Alternatively, it undergoes disproportionation:

$$2O_2^{\bullet -}(ads) + H_2O \rightarrow HO_2^- + O_2 + OH^- \quad \textbf{(3.4)}$$

Leading to the final generation of H_2O_2:

$$HO_2^- + H_2O \rightarrow 2HO^{\bullet} + OH^- \quad \textbf{(3.5)}$$

$$HO^{\bullet} + HO^{\bullet} \rightarrow H_2O_2 \quad \textbf{(3.6)}$$

Through this series of processes, reactive radicals $HO_2^{\bullet}$ and $HO^{\bullet}$ can be formed at the electrode surface, in agreement with literature on electrochemical generation[82-84] and redox potentials[95,96,59-60] of ROS. Accordingly, the process C_{ox} in **Figure 3.7a** corresponds to a multistep electrochemical reduction of dissolved O_2 resulting in the generation of ROS, the signals A_{ox} and A_{hox} being attributable to the oxidation of $O_2^{\bullet -}$ and $HO_2^{\bullet}$, respectively.[97]

The C_{ox} peak shows a weak anodic counterpart (A_{ox}) and is accompanied by an oxidation peak at +0.75 V (A_{hox}). At films of the natural thiazinoquinones **(Figure 3.7 b-d)**, the signals C_{ox} and A_{ox} are depleted and preceded by the first reduction process of the compound (C_1), corresponding, in PBS, to the formation of HQ·. The depletion of the signal is relatively large for **13** and **14** and much less intense for **12** and **15**. Interestingly, in the anodic scan, the oxidation peak at ca. +0.75 V (A_{hox}), appearing in the voltammograms at the

[95] Jinnouchi, R.; Anderson, A.B. *J. Phys. Chem*. **2008**, 112, 8747-8750.
[96] Anderson, A.B.; Jinnouchi, R.; Uddin, J. *J. Phys. Chem.* **2013**, 117, 41-48.
[97] Cofré, P.; Sawyer, D.T. *Anal. Chem*. **1986**, 58, 1057-1062.

unmodified glassy carbon electrode (**Figure 3.7 a**), is also considerably weakened (**Figure 3.7 b-d**).

The voltammetric features in **Figure 3.7** can be rationalized on assuming that there is another pathway operating in the oxidation of dissolved peroxide/hydroperoxide at quinone films, which competes with its electrochemical oxidation. This can be tested by means of voltammetric features for the oxidation of the hydroperoxide radical (signal A_{hox}), as illustrated in **Figure 3.8**, where the square wave voltammograms of air-saturated PBS in contact with unmodified and **14**-modified glassy carbon electrode at two different square wave frequencies, are shown. At a relatively high frequency **(Figure 3.8 a);** and at a short experimentation time, both the unmodified and **14**-modified electrode display an essentially identical signal A_{hox}, thus denoting that the generation of hydroperoxide radical occurs. When the frequency is lowered **(Figure 3.8 b)**, and the time is longer, the peak A_{hox} appears at the unmodified electrode whereas it vanishes at the **14**-modified electrode. This effect was observed with essentially identical extent for the thiazinoquinones in this study.

A rationalization of the above electrochemical features can be proposed taking into account that it has been demonstrated that several quinones modify the activity of superoxide dismutases (SOD) by undergoing equilibrium reactions with superoxide radicals.[98]

For quinones with no or short hydrophobic tails, the radical product is a semiquinone at much lower yield, likely indicating reduction of quinone by superoxide and subsequent loss of most of the semiquinone product by disproportionation.[69] In solution phase, the depletion of the peak A_{hox} at 'long' times **(Figure 3.8 b)** could be attributed to semiquinone disproportionation but, at microparticulate deposits of quinone it appears the most reasonable option to attribute the observed voltammetric features to the result of a relatively slow reaction of HQ·with the electrochemically generated hydroperoxide.

---

[98] Butler, J.; Hoey, B.M. *J. Free Radicals Biol. Med*. **1986**, 2, 77-81.

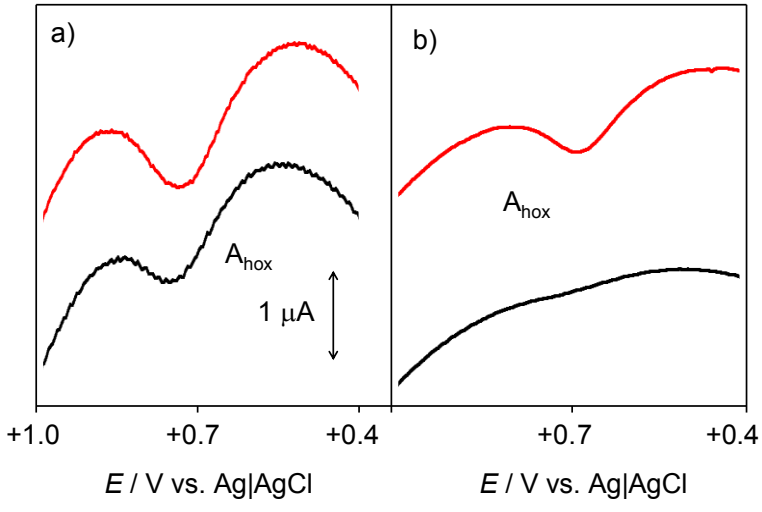

Figure 3.8. Square wave voltammograms at unmodified (red lines) and **14**-modified (black lines) glassy carbon electrode in contact with air-saturated PBS at pH 7.4. Potential scan initiated at -1.05 V in the positive direction; potential step increment 4 mV; square wave amplitude 25 mV; frequencies of a) 5 and b) 50 Hz. Only the region of potentials around the peak A_{ox} is depicted.

Experiments in DMSO solution, also representative of the interaction of the studied products with oxygen and ROS, were used to complement the above scenario.

Figure 3.9 compares the voltammograms of dissolved oxygen in 0.10 M Bu_4NPF_6/DMSO solutions (**Figure 3.9a**), **12** in the same electrolyte previously deoxygenated (**Figure 3.9b**) and air-saturated solutions of **14** (**Figure 3.9c**) and **15 (Figure 3.9d)**. As it is well-known, the electrochemical reduction of dissolved oxygen in aprotic solvents occurs reversibly at potentials ca. –0.9 V (**Figure 3.9 a, C_O/A_O couple**) yielding superoxide radical anion. In the absence of oxygen, the studied quinones produce an essentially reversible one-electron reduction (C_{Q1}/A_{Q1}) to the corresponding semiquinone at ca. –0.75 V followed by a second one-electron reduction at ca. –1.5 V (C_{Q2}/A_{Q2}). Voltammograms of air-saturated DMSO solutions of such compounds consist of superimposed signals for O_2 and Q reduction but remarkably, in the anodic scan the anodic signal A_{Q1} is entirely or almost entirely depleted after passing the peak A_O

which remains essentially unaltered, while the couple C_{Q2}/A_{Q2} is also decreased.

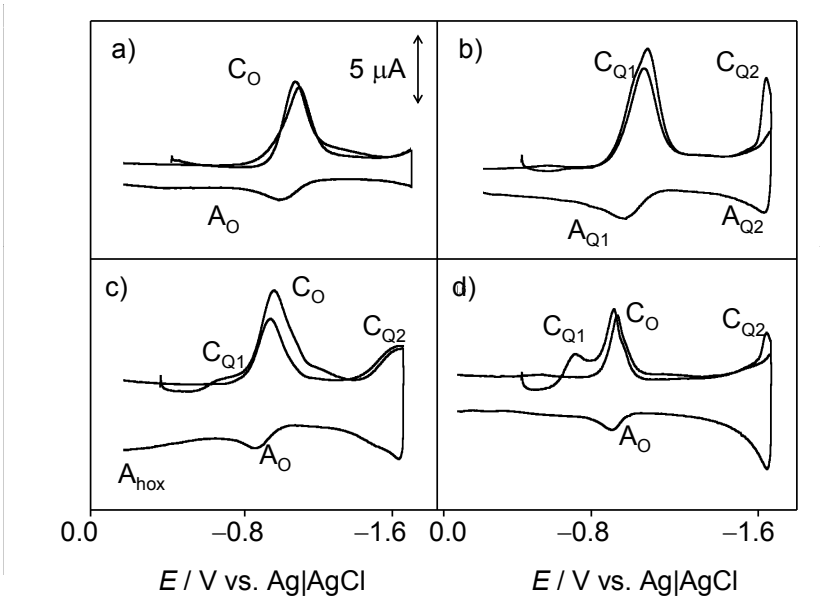

Figure 3.9. Cyclic voltammograms at glassy carbon electrode, after semi-derivative convolution, of different 0.10 M Bu_4NPF_6/DMSO solutions. a) air-saturated electrolyte solution; b) 0.5 mM **12** in deoxygenated electrolyte; c) air-saturated 0.5 mM **14**; d) air-saturated **15**. Potential scan rate mV s^{-1}.

The depletion of the peak A_{Q1} and the C_{Q2}/A_{Q2} couple in the voltammograms of air-saturated thiazinoquinone solutions can be considered as indicative of the occurrence of a relatively fast reaction between dissolved oxygen and the semiquinone radical anion electrochemically generated. The large separation between the two one-electron reduction processes of the thiazinoquinones (**Figure 3.9 b**), in sharp contrast with the signal merging recorded in aqueous media (**Figure 3.5**), denotes that there is no significant disproportionation of the intermediate semiquinone radical anion and there is no interaction of $Q^{\bullet-}$ with the superoxide anion.

Thus, while the voltammetry of microparticulate films of the studied quinones in contact with air-saturated PBS revealed the reduction of the protonated semiquinone radicals by the superoxide radical anion, in air-saturated DMSO

solution, on the contrary, the semiquinone radical anions are oxidized by oxygen.

This difference can be assessed by performing additional experiments in water-containing DMSO solution. This can be seen in **Figure 3.10** for **12** (in **Figure 3.10** compound **13** is reported). In anhydrous DMSO in the absence **(Figure 3.10a)** of dissolved O_2, the voltammetric response is identical to all other thazinoquinones in this study, with well separated couples C_{Q1}/A_{Q1} and C_{Q2}/A_{Q2}. In air saturated DMSO containing a small concentration of water (**Figure 3.10 b**), an additional couple (C_{QH}/A_{QH}) is recorded, corresponding to the overall reduction to hydroquinone, appearing as a unique voltammetric couple in presence of water, that is, when the protonated semiquinone species can be formed (**Figure 3.6**). This new couple is placed at ca. 250 mV more negative potential than the C_{Q1}/A_{Q1} couple corresponding to the reversible formation of $Q^{\bullet-}$. This new couple can be attributed to the reversible one-electron reduction of the protonated semiquinone resulting from the fast protonation of the semiquinone radical anion produced in the cathodic step C_{Q1}. Consistently with this interpretation, even in a medium such as DMSO having high radical scavenging ability[69] a weak anodic signal (A_{hox}) attributable to the formation of some radical hydroperoxide as a result of the presence of residual water, was recorded at the unmodified electrode (**Figure 3.10c**). Again, this signal vanishes more or less intensively in the presence of thiazinoquinones, now in the solution phase (**Figure 3.10b**).

In summary, the results of these voltammetric studies suggest that all the considered natural thiazinoquinones are able to form the semiquinone radical species and that this latter, depending on its protonation state, can be reduced or oxidized in presence of redox-active compounds, such as, in the case of these experiments, O_2 and ROS**.**

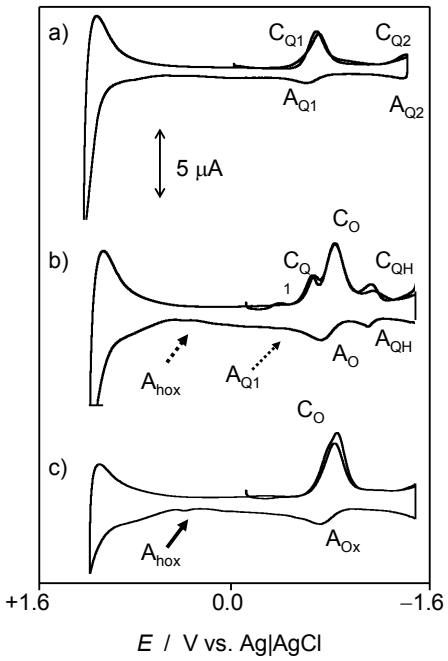

Figure 3.10. Cyclic voltammograms at glassy carbon electrode, after semi-derivative convolution, of different 0.10 M Bu_4NPF_6/DMSO solutions. a) 0.5 mM **13** b) air-saturated 0.5 mM **13** + 0.5 mM water; c) air saturated 0.10 M Bu_4NPF_6/DMSO + 0.5 mM water. Potential scan rate mV s^{-1}.

3.3.3. Interaction with dsDNA

The interaction between the thiazinoquinones and salmon testes dsDNA was studied in DMSO solution. **Figure 3.11** compares the cyclic voltammograms of a) **13**; b) **14**; c) **15**; d) **12** plus dsDNA solutions. Under these experimental conditions, dsDNA remained electrochemically silent. However, the voltammetry of the thiazinoquinones experienced significant modifications relative to the previously observed response (**Figure 3.10**). Thus, the C_{Q1}/A_{Q1} couple showed peak splitting and weakening of the anodic signal. The new cathodic signal (C_{QA}), whose anodic counterpart (A_{QA}) is almost entirely absent, can be attributed to the quinone-localized reduction of the dsDNA-thiazinoquinone complex, a feature parallel to that observed for canthin-6-one

alkaloid-modified electrodes,[99] which can be considered as indicative of the existence of a strong interaction between the thiazinoquinones and dsDNA. The weakness of the anodic signal A_{QA} would be the result of secondary post-electron transfer reactions.

The voltammograms, however, display a weak couple at less negative potentials (C_{QB}/A_{QB}) whose intensity appears to be larger for the compounds displaying the lower C_{QA}/A_{QA} signals. The new couple can be attributed to the reduction of a thiazinoquinone-dsDNA complex different from that responsible of the C_{QA}/A_{QA} couple, so that the overall voltammetric pattern can be described in terms of a square scheme such as depicted in **Figure 3.12**. Assuming reversibility, the aforementioned electron transfer processes would be coupled with the complexation equilibria between the oxidized (quinone) and reduced (semiquinone radical anion) forms of the thiazinoquinone with two binding sites (A and B) of dsDNA.

In this kind of systems, the equilibrium constants for the interaction with the oxidized (K_J^{ox}) and reduced (K_J^{rd}) forms (J=A,B) can be related with the shift of the equilibrium potential of the C_{QJ}/A_{QJ} couple relative to the equilibrium potential of the unbounded thiazinoquinone (C_{Q1}/A_{Q1}) by means of the following relationship (**Equation 3.7**):

$$E_{QJ}^{eq} = E_{Q1}^{eq} + \frac{RT}{nF}\ln\left(\frac{K_{QJ}^{rd}}{K_{QJ}^{ox}}\right) \quad \textbf{(3.7)}$$

Our data indicate that the semiquinone radical anion form is much more stabilized, relative to the quinone, when the interaction occurs in the site B than when the interaction occurs via the site A.

Using equimolar concentrations of thiazinoquinone and dsDNA, the height of the peaks C_{QJ} relative to the peak C_{Q1} **(Figure 3.11**) would be indicative of the intensity of the respective quinone-dsDNA interaction via the J-site. Our data

[99] Doménech-Carbó, A.; Cebrián-Torrejón, G.; De Miguel, L.; Tordera, V.; Rodrigues, D.; Assad-Kahn, S.; Fournet, A.; Figadère, B.; Vázquez, R.; Popuon, E. *Electrochim. Acta.* **2014**, 115, 546-552.

indicate that, under our experimental conditions, the intensity of the thiazinoquinone-dsDNA binding in the A-site decreases in the order **12**> **14** > **13** ≈ **15**, whereas the intensity of the thiazinoquinone-dsDNA binding in the B-site decreases just in the inverse order.

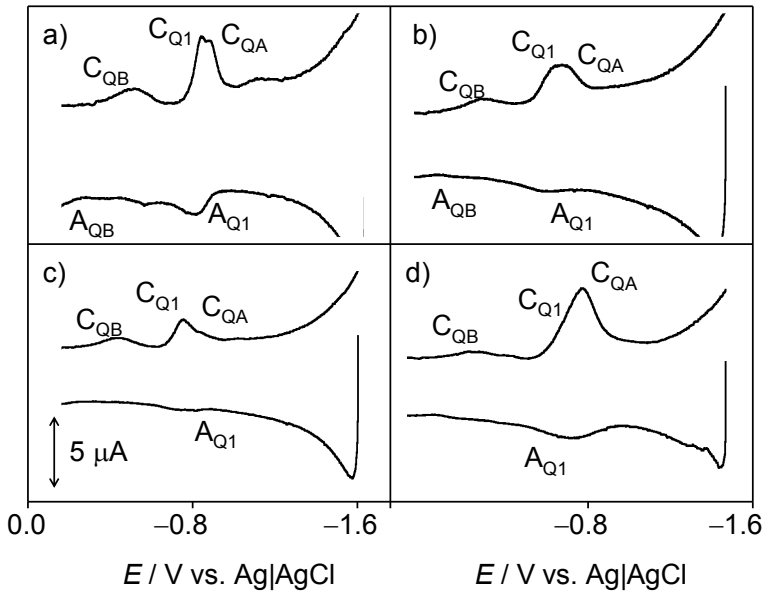

Figure 3.11. Cyclic voltammograms at glassy carbon electrode, after semi-derivative convolution, of different 0.2 mM dsDNA (salmon testes) plus 0.3 mM thiazinoquinone solutions in 0.10 M Bu_4NPF_6/DMSO. a) **13**; b) **14**; c) **15**; d) **12**. Potential scan rate mV s^{-1}.

This feature is in agreement with the competing effect exerted by the two sites for the interaction with thiazinoquinones (**Figure 3.12**). Interestingly, the relative order of A-site interaction of the conithiaquinones: **14** > **15**, is in agreement with the relative cytotoxic ability with respect to human breast adenocarcinoma cells (MCF-7 line).[80] This feature suggests a relation between the interaction with the binding site A and the cytotoxic activity of this family of compounds.

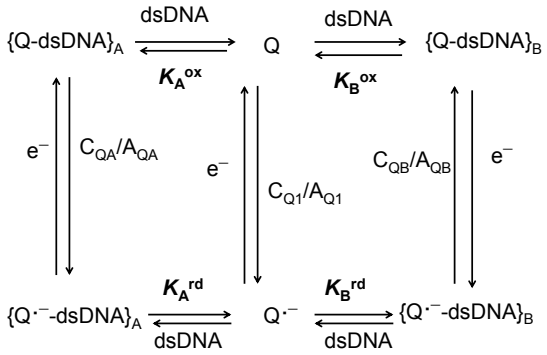

Figure 3.12 Square scheme for the electrochemistry of DMSO solutions of dsDNA plus the studied natural thiazinoquinones.

3.3.4. Computational Studies

Computational studies were performed on the molecular models of compounds **12-15** (**Figure 3.4**) by using a combination of molecular dynamics (MD) and mechanic (MM) calculations with quantum-mechanical (QM) methods (PM7 and DFT) (see the experimental section for details).

The conformational and electronic properties of the compounds were investigated taking into account the reduction pathway of quinones (**Q**) to hydroquinones (**QH_2**) in aqueous systems**.** This involves a sequence of steps in which reversible one-electron reduction reactions are followed by proton uptake reactions producing different intermediate species, as illustrated in **Scheme 3.1**. In the case of the natural thiazinoquinones **12-15**, two possible protonated semiquinone radicals can be produced, named **$QH^{\bullet}_{i}$**, **$QH^{\bullet}_{ii}$**, respectively (**Figure 3.13**).

Firstly, the conformational space of the starting neutral quinone species was sampled by applying a procedure including molecular dynamics (simulated annealing; SA), molecular mechanic (MM), and PM7 calculations. Obtained conformers were grouped into conformational families and ranked by their potential energy values.

Secondly, the lowest energy conformer of each family was selected to be subjected to DFT full optimization. Finally, the DFT global minimum (GM) conformer of each compound was used to generate the reduced species **$Q^{\bullet-}$**,

QH$^{\bullet}_{i}$, **QH$^{\bullet}_{ii}$**, **QH$^{-}_{i}$**, **QH$^{-}_{ii}$**, and **QH_2,** which were again subjected to DFT full optimization (**Figure 3.14**).

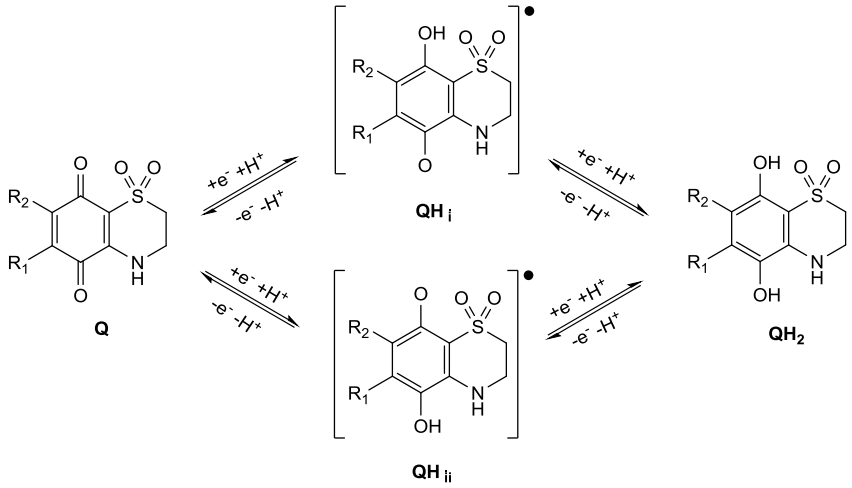

Figure 3.13. Schematic representation of the formation of the two possible protonated semiquinones radicals in the reduction pathway of natural thiazinoquinones.

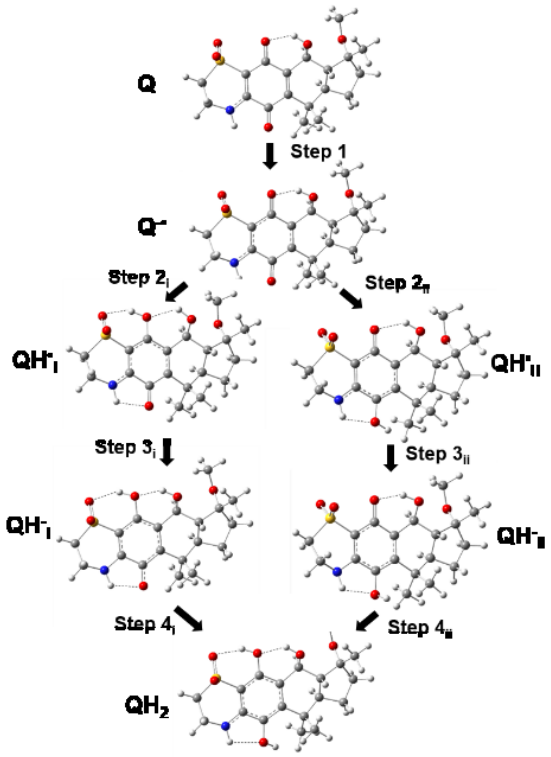

Figure 3.14. $Q^{\bullet -}$, QH$^{\bullet}_{i}$, QH$^{\bullet}_{ii}$, QH$_i^-$, QH$_{ii}^-$, and QH_2 species of **14** obtained from DFT calculations.

Table 3.3 Reaction energy values (**Δ*E*;** kcal/mol) calculated for the proposed reduction pathway **(Scheme 3.1)** considering the formation of the two possible semiquinone species.

Cmp	(Q→QH$_2$)	Step 1	Step 2$_i$	Step 2$_{ii}$	Step 3$_i$	Step 3$_{ii}$	Step 4$_i$	Step 4$_{ii}$
12	-773.6	-60.0	-326.4	-310.2	-54.8	-60.7	-332.4	-342.7
13	-762.6	-50.4	-330.5	-313.2	-44.8	-56.4	-336.9	-342.6
14	-769.4	-60.6	-323.2	-307.5	-53.0	-62.2	-332.6	-339.1
15	-768.4	-53.0	-330.3	-313.6	-48.2	-55.1	-336.9	-346.7

This allowed the calculation of the reaction energies (E_f(Prod.) – E_f(React.)) of each step of the reduction pathway reported in **Scheme 3.1**. Due to the formation of the two possible semiquinone species **QH$^{\bullet}_i$** and **QH$^{\bullet}_{ii}$** (**Figure 3.13**), two different set of reaction steps were calculated for the reduction from **Q** to **QH$_2$** (**Table 3.3; Figure 3.14**).

The first consideration that can be derived is that all compounds present a definite preference for the formation of one of the two possible semiquinone species, namely **QH$^{\bullet}_i$**. **(Step 2$_i$ vs Step 2$_{ii}$; Table 3.3)**. This is likely due to the formation of a hydrogen bond between the SO_2 group and the newly generated hydroxyl group of **QH$^{\bullet}_i$**, which cannot be formed in the alternative **QH$^{\bullet}_{ii}$** semiquinone (**Figures 3.13 and 3.14**).

Regarding the relative compound potency in biological assays **(Table 3.2)**, it has to be underlined that, since **12** and **13** were tested on different cancer cell lines, only **14** and **15** (tested on MCF-7 cells) can be directly compared.[78-80] In this view, the rank order of the calculated reaction energies reported in **Table 3.3** for the whole reduction pathway (**Q→QH$_2$**) reflects the activity order of the compounds (**Table 3.2**). Then, considering each reaction step (**Scheme 3.1; Figure 3.13 and 3.14**), the more active compound **14** shows higher propensity to acquire both the first and the second electron (Step 1 and 3, respectively) with respect to **15** (**Table 3.3; Figures 3.4 and 3.5**). On the contrary, the two protonation steps **(Step 2 and Step 4)** present more favorable reaction energies for **15** with respect to **14**. In any case, according to the data reported in **Table 3.3**, either the formation of the semiquinone species **QH$^{\bullet}_i$**, either its subsequent

reduction to hydroquinone is more favored for **14** (more active) with respect to **15** (less active).

It is noteworthy that the larger contribute to the overall reaction energy comes from the protonation steps and this is in agreement with the role played by semiquinone radical anion protonation on quinone reduction, as evidenced by our electrochemical studies. Actually, many variables can affect the protonation rate of the reduced species, which can significantly differ in a cellular environment.

To further investigate the reactivity of the studied quinones and their semiquinone radical species, we calculated the vertical electron affinity (EA) of **Q** and $\mathbf{QH^{\bullet}_i}$ and the ionization potential (IP) of $\mathbf{Q^{\bullet-}}$ and $\mathbf{QH^{\bullet}_i}$. The vertical *EA* measures the propensity of a molecule to acquire one electron without considering subsequent electronic and/or structural rearrangements which may drive the structure to a lower energy minimum (see the experimental section for details). At the same conditions, the vertical IP measures the propensity of a molecule to lose one electron. The resulting *EA* and *IP* values are reported in **Table 3.4**, together with the energy of the frontier orbitals of i) the neutral quinone **Q** (LUMO), ii) the radical anion $\mathbf{Q^{\bullet-}}$ (SOMO), and iii) the radical semiquinone $\mathbf{QH^{\bullet}_i}$ (SOMO).

Table 3.4 Calculated energy values (kcal/mol) of LUMO and SOMO orbitals, Vertical *IP* and vertical *EA* of the Q, Q•-, and QH•i species of natural thiazinoquinones.

Cmp	**Q**			**$Q^{\bullet-}$**		**$QH^{\bullet}_i$**		
	E_{LUMO}	Vertical EA	ω	E_{SOMO}	Vertical IP	E_{SOMO}	Vertical IP	Vertical EA
12	-86.383	15.35	127.99	-34.074	66.8	-121.47	151.7	49.4
13	-80.083	24.82	93.77	-21.517	56.8	-115.93	151.5	39.2
14	-89.452	30.00	111.81	-32.442	69.2	-127.72	164.8	46.2
15	-81.401	22.52	93.85	-24.950	60.9	-121.88	158.2	41.2

The higher vertical *EA* and lower E_{LUMO} energy of **14** with respect to **15**, as well as, the higher vertical *IP* and lower E_{SOMO} of its $\mathbf{Q^{\bullet-}}$ and $\mathbf{QH^{\bullet}_i}$ radicals (**Table 3.4**), is in agreement with its lower reaction energy to form the semiquinone species (**Table 3.3**). Moreover, the higher propensity of **12,** characterized by an IC_{50} of 3 μM on Jurkat cells (**Table 3.2**), to acquire, both, the first and the second electron (**Step 1 and 3, respectively; Scheme 3.1; Table 3.3**), agrees with i) the LUMO orbital energy of its **Q** form, and ii) the SOMO orbital energy and the vertical *IP* of its $\mathbf{Q^{\bullet-}}$ form (**Table 3.4**). By contrast, some considerations can be made comparing the relatively low vertical *EA* of the neutral quinone form of **12** (**Table 3.4**) to the calculated reaction energy for its one electron reduction **(Step 1, Table 3.3)**. Indeed, contrarily to the vertical *EA*, the reaction energy takes in to account possible structural rearrangements after electron acquisition, by consequence, the results obtained for **12** revealed that the stability of its $\mathbf{Q^{\bullet-}}$ radical anion strongly depends on the ability to extend the electronic conjugation to the extra aromatic ring, as well as, the conformation of the long unsaturated alkyl chain (**Figure 3.6**).

Interestingly, the values reported in **Table 3.4** also indicate that the protonated semiquinone radicals of all compounds ($\mathbf{QH^{\bullet}_i}$) are characterized by a marked vertical *EA*, significantly higher than the one of the corresponding parent quinone **Q**, following the same rank order of the relative activity of the compounds. This can account for their propensity to be reduced by superoxide anions, as resulted from electrochemical studies.

Finally, we calculated the electrophilicity index[100] of all compounds (***ω*; Table 3.4**) as a measure of their propensity to undergo a nucleophilic attack by biological molecules (DNA, protein, etc.). Interestingly, the resulting values resulted to be correlated to the intensity of the thiazinoquinone-dsDNA binding in the A-site calculated from voltammetric data.

---

[100] Parr, R.G.; Szentplay, L.V.; Liu, S. J. *Am. Chem. Soc.* **1999**, 121, 1922-1924.

3.4. Conclusions

In conclusion, the extraction and the chemical analysis of *Phallusia fumigata* led to the isolation of the phallusiasterol C (**6**), a sulfated sterol, which is a possible modulator of the PXR nuclear receptor. Additionally, the electrochemical response of four natural cytotoxic thiazinoquinones (**12-15**), which were previously isolated and characterized from *Aplidium* species, has been investigated. The structural diversity of the metabolites, above reported, highlighted the fact that marine organisms continue to be satisfying sources of chemodiversity, associated with a very large array of pharmacological activities. These products provide a rich source of chemical diversity that can be used to design and develop new potentially useful therapeutic agents.

CHAPTER 4

THE STEREOCHEMISTRY ASSIGNMENT: A GREAT CHALLENGE IN NATURAL PRODUCTS CHEMISTRY

4.1. Introduction

Molecular shape, symmetry and stereogenicity/chirality are the key concepts in natural products research. In the majority of cases, the planar structure elucidation is just the initial step for studying a natural product and many of its important aspects, e.g. the spectroscopic properties and reactivity, as well as the structure-activity relationship or protein-ligand interactions. The latter can only be studied after the structure of a compound, including the stereochemical configurations, has been well determined.[101] Additionally, the bioactive natural product's information, either used for structure-activity relationships or for retrosynthetic design for total synthesis, is precisely represented by its 3D structure.

Generally, NMR, X-ray, synthetic approaches or chiroptical methods, the stereochemistry of natural products. However, in comparison to synthetic organic molecules, the stereochemical elucidation of natural products is significantly more impressive. In most cases, the number of available samples, which were isolated from an uncommon source or from species difficult to collect, is not sufficient. Moreover, while the absolute configuration of synthetic compounds can derive from the chiral educts stereo-information, nothing is known about the natural products configuration, unless related to other previously isolated and structurally related natural metabolites.[102,103,104,105]

The determination of the relative configuration of the stereogenic centers, that in turn determines the conformational properties, is usually the starting point of

---

[101] Mori, K. *Chirality* **2011**, 23, 449–462.
[102] Molinski, T. F. *Nat. Prod. Rep*. **2010**, 27, 321–329.
[103] Halabalaki, M.; Vougogiannopoulou, K.; Mikros, E.; Skaltsounis, A. L. *Curr. Opin. Biotechnol*. **2014**, 25, 1–7.
[104] L.i, K.; Chung-Davidson, Y.; Bussy, U.; Li, W. *Mar. Drugs.* **2015**, 13, 2694-2713.
[105] Allenmark, S. G. *Nat. Prod. Rep.* **2000**, 17, 145–155.

the complete stereochemical assignment, including the absolute configuration of all the stereocenters. Many techniques and approaches have been developed and are nowadays available. Unfortunately, some of them are not always useful in natural products research; for example, X-ray structure determination leads to valid assignment in the case of samples forming suitable crystals. While for the over expressed biomacromolecules or synthetic compounds, this can be easily achieved, for a natural product it can be difficult, that is, an unusual chemical entity, could derive from an uncommon marine organism found in very small amont. The best solution regarding the stereochemical problem, would be the synthesis of all the possible stereoisomers for comparison of spectroscopic data. From a practical standpoint, this task is neither easily obtained nor necessary. The synthesis of 'key' segments for comparison, sometimes may help the stereostructure determination; usually, chemical degradations of the original metabolite to more simple compounds, which are more suitable to synthesis and/or spectroscopic analysis, are required, thus achieving microscale chemical transformations. NMR and CD based methods, assisted by empirical quantum mechanical prediction and/or chemical derivatization, became popular tools for stereochemistry analysis of natural products.[106]

It should be kept in mind, that none of these techniques is predominant in the configuration assignments, however, each of them have their respective goals and limitations. Even today, when planar structures can be determined with microgram samples of molecules available, the stereochemistry assignment is still a great challenge for chemists and, sometimes, the proposed planar structure is completed years later. In fact, regardless of the compound contains only one or several stereocenters, natural products absolute stereostructures are solved on a case-by-case basis.

---

[106] Petrovic, A. G.; Navarro-Vázquez, A.; Alonso-Gómez, J. L. *Curr. Org. Chem*. **2010**, 14, 1612-1628.

Sometimes we could not assign the stereochemistry of a new compound exclusively on the basis of classic methods, therefore we had to refer to other techniques that I am describing in this chapter.

The following section talks about the problem of stereochemistry elucidation of acyclic scaffolds that I have been dealing with during my research. This problem is an important challenge in natural products chemistry and often, integrated approaches are needed, which require a number of rigorously acquired data obtained by combination of different tools, including chemical manipulation of the original molecule and organic synthesis.[107] Databases of spectral information can be a great resource for stereostructure determination, too. For example, Kishi and coworkers, on the basis of their extensive experience on polyketides chemistry and synthesis, developed an NMR database of several motifs common to this natural products family. This data collection, known as the "universal NMR database (UDB)", allowed simplified protocols to be used for the relative and absolute configuration assignment of unknown polyketides without degradation and/or derivatization work.[108,109,110,111]

4.2. Assignment of the Complete Stereochemistry of Phosphoeleganin

Phosphoeleganin (**16, Figure 4.1**), a new phosphorylated polyketide, having a protein tyrosine phosphatase 1B (PTP1B) inhibitory activity, has been recently isolated from the Mediterranean ascidian *Sidnyum elegans*.[112] By combination of spectroscopic analysis and microscale chemical degradation and/or derivatization, the stereostructure of this marine natural product has been established except for the absolute configuration of the carbinolic centers C11 and C12. This provided two alternative stereostructures for the natural

---

[107] Kobayashi; Y.; Lee, J.; Tezuka, K.; Kishi, Y. *Org. Lett*. **1999**, 1, 2181-2184.
[108] Molinski, T. F.; Morinaka, B. I. *Tetrahedron*.**2012**, 68, 9307-91628.
[109]Kobayashi, Y.; Tan, C.-H.; Kishi, Y. *J. Am. Chem. Soc.* **2001**, 123, 2076-2078.
[110] Kishi, Y. *Tetrahedron,***2002**, 58, 6239-6258.
[111] Higashibayashi, S.; Kishi, Y. *Tetrahedron* **2004**, 60, 11977-11982
[112] Imperatore, C.; Luciano, P.; Aiello, A.; Vitalone, R.; Irace, C.; Santamaria, R.; Li, J.; Guo, Y.-W.; Menna, M. *J. Nat. Prod*. **2016**, 79, 1144–1148

metabolite (**Figure 4.1**) corresponding to the 8*S*, 11*S*, 12*R*, 15*S*, 16*R* and 8*S*, 11*R*, 12*S*, 15*S*, 16*R* configuration patterns. Therefore, my research was focused on absolute stereochemistry of C11/C12 determination, which led to the univocal 8*S*, 11*S*, 12*R*, 15*S*, 16*R* stereochemical assignment of phosphoeleganin, performed by combination of organic synthesis and chiral derivatization methods directed to the application of UDB concept. Indeed, the logic used in the universal NMR database approach is that, given a complex molecule composed of structural clusters of stereogenic centers connected with a number of methylene bridges, we can assume that (1) the structural properties of these clusters are inherent to the specific stereochemical arrangement of the (small) substituents on the carbon backbone and (2) the structural properties of these clusters are independent from the rest of molecule, when they are sufficiently separated from each other.[109] In practice, the stereogenic subunits need only to be separated by two or more methylene groups so that they may be treated independently.

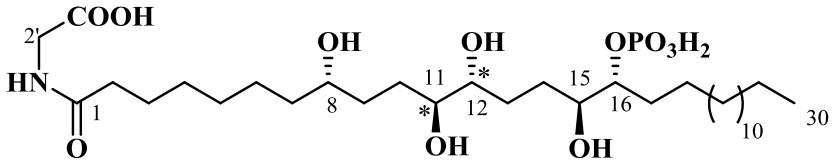

16

Figure 4.1. Structure of phosphoeleganin **(16)**

On this basis, we considered the C8-C12 stereocluster of phosphoeleganin, in which the *S* absolute configuration at C8 and the C11, C12-*erythro* relationship had been previously assigned.[112] It was decided to compare the NMR chemical shifts of this stereocluster with those of synthetic compounds with known stereochemistry. We did not find any suitable model compound for comparison in the Kishi's universal NMR database; therefore, we decided to prepare the four 8,9-*erythro* stereoisomers of 5,8,9-tetradecanetriol for this purpose. (**Scheme 4.1**).

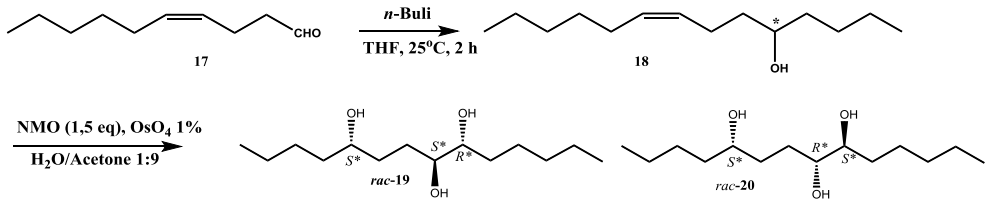

Scheme 4.1. Synthesis of the four 8,9-*erythro* stereoisomers of 5,8,9-tetradecanetriol

The *cis*-4-decenal (**17**) was converted to the (*Z*)-tetradec-8-en-5-ol (racemate) **18** by coupling with *n*-BuLi and, then, treated with NMO and OsO_4 1% to give a mixture of the four 8,9-*erythro* stereoisomers of 5,8,9-tetradecanetriol (*rac*-**19** and *rac*-**20**).

Separation by reverse phase HPLC (Luna C18 MeOH/H_2O 7:3) of the reaction mixture afforded two diastereoisomeric fractions (*rac*-**19** and *rac*-**20**) as racemates. Both *rac*-**19** and *rac*-**20** were separately derivatized with three equivalents of (*R*)-methoxyphenylacetic acid (*R*-MPA) to afford, in each case, a diastereoisomeric mixture of tris-(*R*)-MPA esters, **21**/**22** and **23**/**24**, respectively (**Scheme 4.2**).

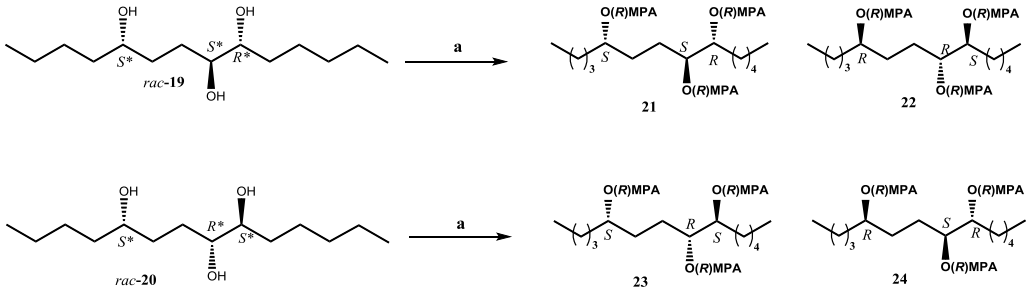

Scheme 4.2. Synthesis of the two diastereomers mixtures of triesters **21**/**22** and **23**/**24**. a) EDC, DMAP, (*R*)-MPA, CH_2Cl_2, r.t. overnight.

The four (*R*)-MPA derivatives were obtained as individual compounds by HPLC separation on silica gel column (hexane/EtOAc 85:15) and their ^1H NMR spectra were registered. According to the approach proposed by Riguera group for the assignment of the relative configuration of acyclic sec/sec-1,*n*-

diols by double derivatization,[113,114] the chemical shift differences (Δδ) in the couples **21**/**22** and **23**/**24** were calculated. It is to be noted that in our case it was not necessary to prepare the two (*R* and *S*) tris-MPA esters since the (*S*)-MPA derivatives of **21** and **23** would be enantiomeric to the (*R*)-MPA derivatives of **22** and **24**, respectively, and, consequently, their NMR chemical shifts would be identical. Δδ values calculation led to negative (or positive) Δδ (δH_{21}-δH_{22} or δH_{22}-δH_{21}) values for C1- C5 protons and positive (or negative) Δδ values for C8-C14 protons in the **21**/**22** couple (**Figure 4.2.a**); on the contrary, all positive (or negative) Δδ (δH_{23}-δH_{24} or δH_{24}-δH_{23}) values were obtained for C5- C8 protons in the **23**/**24** couple (**Figure 4.2.b**). Finally, comparison of the signs distribution in our couples with the trends noted by Riguera in every isomer of acyclic sec/sec-1,4-diols[115] suggested a 5,8-*anti*, 8,9-*anti* configuration in the **21**/**22** couple and a 5,8-*syn*, 8,9-*anti* configuration in the **23**/**24** couple.

a)

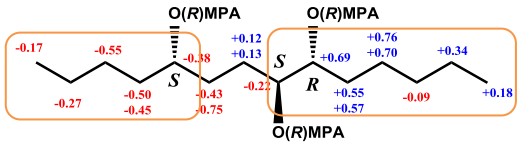

$\Delta\delta_{21/22} = \delta_{H21} - \delta_{H22}$ **or** $\delta_{H22} - \delta_{H21}$; **R** = (*R*)-MPA

b)

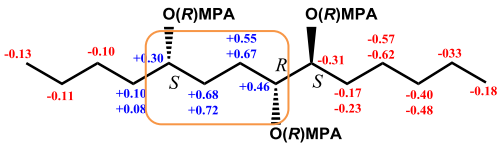

$\Delta\delta_{23/24} = \delta_{H23} - \delta_{H24}$ **or** $\delta_{H24} - \delta_{H23}$; **R** = (*R*)-MPA

Figure 4.2. Δδ signs distribution for the MPA esters of the couple **21**/**22** (a) and **23**/**24** (b)

Actually, as depicted in **Figure 4.2**, the patterns in the Δδ values sign distribution were not perfectly homogeneous, especially in the couple **21**/**22**

---

[113] Freire, F.; Manuel, J.; Quin˜oa´, E.; Riguera, R. *J. Org. Chem*. **2005**, 70, 3778-3790.
[114] Seco, J.M.; Riguera, R. *eMagRes*. **2015**, 4, 1–30.

where anomalies were detected for the protons whose signals are diagnostic. Combined shielding/deshielding effects of the MPA units enough close to each other possibly produce these anomalies, and increase the uncertainty degree in the stereochemical assignment.[115]

Therefore, we considered to substantiate the (5*S**,8*S**,9*R**) and the (5*S**,8*R**,9*S**) relative configuration assignments in compounds **21**/**22** and **23**/**24**, respectively, by chemical means.

To this purpose, we used a one-pot method[116] to perform the stereoselective synthesis of tetrahydrofuran rings via the intermediary of cyclic ortho esters (**19a** and **20a**) generated in situ from the enantiomerically pure tetradecane-5,8,9-triols **19** and **20**, derived from base-catalysed methanolysis of the *tris*-(*R*)-MPA esters **21** and **23 (Scheme 4.3)**.

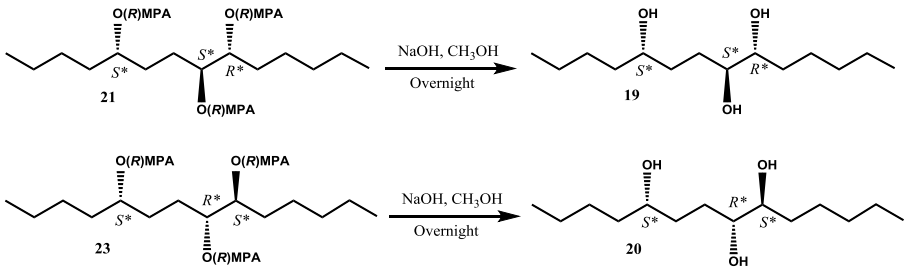

Scheme 4.3. Base-catalysed hydrolysis of compounds **21** and **23**.

Treatment of **19** and **20** with trimethyl orthoacetate and 10 mol % PPTS followed by addition of catalytic $BF_3 \bullet Et_2O$, led to cyclization of the triols to provide excellent yields of **25** and **26**.

The ionization of the intermediate ortho ester, with a Lewis acid, led to a reactive acetoxonium species (**19b**). The reaction proceeded via exo cyclization of the reactive acetoxonium intermediate (**19b**), thereby inverting the configuration at C8.

---

[115] Seco J. M.; Quiñoá, E.; Riguera, R. *Chem. Rev*. **2012**, 112, 4603−4641.

[116] Zheng, T.; Narayan, R. S.; Schomaker, J. M.; Borhan, B. *J. Am. Chem. Soc*. **2005**, 9 VOL. 127, NO. 19, 6947

A *trans* and *cis* relationship across the THF rings in compounds **25** and **26**, respectively, was then established by ROESY experiments. Particularly, strong dipolar couplings were observed between H5 and H8 in compound **26** whereas we did not detect any ROE correlation between these two protons for compound **25** (**Figure 4.3**).

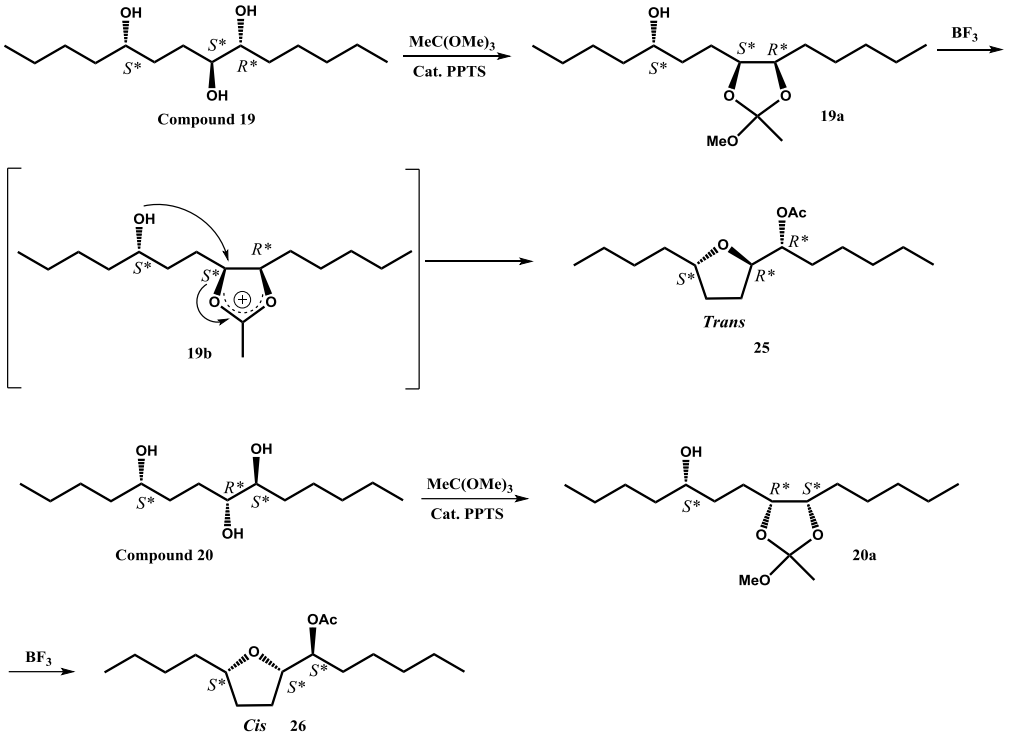

Scheme 4.4. Preparation and stereoselective cyclization of tetradecane-5,8,9-triols **19** and **20**

These results, combined with the stereoselective outcome of the cyclization reaction where the configuration at C8 is inverted, were in agreement with an *anti-anti* relative configuration in compound **19** and a *syn-anti* relative configuration in compound **20**. Thus, the (5*S**,8*S**,9*R**)- and the (5*S**,8*R**,9*S**)- relative configurations were definitely assigned to the tetradecane-5,8,9-triols **19** and **20**, respectively. The chemical characterization of compounds *rac*-**19,** *rac*-**20, 25** and **26** was easily performed through spectral analysis and the data were reported in **Table 4.1** and **Table 4.2.**

Finally, the NMR data of the tetradecane-5,8,9-triols **19** and **20** were compared to those of the natural phosphoeleganin (**16**). This analysis evidenced that proton and carbon NMR resonances of **16** matched with those of

(5*S**,8*S**,9*R**) tetradecane-5,8,9-triol (**19**) suggesting an 8,11-*anti* relative configuration in **16** (**Figure 4.4**).

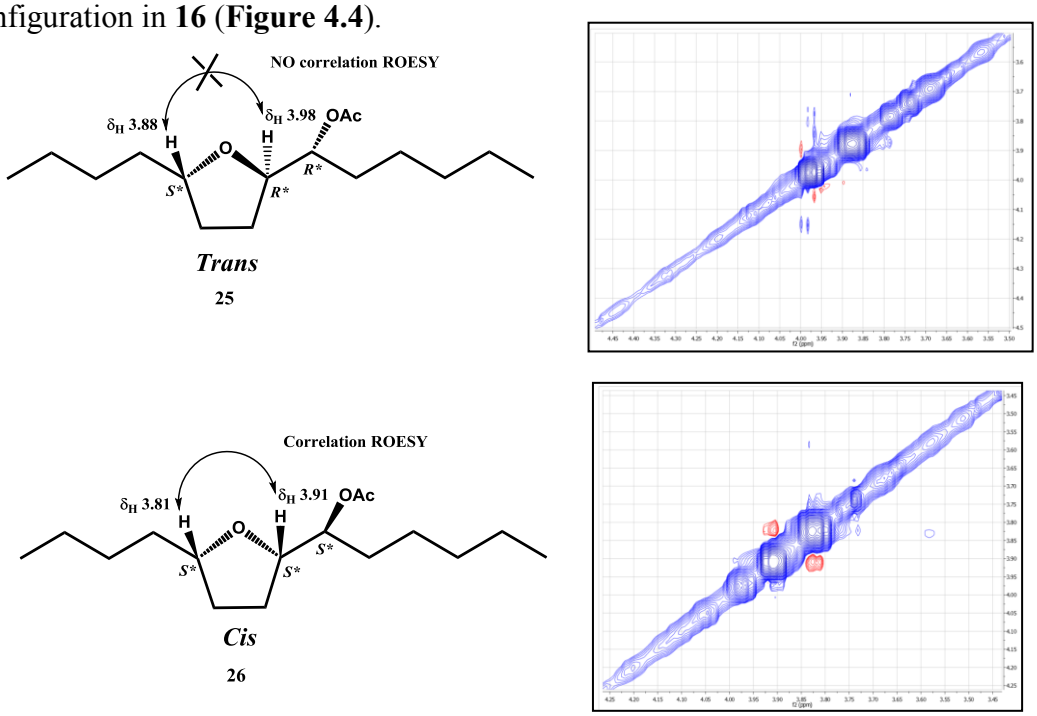

Figure 4.3. Key ROE correlations of compounds **25** and **26**

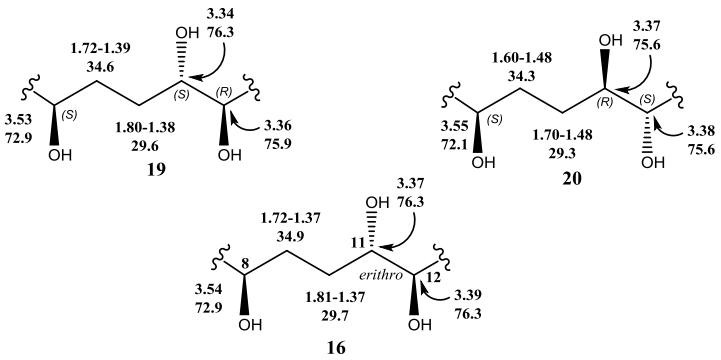

Figure 4.4. ^{1}H and ^{13}C chemical shift values (CD_3OD) of the triol portion of **16** and those of the triols **19** and **20**.

The absolute configuration at C8 in phosphoeleganin has been previously established as *S*. Thus, the assignment of the relative stereochemistry of C8-

C11 segment as *anti* required an absolute configuration at C11 as *S*. Analogously, the C11-C12 *anti* configuration, previously established, too, required an absolute configuration at C12 as *R*. Therefore, the absolute stereochemistry of phosphoeleganin was completely determined as 8*S*, 11*S*, 12*R*, 15*S*, 16*R*.

In conclusion, these data confirmed the *anti-anti* relative configuration of *rac*-**19** and a *syn-anti* relative configuration of *rac*-**20** as previously established by CDA derivatization method.

Table 4.1. ^{1}H (700 MHz) and ^{13}C NMR (175 MHz) data for *rac*-**19** and *rac*-**20** in CD_3OD

	rac–**19**		*rac*–**20**	
Pos	δ_C	δ_H **(mult, *J* in Hz)**	δ_C	δ_H **(mult, *J* in Hz)**
1	14.1	0.92 (t, 7.6)	14.1	0.92 (t, 7.6)
2	28.7	1.32 [a] -1.43 [a]	28.7	1.33 [a] -1.44 [a]
3	32.8	1.32 [a]	32.8	1.32 [a]
4	37.9	1.42 [a] -1.46	37.9	1.42 [a] -1.46 [a]
5	72.9	3.53	72.1	3.55
6	34.6	1.39 [a] - 1.72	34.3	1.53 [a] -1.60 [a]
7	29.6	1.38 [a] - 1.80	29.3	1.48 [a] – 1.70 [a]
8	76.3	3.34	75.6	3.37
9	75.9	3.36	75.6	3.38
10	33.4	1.36 [a] – 1.60 [a]	33.4	1.36 [a] – 1.60 [a]
11	26.4	1.33 [a] -1.54	26.4	1.33 [a] -1.54 [a]
12	32.8	1.32 [a]	32.8	1.32 [a]
13	23.7	1.34 [a]	23.7	1.34 [a]
14	14.1	0.92 (t, 7.6)	14.1	0.92 (t, 7.6)

[a]Partially overlapped by other resonances

Table 4.2. ^{1}H (700 MHz) and ^{13}C NMR (175 MHz) data for **25** and **26** in CD_3OD

	25		**26**	
Pos	δ_C	δ_H **(mult, *J* in Hz)**	δ_C	δ_H **(mult, *J* in Hz)**
1	14.1	0.87 (t, 7.6)	14.1	0.87 (t, 7.6)
2	22.8	1.30 [a]	22.9	1.30 [a]
3	28.4	1.31 [a] - 1.25	28.5	1.31 [a]-1.25
4	35.5	1.38 [a] -1.56	35.5	1.40 [a] -1.56 [a]
5	79.6	3.88	80.1	3.81
6	32.4	1.44 [a] - 1.98	31.2	1.44 [a] -1.92 [a]
7	28.4	1.58 [a] - 1.96	27.8	1.62 [a] – 1.89 [a]
8	79.3	3.98	79.6	3.91
9	75.7	4.86	75.9	4.87
10	31.1	1.53 [a]	31.2	1.56 [a]
11	31.9	1.27 [a]	31.9	1.27 [a]
12	25.6	1.28 [a]	25.2	1.28 [a]
13	22.8	1.30 [a]	22.6	1.29 [a]
14	14.1	0.87 (t, 7.6)	14.1	0.87 (t, 7.6)

[a]Partially overlapped by other resonances

4.3. Conclusions

The assignment of a natural product's absolute configuration is a laborious task and mistakes can occur as well. When a novel natural product is ready for stereochemical assignment, its chemical structure should be carefully studied and its physicochemical properties considered before a preferable method is chosen. So, the configurational assignment in natural products depends on the skills and on the tenacity of the chemist, who must have a great power of observation and extreme perseverance. From these studies, several issues may arise. For example: are all the natural products pure enantiomers? Can a single enantiomer of a biomolecule be always responsible for its bioactivity? Recent results have shown that bioactive natural products are not always enantiomerically pure, the stereochemistry–bioactivity relationships are complicated and the existing dogma about an enantiomer being bioactive must be modified. Additionally, several studies show the complexity and the importance of the stereochemistry for the expression of bioactivity of natural products. Kenji Mori, a well-known researcher in the natural products stereochemistry field, recently pointed out that the so far accepted view regarding only a certain enantiomer responsible for the activity, is not a fixed rule in nature anymore. Furthermore, other examples show different relationships between configuration and bioactivity, e.g. both enantiomers are needed for the bioactivity, or even in the same genus, different species accept different enantiomers.

CHAPTER 5

DEVELOPMENT OF NATURE INSPIRED ANTIMALARIAL HITS POSSESSING THE THIAZINOQUINONE PHARMACOPHORE

5.1. Introduction

Part of my work was also focused on the development of nature inspired antimalarial hits possessing the thiazinoquinone pharmacophore.

The starting point of this research was the identification of the thiazinoquinone scaffold as a new chemotype active against *P. falciparum* based on studies on marine-derived quinone compounds with antiplasmodial activity [117,118,119,120] which inspired the design and synthesis of a series of new derivatives[120-121] (**Figure 5.1**).

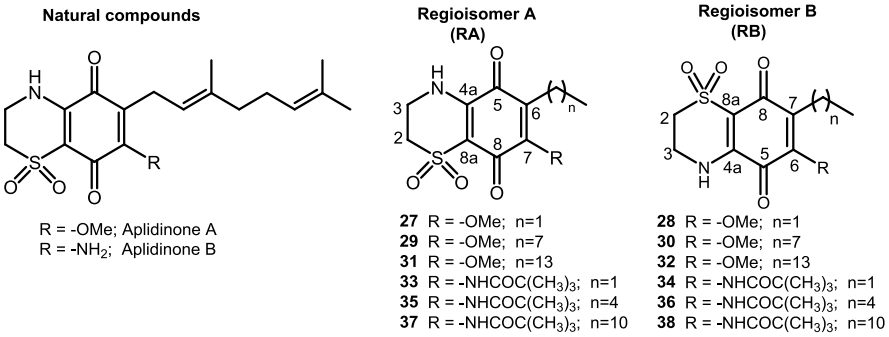

Figure 5.1. Structures of aplidinones A and B and their synthetic analogues

In collaboration with the Department of Biomedical, Surgical and Dental sciences (University of Milan), some previously synthesized thiazinoquinones

---

[117] Laurent, D.; Jullian, V.; Parenty, A.; Knibiehler, M.; Dorin, D.; Schmitt, S.; Lozach, O.; Lebouvier, N.; Frostin, M.; Alby, F.; Maurel, S.; Doerig, C.; Meijer, L.; Sauvain, M. *Bioorg. Med. Chem*. **2006**, 14, 4477-82.

[118] Longeon, A.; Copp, B.R.; Roué, M.; Dubois, J.; Valentin, A.; Petek, S.; Debitus, C.; Bourguet-Kondracki, M. *Bioorg. Med. Chem*. **2010**, 18, 6006-11.

[119] Davis, R. A.; Duffy, S.; Fletcher, S.; Avery, V.M.; Quinn, R. J. *J. Org. Chem*. **2013**, 78, 9608-13.

[120] Aiello, A.; Fattorusso, E.; Luciano, P.; Menna, M.; Calzado, M. A.; Munoz, E.; Bonadies, F.; Guiso, M.; Sanasi, M. F.; Cocco, G.; Nicoletti, R. *Bioorg. Med. Chem*. **2010**, 18, 719-727.

[121] Imperatore, C.; Persico, M.; Aiello, A.; Luciano, P.; Guiso, M.; Sanasi, M. F.; Taramelli, D.; Parapini, S.; Cebrián-Torrejón, G.; Doménech-Carbó, A.; Fattorusso, C.; Menna, M. *RSC Advances*, **2015**, 5, 70689-70702.

have been tested. These compounds showed an interesting *in vitro* antimalarial activity, also on chloroquine-resistant strains of *P. falciparum* (IC_{50} < 1μM), although some of them were strongly cytotoxic. Some structural requirements critical for both the antiplasmodial activity and cytotoxicity were then revealed. In particular, it has been seen that both the regiochemistry of dioxothiazine ring and the type of the substituent on the quinone play an important role on the antiplasmodial effects whereas, in the active regioisomers (**RB**), the presence and/or the length of the side chain distinguishes the antiplasmodial activity from the cytotoxicity. Two new antimalarial hits, compounds **28** and **33**, were thus identified, with an IC_{50} in the low micromolar range and non-toxic[121] (**Figure 5.2**).

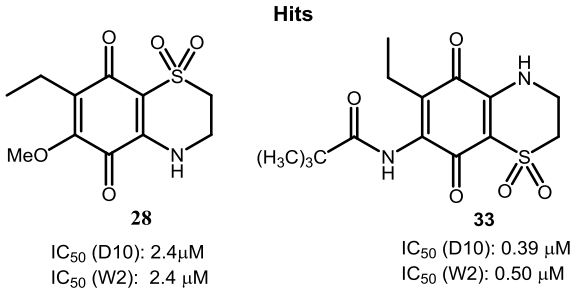

Figure 5.2. New marine inspired thiazinoquinone hits (**28**, **33**)

Additionally, in order to rationalize the structure-activity relationships (SARs), an integrated approach based on computational and electrochemical studies was performed. These studies were carried out by a further collaborating external research group.

These studies led to the hypothesis that the antiplasmodial activity of thiazinoquinones is related to their capacity to form toxic semiquinone species, with the thiazinoquinone ring system planarity favoring the reductive activation of parent quinone and the length of alkyl side chain distinguishing the antiplasmodial from the cytotoxic activity[121].

Accordingly, the electrochemical studies strongly evidenced the relationship between the antiplasmodial activity and an intense interaction with Fe(III)-heme, achieved through the formation of an adduct between the semiquinone

species and Fe(III)-heme.[122] The results obtained by the combination of these studies allowed us to identify new hits candidates.

The newly identified hits compounds **28** and **33** were used as starting point for the synthesis and/or chemical modification of additional analogues, with improved pharmacological proprieties and featuring this chemical scaffold. The structural determination of the new compounds was univocally performed through NMR spectroscopy and mass spectrometry.

In addition, studies on the reaction intermediates and their collateral products have been performed through an extensive spectroscopic analysis in order to improve the yields and/or to expand the chemical diversity.

The final aim of my research was to produce a pool of new compounds to be tested for their antiplasmodial and cytotoxic activity.

Based on the obtained SAR results for the previously developed antiplasmodial thiazinoquinone compounds,[120-121] I performed the synthesis of new analogues containing:

1. a double bond in the thiazine ring
2. different alkyl side chains
3. different benzyl side chains

5.2. Synthesis of derivatives with a double bond in dioxothiazine ring

A first chemical modification has been the introduction of a double bond in dioxothiazine ring. This modification has been inspired by data about Tiaplakortones A and B, reported in literature[123] (**Figure 5.3**).

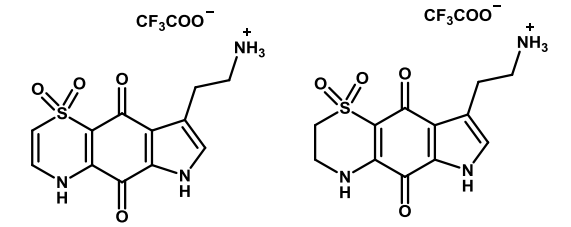

Figure 5.3. Tiaplakortones A and B

[122] Doménech-Carbó, A.; Maciuk, A.; Figadère, B.; Popuon, E.; Cebrián-Torrejón, G. *Anal. Chem*. **2013**, 85, 4014-4021.

[123] Davis, R. A.; Duffy, S.; Fletcher, S.; Avery, V. M.; Quinn, R. J. *J. Org. Chem.*, **2013**, 78 (19), 9608–9613

It has been evidenced that the presence of a double bond in the thiazinoquinone nucleus, produced in these compounds an increasing of the antiplasmodial activity. Moreover, this modification has also been related to computational studies, performed on the compounds of the previous series (**Figure 5.1**), that have evidenced that thiazinoquinone ring system planarity plays an important role in the antiplasmodial activity.[121] In particular, it is shown that the increase of the antiplasmodial activity, in relation to the presence of the double bond, seems to be correlated to a greater planarity and rigidity of the thiazinoquinone nucleus.

In order to perform this modification, the derivatives **28**, **30**, **33** and **34** with an interesting antiplasmodial activity[121], were treated with a solution of potassium hydroxide 1 M for 3h at room temperature.[124]

Subsequently, the reaction mixture was diluted with hydrochloric acid 2 M; then extracted with ethyl acetate and purified by column chromatography on silica gel (EtOAc /hexane=6:4) to afford the pure compounds **39**, **41**, **42** and only the compound **40** as collateral product (**Scheme 5.1**).

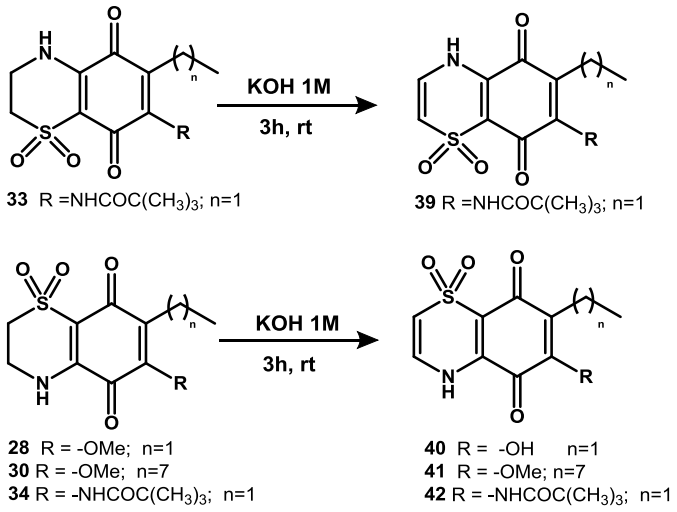

Scheme 5.1. Synthesis of thiazinoquinones **39–42**

[124] Chia, E. W.; Pearce, A. N.; Berridge, M. V.; Larsen, L.; Perry, N. B.; Sansom, C. E.; Godfrey, C. A.; Hanton, L. R.; Lu, G. L.; Walton, M.; Denny, W. A.; Webb, V. L.; Copp, B. R.; Harper, J. L. *Bioorg. Med. Chem*. **2008**, 16, 9432-9442.

The spectroscopic data have evidenced that the reaction performed on the compound **28** has produced the compound **40**, in which beside the formation of the double bond, the substitution of methoxy group with hydroxyl group occurred. This collateral reaction has not been observed in the reaction of the compound **30** which leads only to the formation of the compound **41**, probably because of the longest steric hindrance of the side chain. However, this is an aspect that needs further investigations.

The structures of the new compounds **39-42** were established on the basis of the spectroscopic analysis of the starting compounds[120-121] **28**, **30**, **33** and **34**, as described below. The molecular formula of the compound **40** was determined to be $C_{10}H_9NO_5SNa$ by (+)-HRESIMS of the pseudo-molecular $[M+Na]^+$ ion peak at m/z 278.0098. The spectral data (**Table 5.1**) obtained for compound **40** were nearly identical to those of **28** apart from the presence of two downfield olefin signals resonating in the proton spectrum at δ_H 6.19 (d, *J*=8.9, 1H, H-2), and δ_H 7.04 (d, *J*=8.9, 1H, H-3). These resonances were assigned to one disubstituted double bond, based on the two down-field resonances present in the ^{13}C NMR spectrum at δ_C 109.1 (CH), 130.3 (CH). Furthermore, the spectroscopic data ^1H and ^{13}C NMR have not evidenced the presence of the methyl signal observed in the compound **28**, thus suggesting that during the oxidation reaction, beside the formation of the double bond in the dioxothiazine ring, in the compound **40** the substitution of methoxy group with hydroxyl group occurred.

The chemical characterization of compound **41** was easily performed through spectral analysis (**Table 5.1**). The molecular formula of the compound **41** was determined to be $C_{17}H_{23}NO_5SNa$ on the basis of (+)-HRESIMS of the pseudo-molecular ion $[M+Na]^+$ at m/z 376.1193, differing from that of **30** only for the additional unsaturation. Analysis of ^1H and ^{13}C spectra confirmed that the only difference between **41** and **30** was the presence of a double bond in **41**.

Analogously, the structures of the oxidized compounds **39** and **42** were easily established on the basis of spectroscopic analysis (**Table 5.2**).

The pharmacological results have shown that the compound **40** was completely inactive compared to the starting compound **28**. The lack of any activity can be

due to the presence of hydroxyl group that might be subjected to a tautomeric-equilibrium which could cause a significant deviation from the planarity of benzoquinone ring. Currently, in collaboration with the research group of Prof. Fattorusso (University of Naples "Federico II", Department of Pharmacy), the compound **40** is still subject of computational studies in order to clarify the effects of a possible tautomeric equilibrium on the antiplasmodial activity

Table 5.1. NMR data of compounds **40** (CD_3OD) and **41** (DMSO-d_6).

	40			**41**		
Pos.	**δ_C**	**δ_H, mult. (*J* in Hz)**	**HMBC**	**δ_C**	**δ_H, mult. (*J* in Hz)**	**HMBC**
1	-	-	-	-	-	-
2	109.1	6.19 d (8.9)	3, 8a, 8	111.9	6.41 d (8.9)	3, 8, 8a
3	130.3	7.04 d (8.9)	2, 4a	130.8	7.02 d (8.9)	2, 4a
4	-	-	-	-	-	-
4a	137.7	-	-	138.9	-	-
5	180.6	-	-	175.9	-	-
6	158.8	-	-	154.8	-	-
7	122.6	-	-	138.9	-	-
8	180.2	-	-	181.6	-	-
8a	114.4	-	-	110.1	-	-
1'	17.0	2.45, q (7.5)	6, 7, 8, 2'	23.4	2.46, t (7.5)	6, 7, 8 2'
2'	13.6	1.03, t (7.5)	5, 6, 7, 1'	28.8	1.43, m	
3'	-	-	-	29.5	1.26	7'
4'-5'	-	-	-	29.1	1.26	
6'	-	-	-	31.7	1.24	
7'	-	-		22.3	1.27	
8'	-	-		13.5	0.87, t, (7.5)	
OCH_3	-	-		61.1	3.88	
4-NH	-	-	7, 8, 1'	-	11.1, br s	

Table 5.2. NMR data of compounds **39** and **42** in CD_3OD.

	39			**42**		
Pos.	**δ_C**	**δ_H, mult. (*J* in Hz)**	**HMBC**	**δ_C**	**δ_H, mult. (*J* in Hz)**	**HMBC**
1	-	-	-	-	-	-
2	112.2	6.40 d (8.9)	3, 8a, 8	112.1	6.40 d (8.9)	3, 8, 8a
3	131.7	7.13 d (8.9)	2, 4a	131.6	7.11 d (8.9)	2, 4a
4	-	-	-	-	-	-
4a	140.8	-	-	139.8	-	-
5	180.9	-	-	175.9	-	-
6	142.0	-	-	149.0	-	-
7	139.9	-	-	137.0	-	-
8	180.7	-	-	181.7	-	-
8a	114.6	-	-	112.1	-	-
1'	20.7	2.47, q (7.5)	2', 6, 7, 8	20.2	2.51, q (7.5)	2', 6,7,8
2'	12.1	1.09, t (7.5)	1'	12.8	1.09, t (7.5)	1'
1"	180.6	-		181.3	-	
2"	40.8	-		40.5	-	
Me	27.6	1.32, s		27.8	1.28, s	

5.3. Synthesis of derivatives with different alkyl side chains

The newly identified hit compound **28** was used as starting point for the synthesis of additional analogues, compounds **46-51** with improved pharmacological proprieties and featuring different alkyl chains (**Scheme 5.2**).

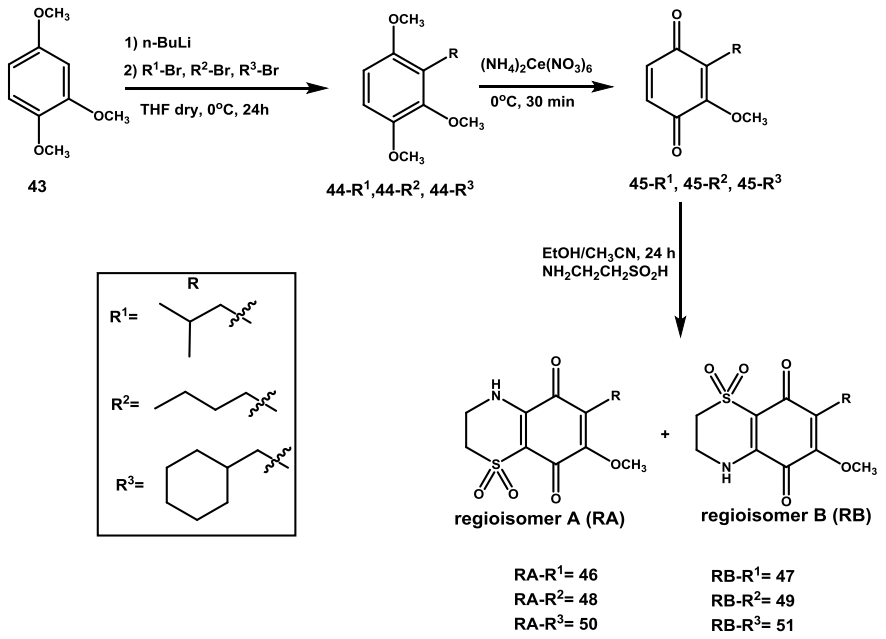

Scheme 5.2. Synthesis of thiazinoquinones **46-51**

A first series of new methoxy-derivatives have been prepared using a synthetic approach very similar to that adopted for the synthesis of the compound **28**.[120] In particular, the first synthetic step has been the lithiation of the commercially available 1,2,4-trimethoxybenzene (**43**) and then the alkylation with three alkyl bromides to obtain the corresponding 1,2,4-trimethoxy-3 alkylbenzenes **44-R^1, 44-R^2,** and **44-R^3** with good yields (80%, 76%, and 77%, respectively). Then, the oxidation of **44-R^1, 44-R^2,** and **44-R^3** with cerium ammonium nitrate (CAN) gave the quinones **45-R^1** (65% yield), 4**5-R^2** (65% yield), and **45-R^3** (74 % yield), respectively. Finally, the condensation reaction with hypotaurine provided the new thiazinoquinones **46-51**. This last reaction is not highly regioselective, and produces for each quinone two regioisomers in a ratio of 8:2 in favor of regioisomer B (**RB**); however, it is simple and cheap in order to obtain the required scaffold. Moreover, the formation of both regioisomers also

enlarges the pool of compounds to include in pharmacological studies. In addition, the regioisomers can be easily separated by HPLC in the same conditions, and then identified by spectroscopic techniques.

The chemical characterization of compounds **46-51** was easily performed through spectral analysis (**Tables 5.3, 5.4**), referring to the NMR spectral assignments made for **27** and **28**.[120] Actually, carbon and proton resonances relative to the bicyclic nucleus of the couples of compounds **46/47**, **48/49** and **50/51** were virtually identical to those of compounds **27** and **28**, respectively, thus defining the structures **46-51** as reported in Scheme 5.2.

Table 5.3. NMR data of compounds **46-49.**

	46		**47**		**48**		**49**	
Pos.	**δ_C**	**δ_H, mult. (*J* in Hz)**	**δ_C**	**δ_H, mult. (*J* in Hz)**	**δ_C**	**δ_H, mult. (*J* in Hz)**	**δ_C**	**δ_H, mult. (*J* in Hz)**
1	-	-	-	-	-	-	-	-
2	48.6	3.29 m	48.7	3.28 m	48.8	3.29 m	48.7	3.28 m
3	39.8	4.06 m	39.5	4.06 m	39.7	4.06 m	39.5	4.06 m
4	-	-	-	-	-	-	-	-
4a	144.2	-	142.8	-	144.3	-	142.8	-
5	179.5	-	176.5	-	179.4	-	176.5	-
6	127.7	-	152.9	-	127.7	-	152.9	-
7	157.6	-	138.8	-	157.6	-	138.8	-
8	174.1	-	178.1	-	174.1	-	178.1	-
8a	109.1	-	110.2	-	109.0	-	110.2	-
1'	34.9	2.28, d (7.3)	34.8	2.38, d (7.3)	22.9	2.38, t (7.5)	23.5	2.47, t (7.5)
2'	28.1	1.75 m	28.3	1.87	28.1	1.45,m	28.8	1.43, m
3'	22.6	0.86, d (6.7)	22.5	0.89, t (7.5)	29.6	1.40, m	29.5	1.38, m
4'	22.6	0.86, d (6.7)	22.5	0.89, t (7.5)	13.9	0.88 t (7.5)	13.8	0.86 t (7.5)
OCH_3	62.2	4.23 s	60.6	3.91 s	62.1	4.26 s	60.7	3.92 s
NH	-	6.71, brs	-	6.50, brs	-	6.81, brs	-	6.40, brs

Table 5.4. NMR data of compounds **50-51.**

	50		**51**	
Pos.	δ_C	δ_H, **mult. (*J* in Hz)**	δ_C	δ_H, **mult. (*J* in Hz)**
1	-	-	-	-
2	48.7	3.28, m	48.9	3.30, m
3	39.7	4.05, m	39.8	4.02, m
4	-	-	-	-
4a	144.6	-	142.5	-
5	180.4	-	176.5	-
6	126.7	-	153.5	-
7	158.6	-	137.8	-
8	173.2	-	179.0	-
8a	109.5	-	110.5	-
CH_2	30.4	2.29, d (7.2)	31.4	2.23, d (7.1)
1'	37.7	1.39, m	38.1	1.55, m
2'-6'	33.2	1.56-0.92, m	33.4	1.53-0.95, m
3'-5'	26.0	1.66-1.14, m	26.2	1.66-1.15, m
4'	26.1	1.60, m	26.7	1.60, m
OCH_3	62.3	4.22 s	60.8	3.88 s
NH	-	6.74, brs	-	6.45, brs

5.4. Synthesis of benzyl-methoxy thiazinoquinones

The previous synthetic protocol has been modified to prepare the benzyl derivatives (**56-61; Scheme 5.3**).

This synthesis has been inspired by date reported in literature about benzylmenadione, a naphthoquinone, whose antimalarial activity has been related to its redox proprieties, probably due to electronic effects of its benzyl chain.[125,126]

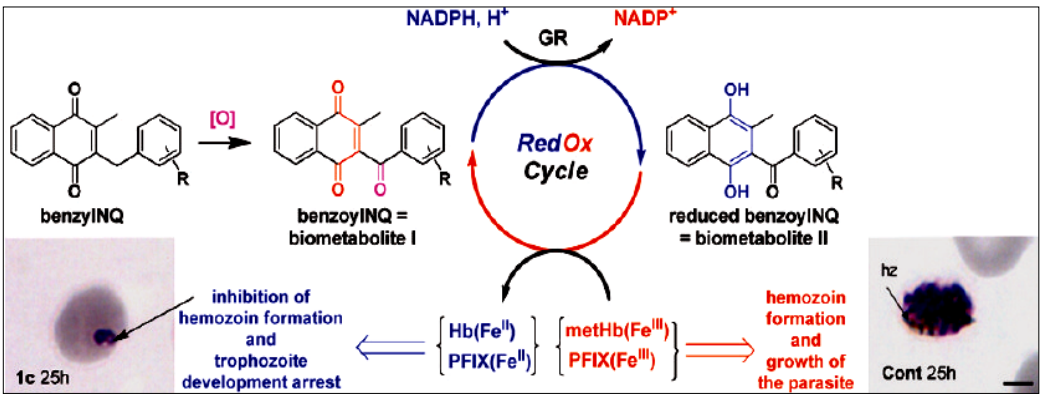

Figure 5.4. Putative redox cascade reactions accounting for the observed antimalarial activity of 3-benzylmenadione derivatives.

Concerning the antimalarial mode of action, it was proposed that the lead benzyl naphthoquinones are initially oxidized at the benzylic chain to benzoyl naphthoquinones in a heme-catalyzed reaction within the digestive acidic vesicles of the parasite. The major putative benzoyl metabolites were then found to function as redox cyclers: (i) in their oxidized form, the benzoyl metabolites are reduced by NADPH in glutathione reductase-catalyzed reactions within the cytosols of infected red blood cells; (ii) in their reduced

---

[125] Muller, T.; Johann, L.; Jannack, B.; Bruckner, M.; Lanfranchi, D. A.; Bauer, H.; Sanchez, C.; Yardley, V.; Deregnaucourt, C.; Schrevel, J.; Lanzer, M.; Schirmer, R. H.; Davioud-Charvet, E. *J. Am. Chem. Soc*. **2011**, 133, 11557–11571.

[126] Bielitza, M.; Belorgey, D.; Ehrhardt, K.; Johann, L.; Lanfranchi, D. A.; Gallo, V.; Schwarzer, E.; Mohring, F.; Jortzik, E.; Williams, D. L.; Becker, K.; Arese, P.; Elhabiri, M.; Davioud-Charvet, E. *Antioxid. Redox Sign*. **2015**, 22, 1337-1351.

forms, these benzoyl metabolites can convert methemoglobin, the major nutrient of the parasite, to indigestible hemoglobin (**Figure 5.4**). Therefore, on the basis of this hypothesis, the benzyl-methoxy derivatives were prepared.

In order to improve the yields, the previous synthetic protocol has been modified. Regarding the synthetic approach, firstly, it was utilized the benzaldehyde instead of the benzylic halide, which was added to the lithiated of 1,2,4 trimethoxybenzene solution (**52**) giving rise to the secondary benzylic alcohols (**53-R^4, 53-R^5, 53-R^6**), followed by their reduction (**54-R^4, 54-R^5, 54-R^6)**, using trifluoracetic acid in dichloromethane and then triethylsilane.[127,128,129] After that, as in the previous protocol, an oxidation and finally a condensation with hypotaurine took place. The last reaction is not highly regioselective in this case too (**Scheme 5.3**).

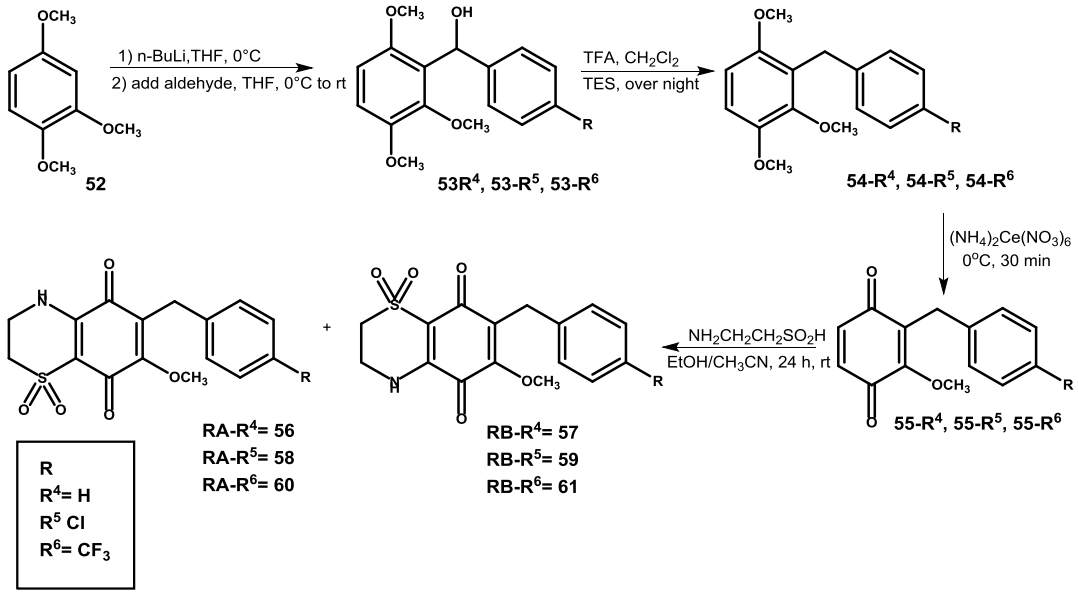

Scheme 5.3. Synthesis of thiazinoquinones **56-61**

Also in this case, all regioisomers **56-61** were isolated as individual compounds by HPLC separations in same conditions. Their chemical characterization

[127] Spyroudis, S. Molecules. **2000**, 5, 1291-1330
[128] Waterlot, C.; Couturier, D.; De Backer, M.; Rigo, B. *Can. J. Chem*. **2000**, 78, 1242-1246
[129] Farmer, J. L.; Froese, R. D. J.; Lee-Ruff, E.; Organ M. G. *Chem. Eur. J*. **2015**, 21, 1888-1893.

(**Tables 5.5, 5.6**) was readily identified by comparison of their spectroscopic data with those reported in literature, for compounds **27** and **28.** [104]

Table 5.5. NMR data of compounds **56-57.**

	56		**57**	
Pos.	δ_C	δ_H, **mult. (*J* in Hz)**	δ_C	δ_H, **mult. (*J* in Hz)**
1	-	-	-	-
2	48.3	3.24, m	49.3	3.24, m
3	40.0	4.02, m	40.6	3.99, m
4	-	-	-	-
4a	144.3	-	142.6	-
5	179.2	-	176.1	-
6	127.0	-	152.9	-
7	157.5	-	136.0	-
8	173.1	-	178.1	-
8a	109.2	-	110.5	-
CH_2	28.7	3.71, s	29.8	3.80, s
1'	138.9	-	138.1	-
2'-6'	128.8	7.19, d, (7.3)	130.0	7.28, d, (7.3)
3'-5'	128.8	7.24, t (7.3)	129.0	7.22, t, (7.3)
4'	126.8	7.17, t (7.3)	127.2	7.15, t, (7.3)
OCH_3	63.3	4.29 s	62.0	3.87 s
NH	-	6.74, brs	-	6.45, brs

Table 5.6. NMR data of compounds **58-61.**

	58		**59**		**60**		**61**	
Pos.	δ_C	δ_H, **mult.** (***J*** **in Hz)**	δ_C	δ_H, **mult.** (***J*** **in Hz)**	δ_C	δ_H, **mult.** (***J*** **in Hz)**	δ_C	δ_H, **mult.** (***J*** **in Hz)**
1	-	-	-	-	-	-	-	-
2	48.2	3.24, m	49.0	3.23, m	48.3	3.24, m	49.3	3.24, m
3	40.1	4.02, m	40.4	3.99, m	40.0	4.02, m	40.6	3.99, m
4	-	-	-	-	-	-	-	-
4a	144.2	-	142.5	-	144.3	-	142.6	-
5	179.1	-	176.2	-	179.2	-	176.1	-
6	127.2	-	152.8	-	127.0	-	152.9	-
7	157.3	-	136.1	-	157.5	-	136.0	-
8	173.0	-	178.0	-	173.1	-	178.1	-
8a	109.1	-	110.4	-	109.2	-	110.5	-
CH_2	28.6	3.71, s	29.8	3.80, s	28.6	3.77, s	29.8	3.85, s
1'	137.8	-	137.8	-	142.3	-	142.1	-
2'-6'	126.8	7.19, d, (8.3)	126.4	7.21, d, (8.3)	127.8	7.30, d, (8.3)	127.6	7.20, d, (8.3)
3'-5'	127.6	7.24, d (8.3)	127.3	7.25, d, (8.3)	126.4	7.49, d (8.3)	126.5	7.24, d (8.3)
4'	133.2	-	133.1	-	128.8	-	128.9	-
CF_3	-	-	-	-	124.2		124.1	
OCH_3	63.2	4.29 s	62.1	3.94 s	63.1	4.29 s	63.3	3.93 s
NH	-	6.80, brs	-	6.45, brs	-	6.80, brs	-	6.55, brs

5.5. Pharmacological activity

In collaboration with the Department of Biomedical, Surgical and Dental sciences (University of Milan), the synthetic analogues of natural thiazinoquinones have been tested for their in vitro antiplasmodial activity against both chloroquine (CQ)-sensitive (D10) and -resistant (W2) strains of *P. falciparum*; cytoxicity against human microvascular endothelial (HMEC-1) cells has been also evaluated.

Regarding the oxidized compounds **39-42**, they haven't shown the expected effects on the antiplasmodial activity (**Table 5.7**). In fact, all compounds with the added insaturation resulted less active than the starting related compounds[120] (**28, 30, 33, 34**). However, while the amide-derivatives **39** and **42** have shown only a slight decrease of the antiplasmodial activity compared to the starting compounds **33-34**, the methoxy-derivative **41** resulted significantly less active than the starting compound **30**. In the case of compound **40** (**Table 5.7**), the lack of any activity can be related to the tautomeric equilibrium due to the presence of the free hydroxyl group that might cause a significant deviation from the planarity of benzoquinone ring. These differences underline the key role of the type of substituent on the quinone, which we are trying to understand through computational studies.

Table 5.7. Pharmacological activity of compounds **39-42**

Compound	D10[a] IC_{50} (μM)	W2[a] IC_{50} (μM)	HMEC-1[a] IC_{50} (μM)
39	0.72	2.1	2.3
40	NA	NA	NA
41	8.9	NA	NA
42	3.5	7.4	NA

[a]Cloroquine (CQ) has been considered as positive control (D10 IC_{50} = 0.04 ± 0.01; W2 IC_{50} = 0.54 ± 0.28; not cytotoxic). Data are the mean ± SD of three different experiments in duplicate; NA: not active (IC_{50} > 10 μM against D10 and W2 strains of P. falciparum and IC_{50} > 100 μM against HMEC-1)

Moreover, the pharmacological screening on the two regioisomers series with different alkyl side chains (**46-51**), have confirmed, above all, the critical role of the regiochemistry on the antiplasmodial effects since the regioisomers **46**, **48**, **50** resulted completely inactive.

In series of the active regioisomers **47**, **49**, **51 (Table 5.8),** although we have not obtained a compound with improved proprieties compared to our starting hit **28**, these results have shown that the presence of a bulky side chain increases the cytotoxic activity, even if a linear correlation length-activity has not been evidenced, suggesting that a particular "shape" of the side chain is required.

Table 5.8. Pharmacological activity of compounds **50-55**

Compound	D10[a] IC_{50} (μM)	W2[a] IC_{50} (μM)	HMEC-1[a] IC_{50} (μM)
46	NA	NA	NA
47	1.3	2.7	26.8
48	NA	NA	NA
49	1.7	2.5	40.2
50	NA	NA	NA
51	2.37	3.03	3.91

[a]Cloroquine (CQ) has been considered as positive control (D10 IC_{50} = 0.04 ± 0.01; W2 IC_{50} = 0.54 ± 0.28; not cytotoxic). Data are the mean ± SD of three different experiments in duplicate; NA: not active (IC_{50} > 10 μM against D10 and W2 strains of P. falciparum and IC_{50} > 100 μM against HMEC-1)

The most interesting pharmacological results were obtained for the compound **57**. It exhibited the highest antiplasmodial activity (less than 1 micromolar) and an acceptable selectivity index, thus representing a new hit with improved proprieties compared to the starting hit **28 (Table 5.9).**

In addition, comparison of the antiplasmodial activity of this compound to those of the totally inactive compounds **56,** its regioisomer, and **55-R[4]**, lacking the thiazine ring, strongly evidenced the crucial role of the dioxothiazine ring for the antiplasmodial effect as well as the importance of the regiochemistry.

Table 5.9. Pharmacological activity of compounds **56-61** and **55-R^4**

Compound	D10[a] IC_{50} (μM)	W2[a] IC_{50} (μM)	HMEC-1[a] IC_{50} (μM)
56	NA	NA	NA
57	0.60	0.70	17.6
58	NA	NA	NA
59	1.63	1.90	8.5
60	NA	NA	NA
61	5.05	5.02	20.4
55-R^4	NA	NA	NA

[a]Cloroquine (CQ) has been considered as positive control (D10 IC_{50} = 0.04 ± 0.01; W2 IC_{50} = 0.54 ± 0.28; not cytotoxic). Data are the mean ± SD of three different experiments in duplicate; NA: not active (IC_{50} > 10 μM against D10 and W2 strains of P. falciparum and IC_{50} > 100 μM against HMEC-1)

As regard to the mechanism of action of the thiazinoquinones, certainly it is related to their redox proprieties. It would seem related to the possibility to form stable toxic semiquinone species acting as "subversive substrates",[121] but it still remains unclear. Further experiments were carried out on the novel hit compound **57**, as described below.

The hemolysis of red blood cells (RBCs), both *P. falciparum* infected and uninfected, was evaluated. The activity of the compound **57** was compared to its inactive regioisomer **56** in each experiment. The hemolysis percentage was monitored with a spectrophotometer (OD 405) measuring the absorbance of the hemoglobin released in the supernatant of the uninfected and infected RBCs. As shown in the **Table 5.10**, the release of hemoglobin was very low both in control RBCs and in those treated with **56** and **57** up to a concentration of 20microg / ml. This demonstrated the almost complete absence of hemolysis in both infected and non-infected red blood cells.

A second experiment was performed in order to evaluate the formation of methemoglobin, the major parasites nutrient. This experiment was carried out using the algorithm of Winterbourn and was performed in both PBS and in complete cell culture medium used for the growth of the parasite.

As reported in **Table 5.11,** both **56** and **57** induced the formation of methemoglobin, with **57** even acting at low concentrations.

Table 5.10. Hemolysis of *P. falciparum* infected and uninfected RBC, in the presence of different concentrations of **56** and **57**.

	OD[a] 405nm RBC		OD[a] 405 nm W2	
Conc. µM	**56**	**57**	**56**	**57**
0.93	0.096	0.098	0.135	0.135
1.86	0.098	0.099	0.135	0.135
3.72	0.098	0.101	0.136	0.134
7.44	0.099	0.105	0.137	0.137
14.88	0.100	0.108	0.139	0.137
29.76	0.100	0.113	0.139	0.141
59.52	0.103	0.117	0.141	0.145
Control	0.091		0.132	

[a]OD indicates the release of hemoglobin

Table 5.11. Formation of methemoglobin

56 in PBS	1%O_2[a]		20%O_2[a]		**57 in PBS**	1%O_2[a]		20%O_2[a]	
Conc. µM	%OXY	%META	%OXY	%META	**Conc. µM**	%OXY	%META	%OXY	%META
0.93	98,30	1,70	97,06	2,94	**0.93**	39,30	60,70	42,29	57,71
1.86	95,19	4,81	93,85	6,15	**1.86**	26,44	73,56	27,47	72,53
3.72	89,83	10,17	88,06	11,94	**3.72**	16,71	83,29	17,21	82,79
7.44	80,31	19,69	79,03	20,97	**7.44**	11,05	88,95	11,71	88,29
14.88	67,26	32,74	64,96	35,04	**14.88**	8,63	91,37	8,48	91,52
29.76	51,14	48,86	49,53	50,47	**29.76**	8,47	91,53	7,75	92,25
59.52	34,71	65,29	32,37	67,63	**59.52**	9,77	90,23	9,98	90,02
Control	99,59	0,41	99,29	0,71	**Control**	99,59	0,41	99,29	0,71

[a]RBCs (3 days of seniority) were treated for 24 hours with **56** or **57** in PBS. Incubation in an atmosphere of 20% O_2 or 1% O_2 (Condition of *P. Falciparum* Growth)

Unfortunately, the addition of N-acetyl Cysteine (NAC) to RBCs was not protective against the formation of methaemoglobin.

Finally, it was evaluated the activity of **56** and **57** against *P. falciparum*, W2 (CQ-R), pretreated with increasing doses of NAC. As shown in **Table 5.12**, in the presence of NAC, an increase of IC_{50} only on **57** occurred.

Table 5.12. Activity against *P. falciparum*, W2 (CQ-R) strain, pretreated with NAC.

Compound	**W2 (CQ-R)**			
	-	**NAC 0.1**	**NAC 1**	**NAC 10**
	IC_{50} (µM)	**IC_{50} (µM)**	**IC_{50} (µM)**	**IC_{50} (µM)**
56	NA	NA	NA	NA
57	0.70	0.70	1.05	1.34

In conclusion, the fact that NAC protects the parasite from the activity of **57**, suggested that the mechanism of action of **57** is related to oxidative stress induced in the presence of the parasite. In addition, both compounds **56 and 57** seemed to have oxidizing capacities given that induce the formation of methemoglobin. However, the formation of methemoglobin did not appear to be related to the compounds mechanism of action, since the NAC, which inhibits the activity of **57** on the parasite, did not prevent the methemoglobin's formation.

5.6. Conclusions

The whole series of data obtained led to the identification of several antimalarial hit candidates, compounds **28, 33, 57**, and shed light on the mechanism of action of this kind of molecules. Particularly, the new hit **57** seemed to have oxidizing capacities, suggesting that the key feature of antimalarial activity resides ultimately in disturbing the redox homeostasis in the parasitized red blood cells.

Currently, the new derivatives are still subject of computational studies in order to clarify even more the mechanism of action and the pharmacological results.

It is to be noted that the presence of an electron withdrawing group on the benzyl group, such as in derivatives **58-61**, did not significantly influenced the antiplasmodial activity compared to compound **57** denoting that not only electronic factors, acting on the stability of the toxic radical species seemingly responsible of the antiplasmodial effects, but further events and factors could be involved in their mode of action. However, these preliminary data clearly point out the thiazinoquinone scaffold as potential new lead structure for antimalarial drugs discovery.

CHAPTER 6

EXPERIMENTAL SECTION

6.1. *Phallusia fumigata*

General Experimental Procedures**.** High-resolution ESI-MS analyses were performed on a Thermo LTQ Orbitrap XL mass spectrometer. The spectra were recorded by infusion into the ESI source using MeOH as solvent. Optical rotations were measured at 589 nm on a Jasco P-2000 polarimeter using a 10-cm microcell. ^{1}H (700 MHz) and ^{13}C (175 MHz) NMR spectra were recorded on an Agilent INOVA spectrometer equipped with a ^{13}C enhanced HCN Cold Probe; chemical shifts were referenced to the residual solvent signal (CHD_2OD: $\delta_H = 3.31$, $\delta_C = 49.0$). For an accurate measurement of the coupling constants, the one-dimensional ^{1}H NMR spectra were transformed at 64K points (digital resolution: 0.09 Hz). Homonuclear ^{1}H connectivities were determined by COSY experiment. Through-space ^{1}H connectivities were evidenced using a ROESY experiment with a mixing time of 500 ms. Two and three bond ^{1}H-^{13}C connectivities were determined by gradient 2D HMBC experiments optimized for a $^{2,3}J$ of 8 Hz. $^{3}J_{H\text{-}H}$ values were extracted from 1D ^{1}H NMR. Medium-pressure liquid chromatographies (MPLC) were performed on a Büchi 861 apparatus with octadecyl-functionalized silica gel (200-400 mesh) packed column. High performance liquid chromatography (HPLC) separations were achieved on a Shimadzu LC-10AT apparatus equipped with a Knauer K-2301 refractive index detector.

Collection, Extraction, and Isolation. Specimens of *Phallusia fumigata* were collected in May 2010 in the bay of Pozzuoli (Napoli, Italy). The samples were frozen immediately after collection and stored at −20 °C until extraction. A reference specimen is deposited at the Department of Pharmacy, University of Naples. The fresh thawed animals (402 g of dry weight after extraction) were homogenized and extracted twice with methanol and then twice with chloroform (4 x 200 mL). The combined extracts were concentrated in vacuo, and the resulting aqueous residue was extracted with EtOAc and subsequently

with *n*-BuOH. Separation of the *n*-BuOH soluble material (3,06 g) was achieved by gradient RP-18 silica gel MPLC (H_2O → MeOH → $CHCl_3$) to yield nine fractions A–I. The fraction eluted with H_2O/MeOH 3:7 v/v, (fraction D, 98.2 mg) was chromatographed by HPLC on a RP-18 column (polar-RP 5 μm, 250 x 4.60 mm) eluting with H_2O/MeOH 35:65 (v/v), yielding a fraction mainly composed of **6** (5.6 mg) which has been further purified by HPLC on a RP-18 column (Synergy 4 μm, 250 x 4.60 mm), eluting with H_2O/MeOH 3:7, thus affording phallusiasterol C (1.1 mg) as pure compound.

Phallusiasterol C (6): colorless amorphous solid, $[\alpha]_D^{25}$ -4.0 (*c* 0.1, CH_3OH); HRESIMS (negative ion mode, CH_3OH) *m*/z 567.2054 ($[M-Na]^-$, calcd. for $C_{26}H_{40}NaO_8S_2^-$ 567.2057); ^1H and ^{13}C NMR (CD_3OD) data are reported in **Table 3.1.**

Transactivation Experiments. To investigate the PXR mediated transactivation, HepG2 cells were plated in a 24-wells plate, at $5x10^4$cells/well, and transiently transfected with 75 ng of pSG5-PXR, 75 ng of pSG5-RXR, 125 ng of pCMV-β-galactosidase, and with 250 ng of the reporter vector pCYP3A4promoter-TKLuc, using Fugene HD transfection reagent (Roche). At 24 hours, post-transfection, cells were primed 18 hours with Rifaximin and **6** (10μM) or with the combination of Rifaximin (10μM) plus compound **6** (50 μM). After treatments, cells were lysed in 100 μL Lysis Buffer (25 mM TRIS-phosphate pH 7.8; 2mM DTT; 10% glycerol; 1% Triton X-100) and 20 μL cellular lysate was assayed for Luciferase activity using the Luciferase Assay System (Promega). Luminescence was measured using an automated luminometer (Glomax 20/20, Promega). Luciferase activities were normalized for transfection efficiencies by dividing the Luciferase relative light units (RLU) by β- galactosidase activity (βgal) expressed from cells co-transfected with pCMVβgal. All experiments were performed in triplicate

Cells culture, RNA extraction and Real-Time PCR. HepG2 cells were cultured at 37 °C in E-MEM supplemented with 10% FBS, 1% l-glutamine and 1%

penicillin/streptomycin. To evaluate PXR target genes expression, serum starved HepG2 cells were stimulated for 18 h with Rifaximin and compound **6** (10μM). Total RNA was extracted using the TRIzol reagent (Invitrogen), purified of the genomic DNA by DNAase I treatment (Invitrogen) and random reverse-transcribed with Superscript II (Invitrogen). 10 ng template was amplified using the following reagents: 0.2 μM of each primer and 10μl of KAPA SYBR FAST Universal qPCR Kit (KAPA BIOSYSTEMS). All reactions were performed in triplicate and the thermal cycling conditions were: 3 min at 95 °C, followed by 40 cycles of 95 °C for 15 s, 58 °C for 20 s and 72 °C for 30 s. The relative mRNA expression was calculated and expressed as $2^{-(\Delta\Delta Ct)}$. Primers used for qRT-PCR were: hGAPDH: GAAGGTGAAGGTCGGAGT and CATGGGTGGAATCATATTGGAA; hCYP3A4: CAAGACCCCTTTGTGGAAAA and CGAGGCGACTTTCTTTCATC; hMDR1: GTGGGGCAAGTCAGTTCATT and CTTCACCTCCAGGCTCAGT.

Statistical Analysis. All values are expressed as means ± standard error (SE) of n observations/group. Comparisons of two groups were made with a one-wayANOVA with post hoc Tukey's test. Differences were considered statistically significant at values of $P < 0.05$.

6.2. Electrochemical and computational studies

Reagents, compound isolation and characterization. Double stranded deoxyribonucleic acid sodium salt from salmon testes (dsDNA) was purchased from Sigma and used as received. Compounds **12-15** (**Figure 3.4**) were isolated and characterized as previously reported.

Electrochemical studies**.** Electrochemical experiments were performed at 298±1 K in a thermostated cell with CH I660 equipment. A BAS MF2012 glassy carbon working electrode (GCE) (geometrical area 0.071 cm^2), a platinum wire auxiliary electrode and an Ag/AgCl (3M NaCl) reference electrode were used in a typical three-electrode arrangement. 0.10 M Phosphate buffer saline (PBS) at pH

7.4 (from Merck reagents) was used for experiments in aqueous solution. Experiments in DMSO (Carlo Erba) were performed using 0.10 M Bu_4NPF_6 (Fluka) as a supporting electrolyte. Prior to electrochemical runs, all solutions were deaerated by bubbling Ar during 15 min.

The electrochemistry of films of the studied receptors on glassy carbon electrode was studied using the methodology previously described by pipeting 10 μL of a solution (1 mg/mL), previously ultrasonicated by 5 min, of the compound in ethanol and allowing the solvent to evaporate in air. As a result, a uniform, fine coating of the quinones was adhered to the basal electrode.

Computational studies. Apparent pK_a values were calculated by using ACD/Percepta software.[130] The compounds were built, taking into account the prevalent ionic forms at physiological pH (7.4), using the Insight 2005 Builder module (Accelrys Software Inc., San Diego). Atomic potentials and charges were assigned using the CFF91 force field.[131] The conformational space of the compounds was sampled through 200 cycles of Simulated Annealing (ε = 80**r*). The following protocol was applied: the system was heated up to 1000 K over 2000 fs (time step = 3.0 fs); the temperature of 1000 K was applied to the system for 2000 fs (time step = 3.0 fs) with the aim of surmounting torsional barriers; successively, temperature was linearly reduced to 300 K in 1000 fs (time step = 1.0 fs). Resulting conformations were then subjected to molecular mechanic (MM) energy minimization within Insight 2005 Discover module (CFF91 force field; ε = 80**r*) until the maximum RMS derivative was less than 0.001 kcal/Å, using Conjugate Gradient[132] as minimization algorithm. MM conformers were then subjected to a full geometry optimization by semi-empirical calculations, using the quantum mechanical method PM7[133] in the

[130]ACD/Percepta, Advanced Chemistry Development, Inc., Toronto, ON, Canada, 2015, http://www.acdlabs.com.

[131] Maple, J.R.; Hwang, M.J.; Stockfisch, T.P.; Dinur, U.; Waldman, M.; Ewig, C.S.; Hagler, A.T. J. *Comput. Chem*. **1994**, 15, 162−182.

[132] Fletcher, R.; Unconstrained Optimization. In Practical Methods of Optimization; John Wiley & Sons: New York, **1980**, vol. 1.

[133] Stewart, J.J. *J. Mol. Model*. **2013**, 19, 1–32.

Mopac2012 package[134] and EF (Eigenvector Following routine)[135] as geometry optimization algorithm. GNORM value was set to 0.01. To reach a full geometry optimization, the criteria for terminating all optimizations were increased by a factor of 100, using the keyword PRECISE. Resulting conformers were ranked by their potential energy values (i.e., ΔE from the global energy minimum) and grouped into conformational families. The occurrence rates and ΔE_{GM} range for each conformational family were calculated. The lowest energy minima of each family have been then subjected to DFT calculations. All structures were fully optimized in gas-phase and characterized as minima at the B3LYP/6-31+G (d, p) level.[136] The calculations were carried out using the Gaussian 09 package.[137]

Starting from the structure of the Q (i.e., the starting quinone species) GM conformers, the redox states $Q^{\bullet -}$, $QH^{\bullet}_{i}$, $QH^{\bullet}_{ii}$, QH_i^-, QH_{ii}^-, QH_2 were generated. In particular, following the reduction pathway of quinones reported in **Scheme 3.1**, each species was generated starting from the DFT optimized species of the previous step. The reaction energies (kcal/mol) for the electron/proton transfer of each step of the reduction reaction $\Delta E_{(Q \rightarrow Q^{\bullet -})}$ were calculated: In particular, gas phase reaction energy calculations for electron attachment were accomplished by determining ΔE of the reaction $Y + e^- \rightarrow Y^-$ that is, $\Delta E = E(Y^-) - E(Y)$, where Y is the Q or $QH^{\bullet}$ DFT conformer. Reaction energies for proton

---

[134] MOPAC2012; Stewart Computational Chemistry: Colorado Springs, CO, USA; http://OpenMOPAC.net (2012)

[135] Baker, J. *J. Comput. Chem*. **1986**, 7, 385−395.

[136] a) Becke, A. D. *J. Chem. Phys*. **1993**, 98, 5648−5652; (b) Lee, C.; Yang, W.; Parr, R. G. Phys. Rev. B: Condens. Matter Mater. Phys. **1988**, 37, 785−789.

[137] Frisch, M.J.; Trucks, G.W.; Schlegel, H.B.; Scuseria, G.E.; Robb, M.A.; Cheeseman, J.R.; Scalmani, G.; Barone, V.; Mennucci, B.; Petersson, G.A.; Nakatsuji, H.; Caricato, M.; Li, X.; Hratchian, H.P.; Izmaylov, A.F.; Bloino, J.; Zheng, G.; Sonnenberg, J.L.; Hada, M.; Ehara, M.; Toyota, K.; Fukuda, R.; Hasegawa, J.; Ishida, M.; Nakajima, T.; Honda, Y.; Kitao, O.; Nakai, H.; Vreven, T.; Montgomery, J.A.Jr.; Peralta, J.E.; Ogliaro, F.; Bearpark, M.; Heyd, J.J.; Brothers, E.; Kudin, K.N.; Staroverov, V.N.; Kobayashi, R.; Normand, J.; Raghavachari, K.; Rendell, A.; Burant, J.C.; Iyengar, S.S.; Tomasi, J.; Cossi, M.; Rega, N. ; Millam, N.J.;. Klene, M.; Knox, J.E.; Cross, J.B.; Bakken, V.; Adamo, C.; Jaramillo, J.; Gomperts, R.; Stratmann, R.E.; Yazyev, O.; Austin, A.J.; Cammi, R.; Pomelli, C.; Chterski, J.W.; Martin, R.L.; Morokuma, K.; Zakrzewski, V.G.; Voth, G.A.; Salvador, P.; Dannenberg, J.J.; Dapprich, S.; Daniels, A.D.; Farkas, O.; Foresman, J.B.; Ortiz, J.V.; Cioslowski, J.; Fox, D.J. Gaussian 09, revision A.1. Gaussian Inc. Wallingford, **2009**.

attachment were calculated by determining ΔE of the reaction $Y + H^+ \rightarrow YH$ that is $\Delta E = E(YH) - E(Y)$, where Y is $Q^{\bullet-}$ or QH^- DFT conformer.[138]

For each considered redox state, the energy of the frontier molecular orbitals (HOMO, LUMO, and SOMO) were used to calculate the following parameters: i) the electrophilicity index (ω), ii) the vertical ionization potential (*IP*), iii) the vertical electron affinity (*EA*). The electrophilicity indexes (ω) were calculated following the expression $\omega = (\mu^2/2\eta)$, where μ is the chemical potential given by $\mu = -(IP + EA)/2$ and η is the chemical hardness given by $\eta = (IP - EA)$, where $IP = E(N=N_{0-1}) - E(N=N_0)$ and $EA = E(N=N_0) - E(N=N_{0+1})$. Here, N_0 is the number of electrons in the ground state of the (usually neutral) system. Thus, the single point energies (E) of the cationic (N_{0-1} electron system), and anionic (N_{0+1} electron system) forms for each considered species were calculated for each compound.

6.3. Synthesis of phosphoeleganin's analogues

General Experimental Procedures. Optical rotations were measured at 589 nm with a Jasco P-2000 polarimeter using a 10-cm microcell. HRMS (ESI positive mode) was performed with a Thermo LTQ Orbitrap XL mass spectrometer. The spectra were recorded by infusion into the ESI source using MeOH as solvent. CD spectra were recorded with a J-710 spectropolarimeter (Jasco, Tokyo, Japan) with J-710 for Windows software (Jasco). ^1H (700 MHz) and ^{13}C (175 MHz) NMR spectra were recorded on an Agilent INOVA spectrometer; chemical shifts were referenced to the residual solvent signal (CD_3OD: $\delta_H = 3.31$, $\delta_C = 49.0$; $CDCl_3$: $\delta_H = 7.26$, $\delta_C = 77.0$). Homonuclear ^1H connectivities were determined by COSY experiments. Two and three bond ^1H-^{13}C connectivities were determined by gradient 2D HMBC experiments optimized for a $^{2,3}J$ of 8 Hz. Medium-pressure liquid chromatographies (MPLC) were performed on a Büchi 861 apparatus with octadecyl-functionalized silica gel (200-400 mesh) packed column. High performance

[138] Sawyer, A.; Sullivan, E.; Mariam, Y.H. *J. Comput. Chem*. **1996**, 17, 204-225.

liquid chromatography (HPLC) separation was achieved on a Knauer K-501 apparatus equipped with an Knauer K-2301 RI detector.

Collection, Extraction, and Isolation. Compound **16** (**Figure 4.1**) was isolated and characterized as previously reported.

Synthesis of compound 18. Compound **18** was prepared from a solution of cis-4-decenal (424 mg, 2,75 mmol, 1.0 equiv) in anhydrous THF (20mL) to which was added *n*-BuLi dropwise (2.06 mL, 1.6 M in hexane, 3.30 mmol, 1.2 equiv). The reaction mixture was stirred at -78°C for 10 min and after for an additional 8h at rt. The reaction was quenched with saturated NH_4Cl and extracted with EtOAc. The organic phase was dried over anhydrous Na_2SO_4 and solvent removed with rotary evaporation. **(18)**: ^{1}H-NMR (700 MHz, $CDCl_3$) δ 0.84 (m, 6H), 1.20-1.51 (m, 14H), 1.95 (m, 2H), 2.05 (m, 1H), 2.12 (m, 1H), 3.54 (m, 1H), 5.32 (m, 2H). ^{13}C-NMR (175 MHz, $CDCl_3$) δ 14.0, 22.5, 22.7, 23.4, 27.1, 27.7, 29.3, 31.4, 37.0, 37.1, 71.5, 129.1, 130.5. ESI-MS (pos.) m/z 213.22 $[M+H]^+$.

Synthesis of compounds 19* and 20*. 495 mg of compound **18** (2.3 mmol, 1 equiv) were dissolved with acetone/H_2O (9:1, 10 mL), added NMO (410 mg, 3.5 mmol, 1.5 equiv) and OsO_4 (1 mol%, 6mg). The reaction mixture was stirred overnight at rt. The reaction was quenched with saturated Na_2SO_3 solution and extracted with EtOAc (3x). Organic layer was dried over anydrous Na_2SO_4, filtered and concentrated in vacuo. Separation by reverse phase HPLC (Luna C18 10μ MeOH/H2O 7:3) of the obtained stereisomeric triols mixture gave two diastereoisomeric fractions, *rac*-**19** (55.1 mg, *tr* 12.6 min) and *rac*-**20** (61.4 mg, *tr* 14.4 min), as enatiomeric mixtures. ESI-MS (pos.) m/z 247.22 $[M+H]^+$.

Synthesis of compounds 21-22 and 23-24. Esterification reaction was carried out both on fraction *rac*-**19** (5.1 mg, 0.048 mmol) that *rac*-**20** (18.1 mg, 0.074 mmol) respectively each dissolved in CH_2Cl_2 dry (3mL). To a *rac*-**19**

compound solution was added EDC (37.4 mg, 0.195 mmol), DMAP (11.8 mg, 0.096 mmol) and (*R*)-methoxyphenylacetic acid (6.32 mg, 0.195 mmol). Instead, to a *rac*-**20** compound solution was added EDC (63.3 mg, 0.334 mmol), DMAP (18.1 mg, 0.148 mmol), (*R*)-methoxyphenylacetic acid (54.8 mg, 0.334 mmol). Each mixture was stirred overnight under N_2 atmosphere at rt. After solvent evaporation, HPLC purification of two mixtures on SiO_2 column (Luna SiO_2 3µ), eluiting with Hexane/ EtOAc 85:15 (v/v), each gave two diastereoisomeric triesters **21 (**2.1 mg, *tr* 3.74 min), **22** (2.3, *tr* 4.64 min), **23** (7.8 mg, *tr* 3.12 min) and **24** (8.0 mg, *tr* 4.32 min).

(21): ^{1}H NMR (700 MHz, $CDCl_3$, J in Hz) δ 0.67 (t, 7.6, 3H, H-1), 0.98 (overlapped, 2H, H-2), 0.61 (m, 2H, H-3), 0.94 (overlapped, 1H, H-4a), 0.98 (overlapped,1H, H-4b), 4.42 (m, 1H, H-5), 0.56 (m, 1H, H-6a), 0.88 (overlapped, 1H, H-6b), 0.93 (overlapped, 1H, H-7a), 1.14 (m, 1H, H-7b), 4.66 (m, 1H, H-8), 5.09 (m, 1H, H-9), 1.36 (overlapped, 1H, H-10a), 1.39 (overlapped, 1H, H-10b), 1.22 (overlapped, 2H, H-11), 1.22 (overlapped, 2H, H-12), 1.25 (overlapped, 2H, H-13), 0.86 (t, 7.6, 3H, H-14); ^{13}C NMR ($CDCl_3$, signals assigned from HSQC data) δ 13.5 (C-1), 22.1 (C-2), 26.2 (C-3), 33.4 (C-4), 74.9 (C-5), 29.1 (C-6), 24.0 (C-7), 74.7 (C-8), 74.1 (C-9), 29.9 (C-10), 24.9 (C-11), 31.1 (C-12), 22.3 (C-13), 13.7 (C-14). HRMS (ESI): m/z [M +Na] $^+$ calcd. for $C_{41}H_{54}O_9Na^+$: 713.3660, found: 713.3680.

(22): ^{1}H NMR (700 MHz, $CDCl_3$, J in Hz) δ 0.84 (t, 7.6, 3H, H-1), 1.25 (overlapped, 2H, H-2), 1.16 (overlapped, 2H, H-3), 1.39 (m, 1H, H-4a), 1.48 (m,1H, H-4b), 4.80 (m, 1H, H-5), 1.31 (overlapped, 2H, H-6), 0.80 (overlapped, 1H, H-7a), 1.02 (m, 1H, H-7b), 4.88 (m, 1H, H-8), 4.40 (m, 1H, H-9), 0.79 (overlapped, 1H, H-10a), 0.84 (overlapped, 1H, H-10b), 0.46 (m, 1H, H-11a), 0.52 (m, 1H, H-11b) 1.31 (overlapped, 2H, H-12), 0.91 (m, 2H, H-13), 0.68 (t, 7.6, 3H, H-14); ^{13}C NMR ($CDCl_3$, signals assigned from HSQC data) δ 13.8 (C-1), 22.3 (C-2), 27.1 (C-3), 33.9 (C-4), 74.7 (C-5), 30.4 (C-6), 25.5 (C-7), 74.4 (C-8), 74.7 (C-9), 26.9 (C-10), 23.9 (C-11), 30.3 (C-12), 22.1 (C-13), 13.5 (C-14). HRMS (ESI): m/z [M +Na] $^+$ calcd. for $C_{41}H_{54}O_9Na^+$: 713.3660, found: 713.3677.

(23): ^{1}H NMR (700 MHz, $CDCl_3$, J in Hz) δ 0.68 (t, 7.6, 3H, H-1), 1.05 (m, 2H, H-2), 0.83 (overlapped, 2H, H-3), 1.29 (overlapped, 1H, H-4a), 1.31 (overlapped,1H, H-4b), 4.83 (m, 1H, H-5), 1.42 (overlapped, H, H-6a), 1.46 (overlapped, 1H, H-6b), 1.37 (overlapped, 1H, H-7a), 1.44 (overlapped, 1H, H-7b), 5.07 (m, 1H, H-8), 4.69 (m, 1H, H-9), 0.99 (overlapped, 2H, H-10), 0.54 (overlapped, 1H, H-11a), 0.59 (overlapped, 1H, H-11b), 0.74 (m, 1H, H-12a), 0.82 (overlapped, 1H, H-12b), 0.91 (m, 2H, H-13), 0.67 (t, 7.6, 3H, H-14); ^{13}C NMR ($CDCl_3$, signals assigned from HSQC data) δ 13.7 (C-1), 22.1 (C-2), 26.7 (C-3), 33.4 (C-4), 74.2 (C-5), 29.9 (C-6), 25.9 (C-7), 74.5 (C-8), 74.8 (C-9), 27.6 (C-10), 23.9 (C-11), 30.9 (C-12), 22.1 (C-13), 13.7 (C-14). HRMS (ESI): m/z $[M+Na]^+$ calcd. for $C_{41}H_{54}O_9Na^+$: 713.3660, found: 713.3681.

(24): ^{1}H NMR (700 MHz, $CDCl_3$, J in Hz) δ 0.81 (t, 7.6, 3H, H-1), 1.16 (overlapped, 2H, H-2), 0.93 (overlapped, 2H, H-3), 0.99 (overlapped, 1H, H-4a), 1.21 (overlapped,1H, H-4b), 4.53 (m, 1H, H-5), 0.74 (overlapped, 2H, H-6), 0.77 (overlapped, 1H, H-7a), 0.89 (overlapped, 1H, H-7b), 4.61 (m, 1H, H-8), 5.00 (m, 1H, H-9), 1.16 (overlapped, 1H, H-10a), 1.22 (overlapped, 1H, H-10b), 1.16 (overlapped, 2H, H-11), 1.22 (overlapped, 2H, H-12), 1.24 (overlapped, 2H, H-13), 0.85 (t, 7.6, 3H, H-14); ^{13}C NMR ($CDCl_3$, signals assigned from HSQC data) δ 13.8 (C-1), 22.4 (C-2), 27.1 (C-3), 33.4 (C-4), 73.9 (C-5), 28.8 (C-6), 22.6 (C-7), 74.2 (C-8), 74.4 (C-9), 29.6 (C-10), 24.9 (C-11), 31.4 (C-12), 22.4 (C-13), 13.9 (C-14). HRMS (ESI): m/z $[M+Na]^+$ calcd. for $C_{41}H_{54}O_9Na^+$: 713.3660, found: 713.3688.

Synthesis of compound 19. Pure enantiomeric **19** triol was obtained by **21** (2 mg, 0.003 mmol) compound's hydrolysis reaction with NaOH (400 mg, 10 mmol) in MeOH (3mL) and any water drops. The mixture was stirred at rt overnight, then diluted with HCl (1% solution), washed with brine and the triol was extracted with 20 mL BuOH (3x). The organic extract was dried over anhydrous Na_2SO_4 and then concentrated in vacuo. Reverse phase HPLC (Luna 5μ C18), eluiting with MeOH: H2O 7:3, allowed triol purification (2mg, *tr* 10.5 min). **(19)**: ^{1}H NMR (700 MHz, CD_3OD, J in Hz), view δ_H and δ_C **(*rac*-**

19) in **Table 4.1**. ESI-MS (pos.) m/z 247.22 $[M+H]^+$ $[\alpha]_D^{25}$: +3.71 (0.009, MeOH).

Synthesis of compound 20. **20** triol (3.6mg, *tr* 12.0 min) was obtained by the same reaction and purification (reverse phase HPLC MeOH: H2O 7:3) of **19** reported above, using 4,8 mg (0.007 mmol) of **23**. **(20)**: ^{1}H NMR (700 MHz, CD_3OD, J in Hz), view δ_H and δ_C **(***rac***-20)** in **Table 4.1**. ESI-MS (pos.) m/z 247.22 $[M+H]^+$. $[\alpha]_D^{25}$: +1.56 (0.015, MeOH).

Cyclization of 19* enantiomeric mixture. 10.4 mg of *rac*-**19** (0.0422 mmol, 1.0 equiv) were dissolved in CH_2Cl_2 (5 mL) and added trimethyl orthoacetate (7 μL, 1.2 equiv), PPTS (0.100 mg, 0.01 equiv) at rt. Spent 15 min, BF_3•Et2O (0.53 μL, 0.1 equiv) was added at 0°C and when TLC showed orthoester absence, the mixture was quenched with H_2O/Acetone 9:1 and after solvent was removed in vacuo. Cyclised product **25** was obtained quantitatively. **(25)**: ^{1}H NMR (700 MHz, CD_3OD, J in Hz), view δ_H and δ_C in **Table 4.2**. HRMS (ESI): m/z $[M+Na]^+$ calcd. for $C_{16}H_{30}O_3Na^+$: 293.2087, found: 293.2075.

Cyclization of 20* enantiomeric mixture: Using 10.5 mg of *rac*-**20** (0.0422 mmol, 1.0 equiv), compound **26** was obtained with the same conditions of **25** reported above. **(26)**: ^{1}H NMR (700 MHz, CD_3OD, J in Hz), view δ_H and δ_C in **Table 4.2**. HRMS (ESI): m/z $[M+Na]^+$ calcd. for $C_{16}H_{30}O_3Na^+$: 293.2087, found: 293.2083.

6.4. Synthesis of thiazinoquinone derivatives

General experimental procedures. High-resolution ESI-MS analyses were performed on a Thermo LTQ Orbitrap XL mass spectrometer (Thermo-Fisher, San Josè, CA, USA). The spectra were recorded by infusion into the ESI (Thermo-Fisher, San Josè, CA, USA) source dissolving the sample in MeOH. ^{1}H (700 MHz) and ^{13}C (175 MHz) NMR spectra were recorded on an Agilent INOVA spectrometer (Agilent Technology, Cernusco sul Naviglio, Italy)

equipped with a ^{13}C enhanced HCN Cold Probe; chemical shifts were referenced to the residual solvent signal ($CDCl_3$: δ_H = 7.26, δ_C = 77.0; DMSO-*d6* δ_H = 2.39, δ_C = 39.0). For an accurate measurement of the coupling constants, the one-dimensional ^1H NMR spectra were transformed at 64 K points (digital resolution: 0.09 Hz). Homonuclear (^1H- ^1H) and heteronuclear (^1H-^{13}C) connectivities were determined by COSY and HSQC experiments, respectively. Two and three bond ^1H-^{13}C connectivities were determined by gradient 2D HMBC experiments optimized for a $^{2,3}J$ of 8 Hz. $^3J_{H\text{-}H}$ values were extracted from 1D ^1H NMR. High performance liquid chromatography (HPLC) separations were achieved on a Shimadzu LC-10AT (Shimadzu, Milan, Italy) apparatus equipped with a Knauer K-2301 (LabService Analytica s.r.l., Anzola dell'Emilia, Italy) refractive index detector.

Reagents. Sigma–Aldrich. Solvents: Carlo Erba. TLC: Silica Gel 60 F254 (plates 5 x 20, 0.25 mm) Merck. Preparative TLC: Silica Gel 60 F254 plates (20 x 20, 2 mm). Spots revealed by UV lamp then by spraying with 2 N sulfuric acid and heating at 120 °C. Anhydrous solvents: Sigma–Aldrich or prepared by distillation according to standard procedures

Synthesis of compounds 39-42. Aqueous sodium hydroxide (1 M; 1 mL) was added to a solution of 0.055 mmol of each starting compound (15 mg of **28**, 19.5 mg of **30**, 18.7 mg of **33** and **34**) dissolved in 2 mL of methanol**.** The mixture was stirred for 3 hours at room temperature. Subsequently, the reaction mixture was diluted with hydrochloric acid (2 M; 5 mL); then extracted with ethyl acetate three times. The combined organic phases were dried over $MgSO_4$ and the solvent was evaporated. The residue was purified by column chromatography on silica gel (EtOAc/hexane 6:4) to afford the pure compounds **39** (6 mg, 28%), **41** (6.0 mg, 32%), **42** (5.8 mg, 31%) and only the only compound **40** (4 mg, 28%) as collateral product. NMR data of compounds **39, 40, 42** (CD_3OD) and **41** (DMSO-d_6) are reported in **Tables 5.1** and **5.2**. **(39)**: ESI MS (positive ions): m/z 337 ($[M\text{-}H]^-$). **(40)**: ESI MS (positive ions):

m/z 278 ([M+Na] $^{+}$). **(41)** ESI MS (positive ions): m/z 376 ([M+Na] $^{+}$). **(42)**: ESI MS (positive ions): m/z 337 ([M-H] $^{-}$).

Synthesis of compounds 44-R^1, 44-R^2 and 44-R^3. 1.68 g (10 mmol) of 1,2,4-trimethoxybenzene (**43**) were dissolved in 25 mL of anhydrous THF and 12.5 mL of a *n*-BuLi 1.6 M solution (20 mmol) were added, under argon atmosphere at rt; the mixture was stirred for 1 h. Then, the bromoalkane (20 mmol; 2.2 mL of 1-bromo-2-methylpropane**,** 2.1 mL of 1-bromobutane and 2.8 mL of (bromomethyl)cyclohexane) were added and the mixture was left under stirring for 24 h (the end of the reaction was controlled with TLC, eluent: chloroform/hexane 7:3). After this time, the mixture was poured into cold water (150 mL) and extracted three times with ether. The ethereal solution was washed with brine several times ,dried over sodium sulfate, filtered and concentrated. The residue was purified by column chromatography on silica gel (hexane/EtOAc 9:1) to afford **44-R^1** (1.8 g, 80.3% yield) , **44-R^2** (1.7 g, 76.0% yield) and **44-R^3** (2.0g, 76.5% yield) as colorless oil.

44-R^1*:* ^{1}H-NMR ($CDCl_3$): 6.68 (^{1}H, d, *J* = 8.8 Hz, H-6); 6.51 (1H, d, *J* = 8.8 Hz, H-5); 3.79 (3H, s, -OCH_3); 3.78 (3H, s, -OCH_3); 3.73 (3H, s, -OCH_3); 2.49 (2H, d, *J* = 7.3 Hz, CH_2); 1.89 (1H, m, *J* = 7.3 Hz-6.7 Hz, CH); 0.86 (6H, d, *J* = 6.7Hz, CH_3). HRMS (ESI): m/z [M +Na]$^{+}$ calcd. for $C_{13}H_{20}O_3Na^{+}$: 247.1305, found: 247.1314.

44-R^2*:* 247.1315; ^{1}H-NMR ($CDCl_3$): 6.69 (^{1}H, d, *J* = 8.8 Hz, H-6); 6.52 (1H, d, *J* = 8.8 Hz, H-5); 3.77 (3H, s, -OCH_3); 3.74 (3H, s, -OCH_3); 3.72 (3H, s, -OCH_3); 2.63 (2H, t, *J* = 7.4 Hz, $\underline{CH_2}CH_2CH_2CH_3$); 1.49 (2H, m, $CH_2\underline{CH_2}CH_2CH_3$); 1.38 (2H, m, $CH_2CH_2\underline{CH_2}CH_3$); 0.92 (3H, d, *J* = 6.7Hz, CH_3). HRMS (ESI): m/z [M +Na]$^{+}$ calcd. for $C_{13}H_{20}O_3Na^{+}$: 247.1305, found:

44-R^3*:* ^{1}H-NMR ($CDCl_3$): 6.69 (^{1}H, d, *J* = 8.8 Hz, H-6); 6.52 (1H, d, *J* = 8.8 Hz, H-5); 3.80 (3H, s, -OCH_3); 3.78 (3H, s, -OCH_3); 3.74 (3H, s, -OCH_3); 2.50 (2H, d, *J* = 7.4 Hz, $\underline{CH_2}$-cyclohexyl); 1.55 (1H, m, CH); 1.53-0.95 (4H, m); 1.15-1.66 (4H, m), 1.60(2H, m). HRMS (ESI): m/z [M +Na]$^{+}$ calcd. for $C_{16}H_{24}O_3Na^{+}$: 287.1618, found: 287.1626.

Synthesis of compounds 45-R^1, 45-R^2 and 45-R^3. 3.5 mmol of each compound (680 mg of **44-R^1,** 680 mg of **44-R^2**, 820 mg of **44-R^3**) dissolved in 90 mL of acetonitrile were added dropwise to a solution of CAN (9.6 g, 17.5 mmol) in water (100mL) at 0°C. The mixture was stirred for 30 minutes at room temperature (the end of the reaction was checked by TLC, eluent: chloroform/ EtOAc 7:3). The orange liquid was then poured into 100 mL of cold water and extracted three times with ether. The combined organic layers were washed with brine, dried over sodium sulfate, and filtered. The solvent removal under reduced pressure afforded **45-R^1** (382 mg, 65%), **45-R^2** (382 mg, 65%) and **45-R^3** (540 mg, 74 %) sufficiently pure for the following reaction.

(**45-R^1**)*:* ^{1}H-NMR ($CDCl_3$): 6.66 (^{1}H, d, *J* = 10.0 Hz, H-6); 6.51 (1H, d, *J* = 10.0 Hz, H-5); 3.99 (3H, s, -OCH_3); 2.34 (2H, d, *J* = 7.3 Hz, CH_2); 1.81 (1H, m, *J* = 7.3 Hz-6.7 Hz, CH); 0.89 (6H, d, *J* = 6.7Hz, CH_3). HRMS (ESI): m/z [M +Na]$^+$ calcd. for $C_{11}H_{14}O_3Na^+$: 217.0835, found: 217.0841;

(45-R^2): ^{1}H-NMR ($CDCl_3$): 6.66 (^{1}H, d, *J* = 10.0 Hz, H-6); 6.51 (1H, d, J = 10.0 Hz, H-5); 4.01 (3H, s, -OCH_3); 2.42 (2H, t, *J* = 7.4 Hz, $\underline{CH_2}CH_2CH_2CH_3$); 1.47 (2H, m, $CH_2\underline{CH_2}CH_2CH_3$); 1.39 (2H, m, $CH_2CH_2\underline{CH_2}CH_3$); 0.92 (3H, d, *J* = 6.7Hz, CH_3). HRMS (ESI): m/z [M +Na^+]$^+$ calcd. for $C_{11}H_{14}O_3Na^+$: 217.0835, found: 217.0843.

(45-R^3): ^{1}H-NMR ($CDCl_3$): 6.69 (^{1}H, d, *J* = 8.8 Hz, H-6); 6.52 (1H, d, *J* = 8.8 Hz, H-5); 4.01 (3H, s, -OCH_3); 2.35 (2H, d, *J* = 7.4 Hz, $\underline{CH_2}$-cyclohexyl); 1.55 (1H, m, CH); 1.53-0.95 (4H, m); 1.15-1.66 (4H, m), 1.60 (2H, m). HRMS (ESI): m/z [M +Na^+]$^+$ calcd. for $C_{14}H_{18}O_3Na^+$: 257.1148, found: 257.1139.

Synthesis of compounds 46-51. 1.5 mmol of each quinone (290 mg of **45-R^1**, 290 mg of **45-R^2**, 350 mg of **45-R^3**) were dissolved in a mixture of EtOH/CH_3CN 1:1 and heated in a water bath under stirring; then, a solution of hypotaurine (163.7 mg, 1.5 mmol) in 8 mL of water and a catalytic amount of salcomine were added in portions. The mixture was stirred for 24 h at room temperature and the yellow solution became orange/red. Most of the ethanol was removed in vacuo and the residue was poured into water. The mixture was extracted with ether (three times) and the organic phase was washed with brine,

dried over sodium sulfate, and filtered. Solvent removal gave residues containing mixtures of compounds **46/47** (from **45-R^1**, 170 mg, 38 % yield), **48/49** (from **45-R^2**, 173 mg, 39 % yield) as well as of compounds **50/51** (from **45-R^3**, 167 mg, 33 % yield); they were separated as reported below.

Separation of crude mixtures of 46/47, 48/49 and 50/51 isomers. Separation of isomers **46/47** mixture (170 mg) was achieved by HPLC on a SiO_2 column (Luna 5µm, 250 x 4.60 mm) eluting with EtOAc/hexane 6:4 (v/v) and afforded pure compounds **46** (16 mg) and **47** (62 mg). Mixture of isomers **48/49** (170 mg), as well as that of **50/51 (**167 mg), were separated in the same conditions and yielded pure compounds **48** (14 mg), **49** (60 mg), **50** (11 mg), and **51** (43 mg).

(**46**): HPLC EtOAc/hexane 6:4 (v/v), (t_R): 13.5 min (single peak). ^{1}H and ^{13}C NMR data are reported in **Table 5.3**. HRMS (ESI): m/z [M +Na] $^+$ calcd. for $C_{13}H_{17}NO_5SNa^+$: 322.0720, found: 322.0727.

(**47**): HPLC EtOAc/hexane 6:4 (v/v), (t_R): 24 min (single peak). ^{1}H and ^{13}C NMR data are reported in **Table 5.3**. HRMS (ESI): m/z [M +Na] $^+$ calcd. for $C_{13}H_{17}NO_5SNa^+$: 322.0720, found: 322.0729.

(**48**)*:* HPLC EtOAc/hexane 6:4 (v/v), (t_R): 11.5 min (single peak). ^{1}H and ^{13}C NMR data are reported in **Table 5.3**. HRMS (ESI): m/z [M +Na] $^+$ calcd. for $C_{13}H_{17}NO_5SNa^+$: 322.0720, found: 322.0733.

(**49**): HPLC EtOAc/hexane 6:4 (v/v), (t_R): 22 min (single peak). ^{1}H and ^{13}C NMR data are reported in **Table 5.3**. HRMS (ESI): m/z [M +Na] $^+$ calcd. for $C_{13}H_{17}NO_5SNa^+$: 322.0720, found: 322.0735.

(**50**): HPLC EtOAc/hexane 6:4 (v/v), (t_R): 11.8 min (single peak). ^{1}H and ^{13}C NMR data are reported in **Table 5.4**. HRMS (ESI): m/z [M +Na] $^+$ calcd. for $C_{16}H_{21}NO_5SNa^+$: 362.1033, found: 362.1042.

(**51**): HPLC EtOAc/hexane 6:4 (v/v), (t_R): 21.4 min (single peak). ^{1}H and ^{13}C NMR data are reported in **Table 5.4**. HRMS (ESI): m/z [M +Na] $^+$ calcd. for $C_{16}H_{21}NO_5SNa^+$: 362.1033, found: 362.1038.

Synthesis of compounds 53-R^4, 53-R^5 and 53-R^6. To a solution of 1,2,4-trimethoxybenzene (**52**, 1.0 mL, 6.7 mmol) in THF (25 mL) was added 6 mL *n*-BuLi 1.6 M solution (10 mmol) under argon atmosphere at 0 °C; the mixture was stirred for 1 h. Then, the aldehyde (10 mmol; 1.0 mL of benzaldehyde, 1.4 g of 4-chlorobenzaldehyde, 1.3 mL of 4-(trifluoromethyl)benzaldehyde were added and the mixture was left under stirring at room temperature overnight. and quenched by adding saturated aqueous NH_4Cl (30 mL). The two layers were separated and the aqueous layer was extracted with ether (three times). The combined organic layers were washed with brine, dried over anhydrous sodium sulfate, and concentrated. The crude material was purified by column chromatography on silica gel (hexane/EtOAc 8:2) to afford the corresponding secondary benzylic alcohols **53-R^4** (1.3 g, 70% yield), **53-R^5** (1.5 g, 73% yield), **53-R^6** (1.6 g, 70% yield): (1.3 g, 70% yield).

(53-R^4) ^{1}H-NMR ($CDCl_3$): 6.82 (1H, d, *J* = 8.8 Hz, H-6); 6.62 (1H, d, *J* = 8.8 Hz, H-5); 3.82 (3H, s, -OCH_3); 3.74 (3H, s, -OCH_3); 3.61 (3H, s, -OCH_3); 6.25 (1H, d, *J* = 11.7 Hz, CH-OH); 7.36 (2H, d, *J* = 7.0 Hz); 7.28 (2H, t, *J* = 7.6Hz); 7.19 (1H, t, *J* = 7.6Hz); 4.29 (1H, d, *J* = 11.7Hz, OH). HRMS (ESI): m/z [M +$Na^{\cdot}$] $^+$ calcd. for $C_{16}H_{18}O_4Na^+$: 297.1097, found: 297.1109.

(53-R^5) ^{1}H-NMR ($CDCl_3$): 6.82 (1H, d, *J* = 8.8 Hz, H-6); 6.62 (1H, d, *J* = 8.8 Hz, H-5); 3.81 (3H, s, -OCH_3); 3.72 (3H, s, -OCH_3); 3.62 (3H, s, -OCH_3); 6.24 (1H, d, *J* = 11.7 Hz, CH-OH); 7.23 (2H, d, *J* = 8.3 Hz); 7.27 (2H, d, *J* = 8.3Hz); 4.29 (1H, d, *J* = 11.7Hz, OH). HRMS (ESI): m/z [M +Na] $^+$ calcd. for $C_{16}H_{17}ClO_4Na^+$: 331.0708, found: 331.0719.

(53-R^6) ^{1}H-NMR ($CDCl_3$): 6.82 (1H, d, *J* = 8.8 Hz, H-6); 6.62 (1H, d, *J* = 8.8 Hz, H-5); 3.78 (3H, s, -OCH_3); 3.68 (3H, s, -OCH_3); 3.63 (3H, s, -OCH_3); 6.30 (1H, brs, CH-OH); 7.53 (2H, d, *J* = 8.3 Hz); 7.50 (2H, d, *J* = 8.3Hz); 4.29 (1H, brs, OH). HRMS (ESI): m/z [M +Na] $^+$ calcd. for $C_{17}H_{17}F_3O_4Na^+$: 365.10971, found: 365.0954.

Synthesis of compounds 54-R^4, 54-R^5 and 54-R^6. Trifluoracetic acid (0.5 mL, 7,1 mmol) was slowly added to a solution of each compound (2.4 mmol; 650 mg of **53-R^4**, 740 mg of **53-R^5**, 821 mg of **53-R^6**) and triethylsilane (1.1 mL,

7.1 mmol) in dichloromethane (30 mL). The mixture was stirred at room temperature overnight. The organic phase was washed with a sodium carbonate solution (30 mL) and dried. The solvent removal afforded **54-R^4** (570 mg, 93%) **54-R^5** (661 mg, 94%), **54-R^6** (720 mg, 92%) sufficiently pure for the following reaction.

(54-R^4) ^{1}H-NMR ($CDCl_3$): 6.73 (1H, d, *J* = 8.8 Hz, H-6); 6.56 (1H, d, *J* = 8.8 Hz, H-5); 3.80 (3H, s, -OCH_3); 3.72 (3H, s, -OCH_3); 3.68 (3H, s, -OCH_3); 4.01 (1H, s, CH_2-benzyl); 7.22 (2H, d, *J* = 7.0 Hz); 7.18 (2H, t, *J* = 7.6Hz); 7.09 (1H, t, *J* = 7.6Hz). HRMS (ESI): m/z [M +Na] $^+$ calcd. for $C_{16}H_{18}O_3Na^+$: 281.1148, found: 281.1154.

(54-R^5) ^{1}H-NMR ($CDCl_3$): 6.76 (1H, d, *J* = 8.8 Hz, H-6); 6.57 (1H, d, *J* = 8.8 Hz, H-5); 3.80 (3H, s, -OCH_3); 3.72 (3H, s, -OCH_3); 3.70 (3H, s, -OCH_3); 3.99 (1H, s, CH_2-benzyl); 7.19 (2H, s); 7.17 (2H, s). HRMS (ESI): m/z [M +Na] $^+$ calcd. for $C_{16}H_{17}ClO_3Na^+$: 315.0758, found: 315.0770.

(54-R^6) ^{1}H-NMR ($CDCl_3$): 6.85 (1H, d, *J* = 8.8 Hz, H-6); 6.65 (1H, d, *J* = 8.8 Hz, H-5); 3.88 (3H, s, -OCH_3); 3.85 (3H, s, -OCH_3); 3.80 (3H, s, -OCH_3); 4.20 (1H, s, CH_2-benzyl); 7.57 (2H, d, *J* = 8.0 Hz); 7.48 (2H, d, *J* = 8.0 Hz). HRMS (ESI): m/z [M +Na] $^+$ calcd. for $C_{17}H_{17}F_3O_3Na^+$: 349.1022, found: 281.1004.

Synthesis of compounds 55-R^4, 55-R^5 and 55-R^6. 2.2 mmol of each compound (570 mg of **54-R^4,** 643 mg of **54-R^5**, 717 mg of **54-R^6)** dissolved in 90 mL of acetonitrile were added dropwise to a solution of CAN (6.0 g, 11.0 mmol) in water (110 mL) at rt. The mixture was stirred for 30 minutes at room temperature (the end of the reaction was checked by TLC, eluent: chloroform/ EtOAc 7:3). The orange liquid was then poured into 100 mL of cold water and extracted three times with ethyl acetate. The combined organic layers were washed with brine, dried over sodium sulfate, and filtered. The solvent removal under reduced pressure afforded **55-R^4** (324 mg ,65%), **55-R^5** (372 mg ,64%), **55-R^6** (427 mg, 65%), sufficiently pure for the following reaction. **(55-R^4)** ^{1}H-NMR ($CDCl_3$): 6.66 (1H, d, *J* = 10.0 Hz, H-6); 6.57 (1H, d, *J* = 10.0 Hz, H-5); 4.02 (3H, s, -OCH_3); 3.77 (1H, s, CH_2-benzyl); 7.25 (2H, d, *J* = 7.0 Hz); 7.23

(2H, t, *J* = 7.6Hz); 7.16 (1H, t, *J* = 7.6Hz). HRMS (ESI): m/z [M +Na] $^{+}$ calcd. for $C_{14}H_{12}O_3Na^+$: 251.0679, found: 251.0689.

(55-R^5) ^{1}H-NMR ($CDCl_3$): 6.66 (1H, d, *J* = 10.0 Hz, H-6); 6.57 (1H, d, *J* = 10.0 Hz, H-5); 4.04 (3H, s, -OCH_3); 3.71 (1H, s, CH_2-benzyl); 7.19 (2H, d, *J* = 8.5 Hz); 7.17 (2H, d, *J* = 8.5 Hz); HRMS (ESI): m/z [M +Na] $^{+}$ calcd. for $C_{14}H_{11}ClO_3Na^+$: 315.0758, found: 315.0770.

(55-R^6) ^{1}H-NMR ($CDCl_3$): 6.67 (1H, d, *J* = 10.0 Hz, H-6); 6.59 (1H, d, *J* = 10.0 Hz, H-5); 4.06 (3H, s, -OCH_3); 3.80 (1H, s, CH_2-benzyl); 7.50 (2H, d, *J* = 8.0 Hz); 7.36 (1H, d, *J* = 8.0Hz). HRMS (ESI): m/z [M +Na] $^{+}$ calcd. for $C_{15}H_{11}F_3O_3Na^+$: 319.0553, found: 319.0545.

Synthesis of compounds 56-61. 1.42 mmol of each quinone (324 mg of **55-R^4**, 372 mg of **55-R^5**, 420 mg of **55-R^6**) were dissolved in 26 mL of a mixture of EtOH/CH_3CN 1:1 and heated in a water bath under stirring; then, a solution of hypotaurine (155 mg, 1.42 mmol) in 2 mL of water and a catalytic amount of salcomine were added in portions. The mixture was stirred for 24 h at room temperature. The yellow solution became orange/red. Most of the ethanol was removed in vacuo and the residue was poured into water. The mixture was extracted with ether (three times) and the organic phase was washed with brine, dried over sodium sulfate, and filtered. Solvent removal gave residues containing a mixture of the isomers **56/57** (from **55-R^4**, 175 mg, 37 % yield), **58/59** (from **55-R^5**, 181 mg, 35 % yield) as well as of compounds **60/61** (from **55-R^6**, 213 mg, 37 % yield); they were separated as reported below.

Separation of crude mixtures of 56-61 isomers. Separation of isomers **56/57** mixture (175 mg) was achieved by HPLC on a SiO_2 column (Luna 5µm, 250 x 4.60 mm) eluting with EtOAc/hexane 6:4 (v/v) and afforded pure compounds **56** (14 mg) and **57** (56 mg). Mixture of isomers **58/59** (181 mg), as well as that of **60/61** (213 mg), were separated in the same conditions and yielded pure compounds **58** (10 mg), **59** (42 mg), **60** (11 mg), and **61** (49 mg).

(**56**): HPLC EtOAc/hexane 6:4 (v/v), (t_R): 14 min (single peak). ^{1}H and ^{13}C NMR data are reported in **Table 5.5**. HRMS (ESI): m/z [M +Na] $^+$ calcd. for $C_{16}H_{15}NO_5SNa^+$: 356.0563, found: 356.0565.

(**57**): HPLC EtOAc/hexane 6:4 (v/v), (t_R): 27 min (single peak). ^{1}H and ^{13}C NMR data are reported in **Table 5.5**. HRMS (ESI): m/z [M +Na] $^+$ calcd. for $C_{16}H_{15}NO_5SNa^+$: 356.0563, found: 356.0565.

(58) HPLC: EtOAc/hexane 6:4 (v/v), (t_R): 7 min (single peak). ^{1}H and ^{13}C NMR data are reported in **Table 5.6**. HRMS (ESI): m/z [M +Na] $^+$ calcd. for $C_{16}H_{14}ClNO_5SNa^+$: 390.0173, found: 390.0169.

(59) HPLC: EtOAc/hexane 6:4 (v/v), (t_R): 14 min (single peak). ^{1}H and ^{13}C NMR data are reported in **Table 5.6**. HRMS (ESI): m/z [M +Na] $^+$ calcd. for $C_{16}H_{14}ClNO_5SNa^+$: 390.0173, found: 390.0169.

(60) HPLC: EtOAc/hexane 6:4 (v/v), (t_R): 11 min (single peak). ^{1}H and ^{13}C NMR data are reported in **Table 5.6** HRMS (ESI): m/z [M-H]$^-$ calcd. for $C_{17}H_{13}F_3NO_5S$: 400.0461, found: 400.0491.

(61) HPLC: EtOAc/hexane 6:4 (v/v), (t_R): 21 min (single peak). ^{1}H and ^{13}C NMR data are reported in **Table 5.6.** HRMS (ESI): m/z [M-H]$^-$ calcd. for $C_{17}H_{13}F_3NO_5S$: 400.0461, found: 400.0492.

CHAPTER 7

SUPPORTING DATA

7.1. Mass Spectra

HRESI MS spectrum of phallusiasterol C (**6**)

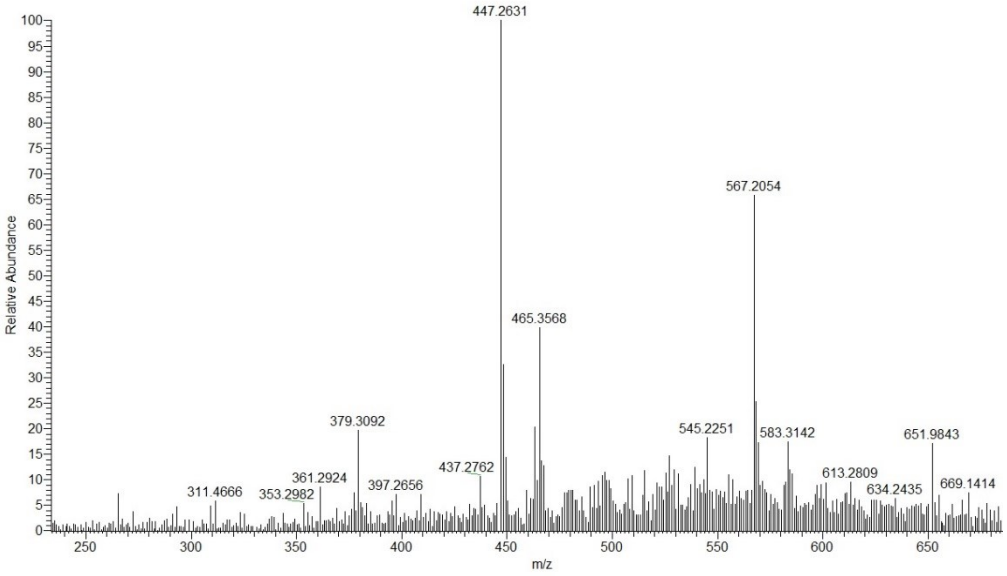

HRESI MS spectrum of compound **21**

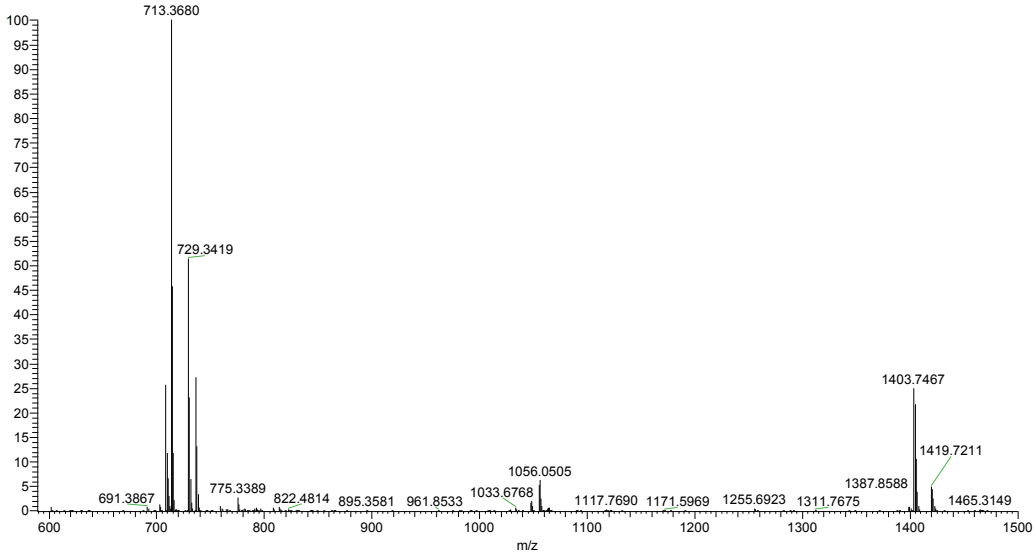

HRESI MS spectrum of compound **22**

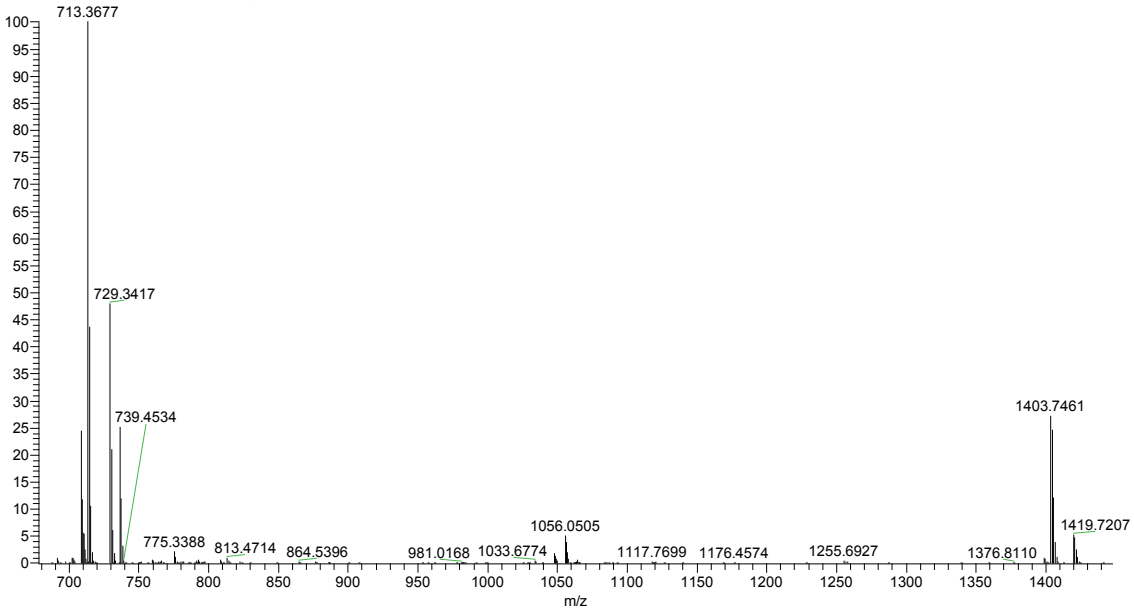

HRESI MS spectrum of compound **23**

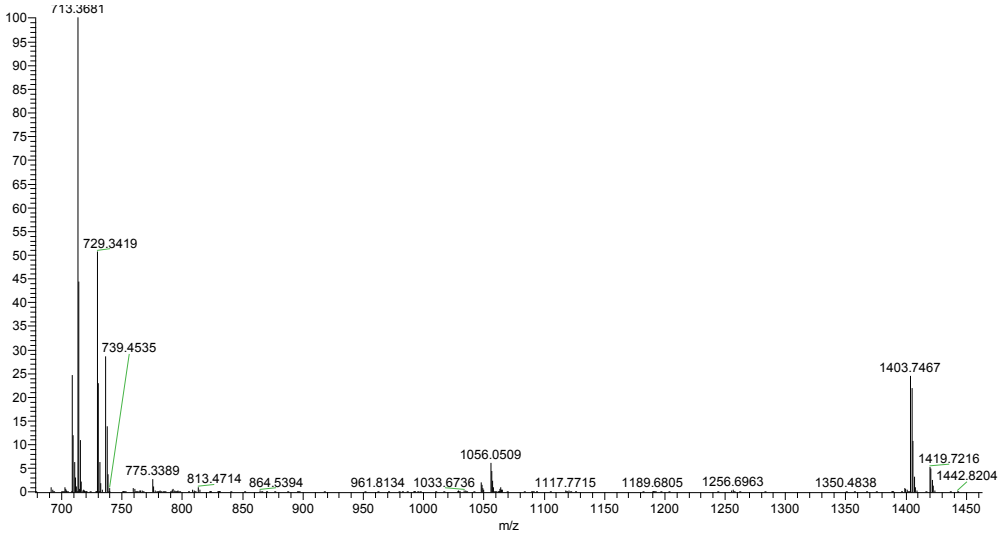

HRESI MS spectrum of compound **24**

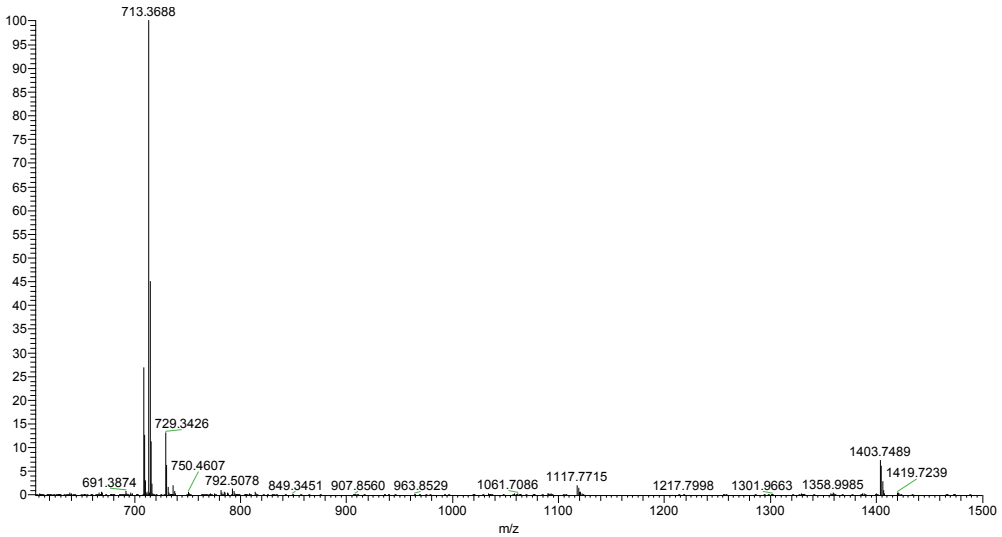

HRESI MS spectrum of compound **25**

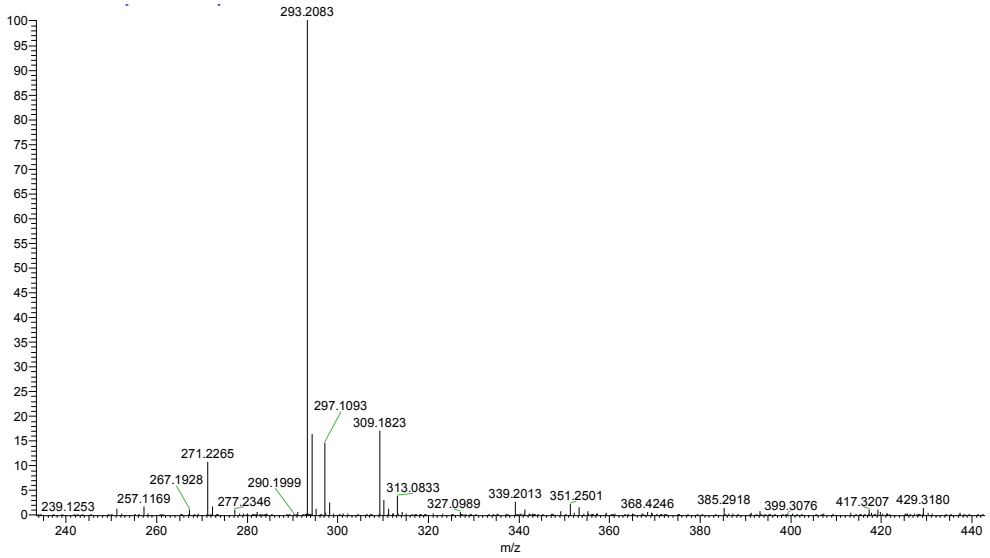

HRESI MS spectrum of compound **26**

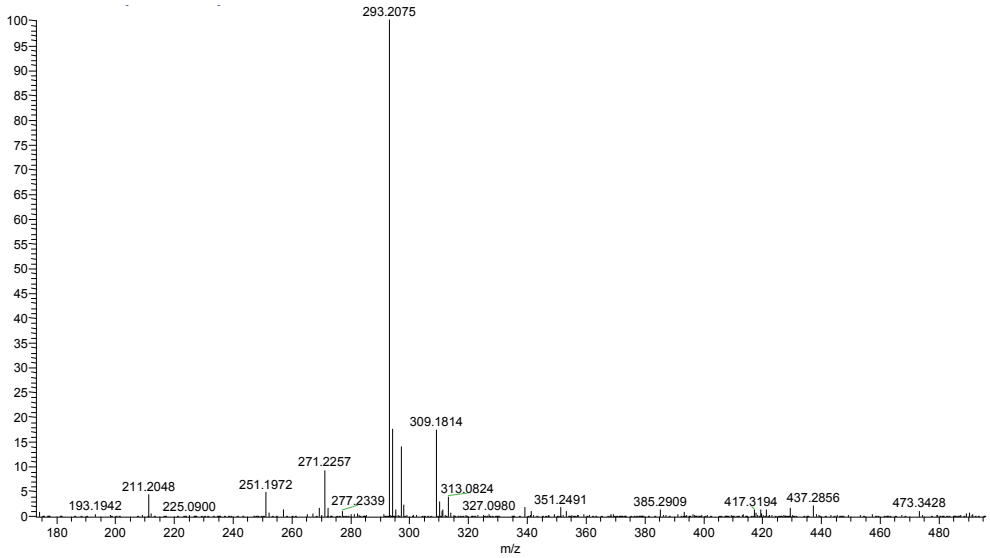

ESI MS spectrum of compound **39**

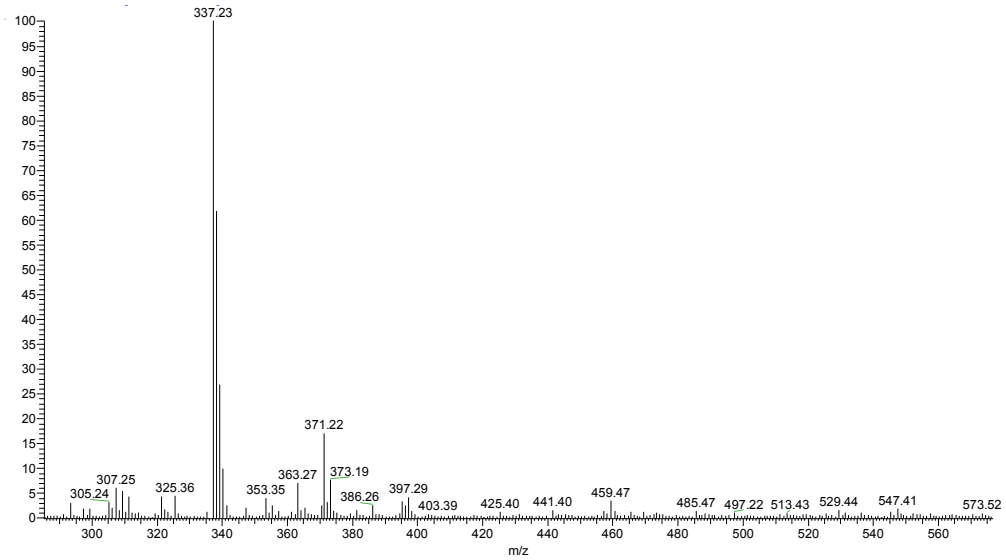

ESI MS spectrum of compound **40**

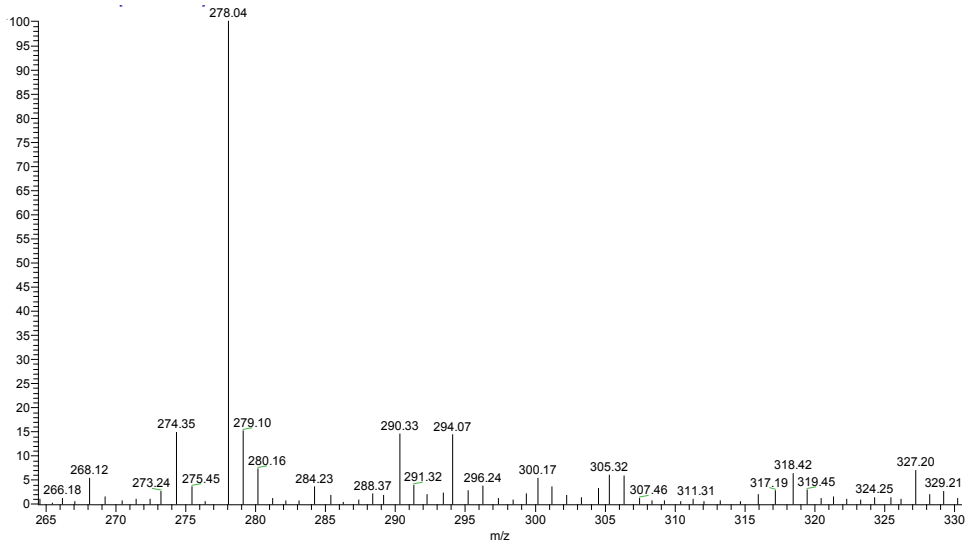

ESI MS spectrum of compound **41**

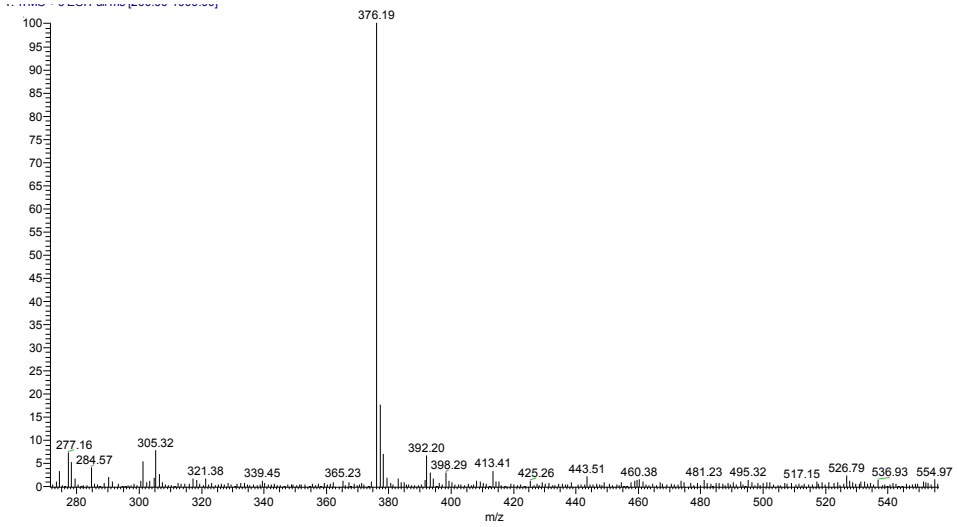

ESI MS spectrum of compound **42**

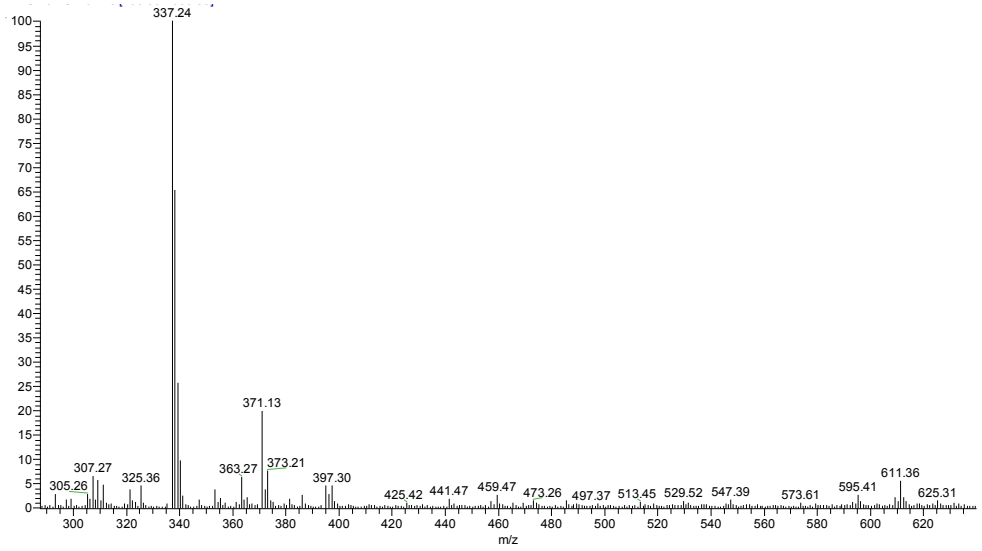

HRESI MS spectrum of compound **46**

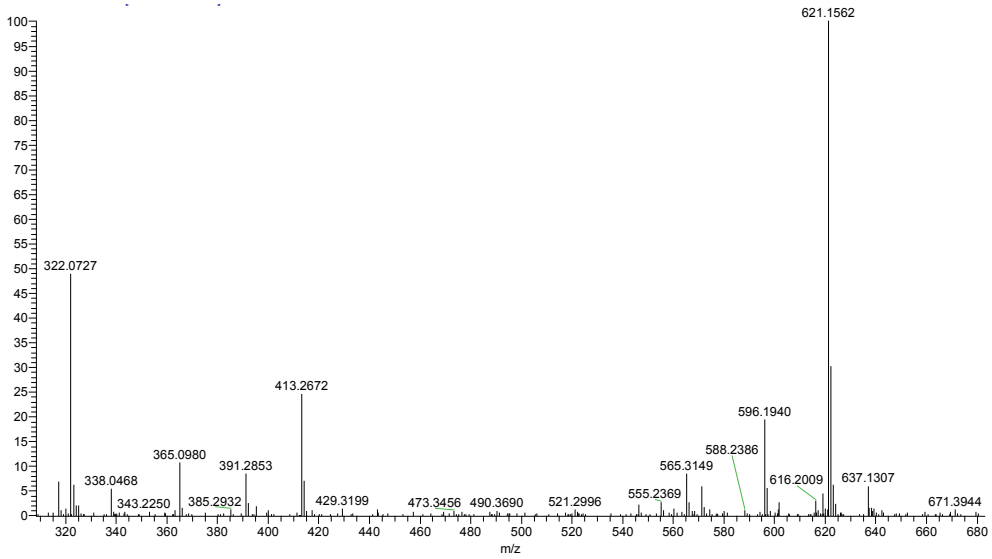

HRESI MS spectrum of compound **47**

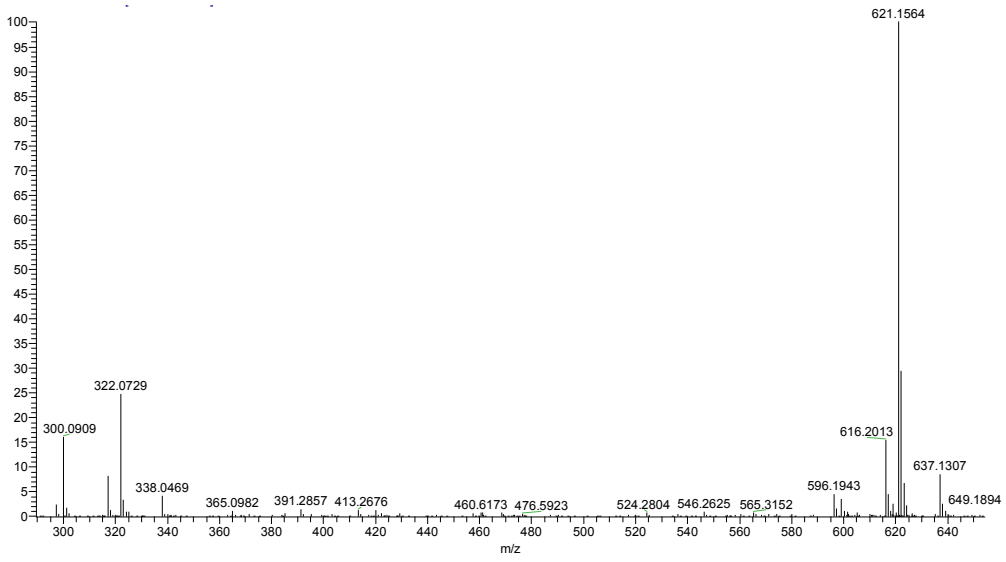

HRESI MS spectrum of compound **48**

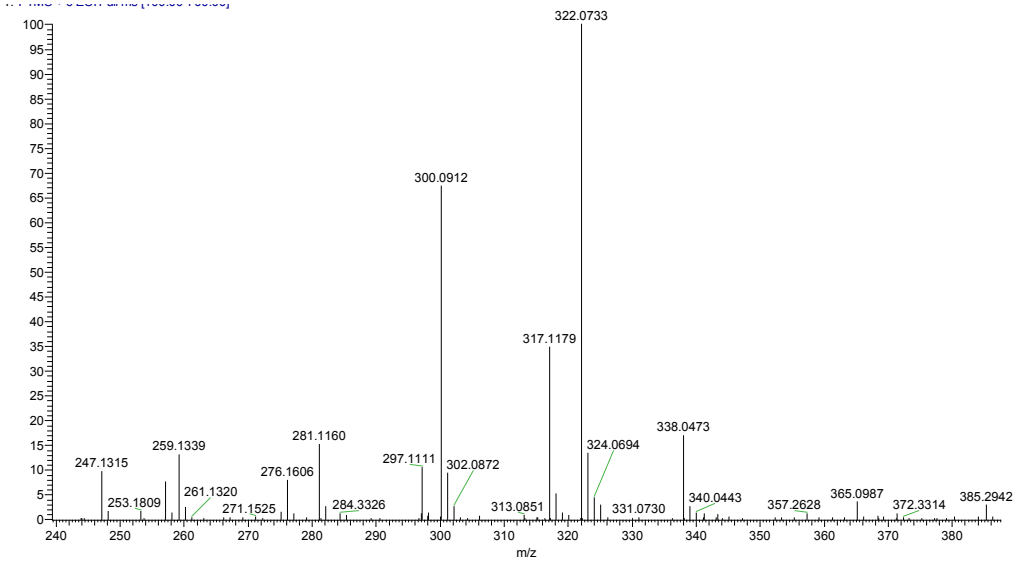

HRESI MS spectrum of compound **49**

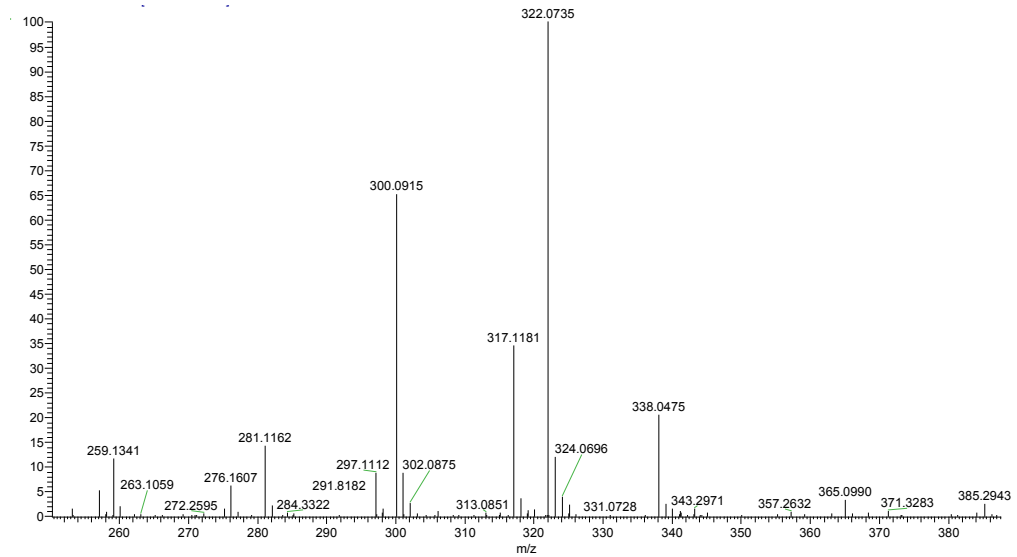

HRESI MS spectrum of compound **50**

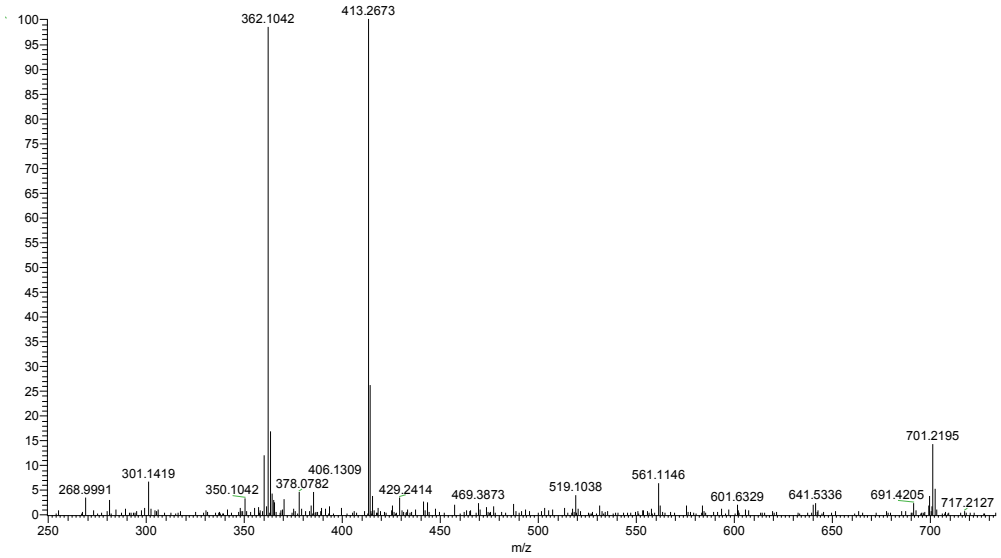

HRESI MS spectrum of compound **51**

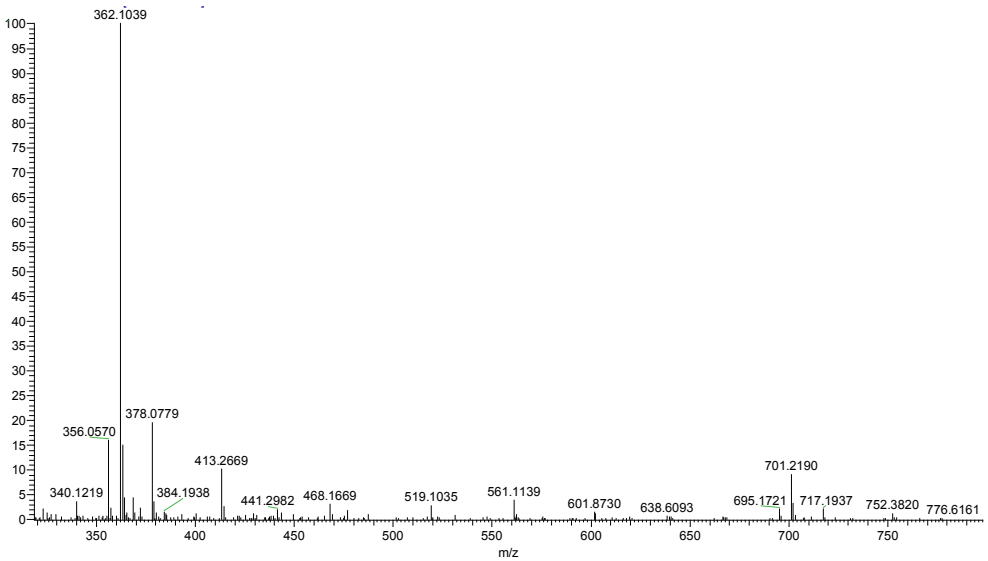

HRESI MS spectrum of compound **56**

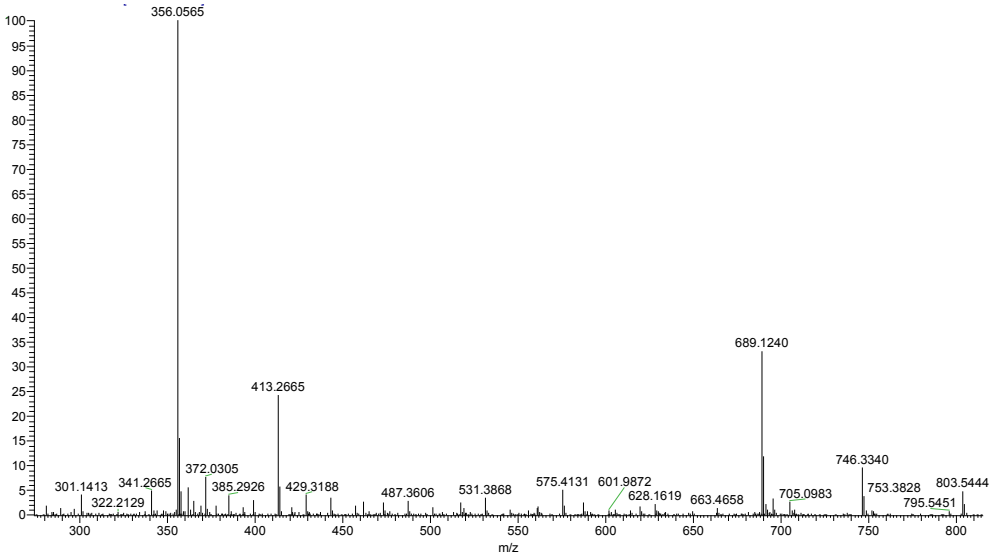

HRESI MS spectrum of compound **57**

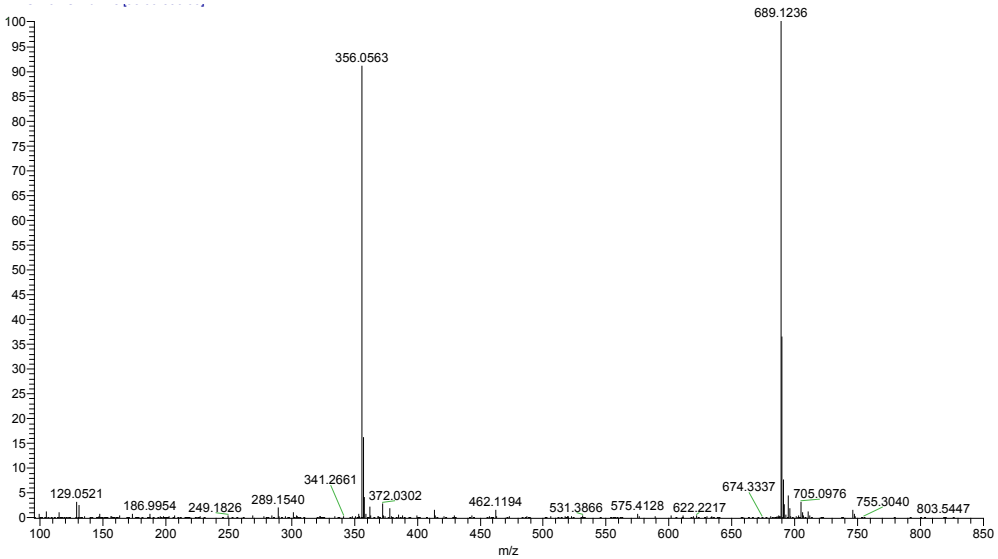

HRESI MS spectrum of compound **58**

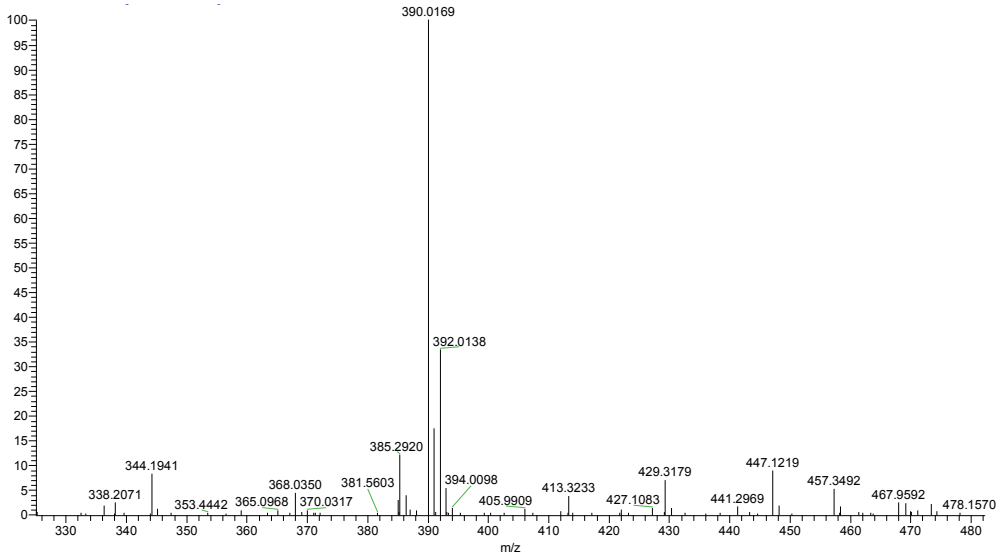

HRESI MS spectrum of compound **59**

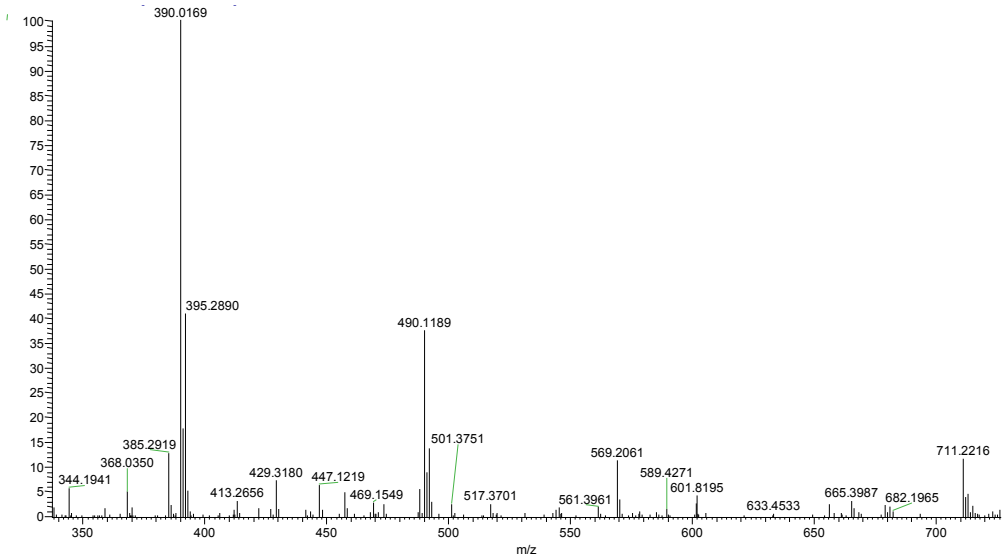

HRESI MS spectrum of compound **60**

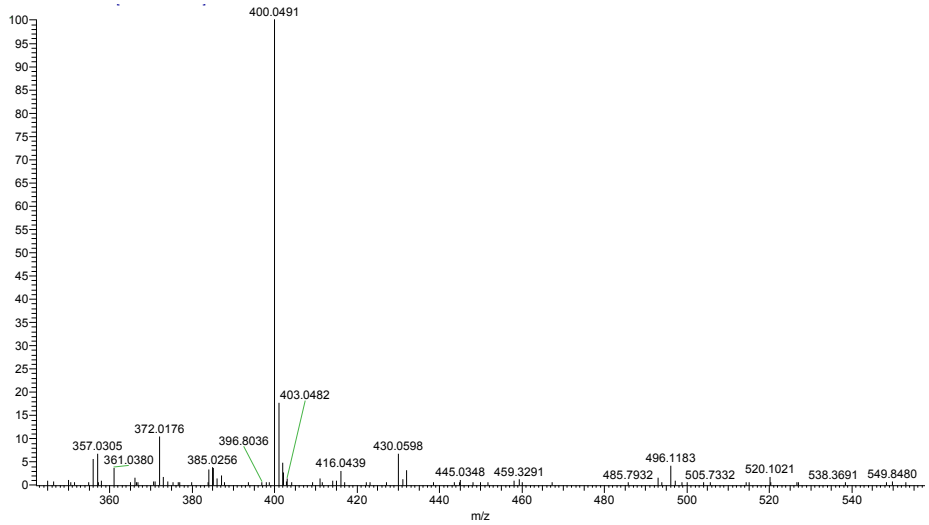

HRESI MS spectrum of compound **61**

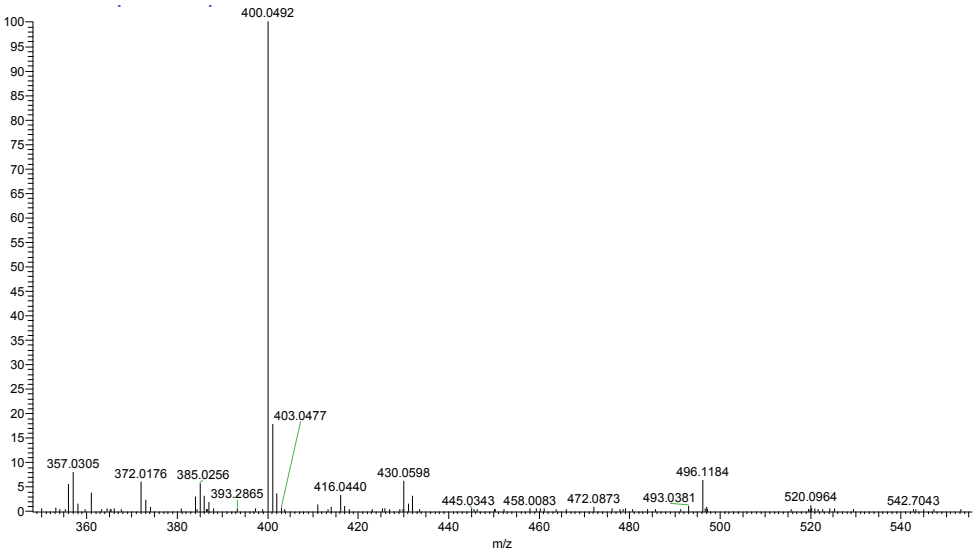

7.2. NMR Spectra

^{1}H-NMR CD_3OD of compound **6**

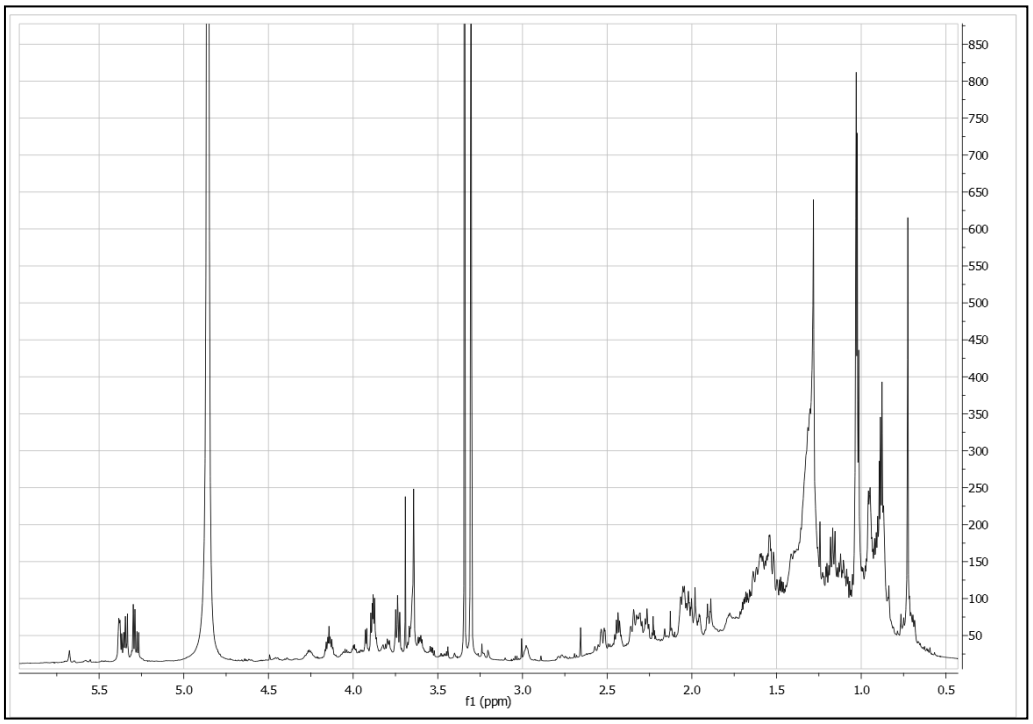

^{13}C-NMR CD_3OD of compound **6**

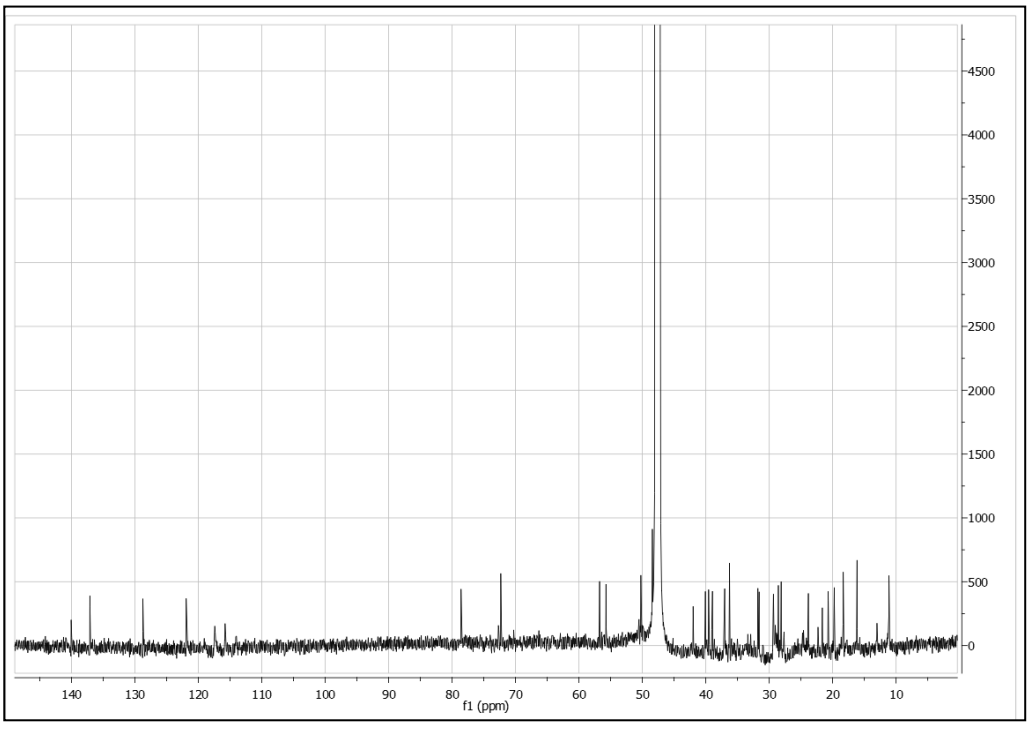

COSY of compound **6** (CD_3OD)

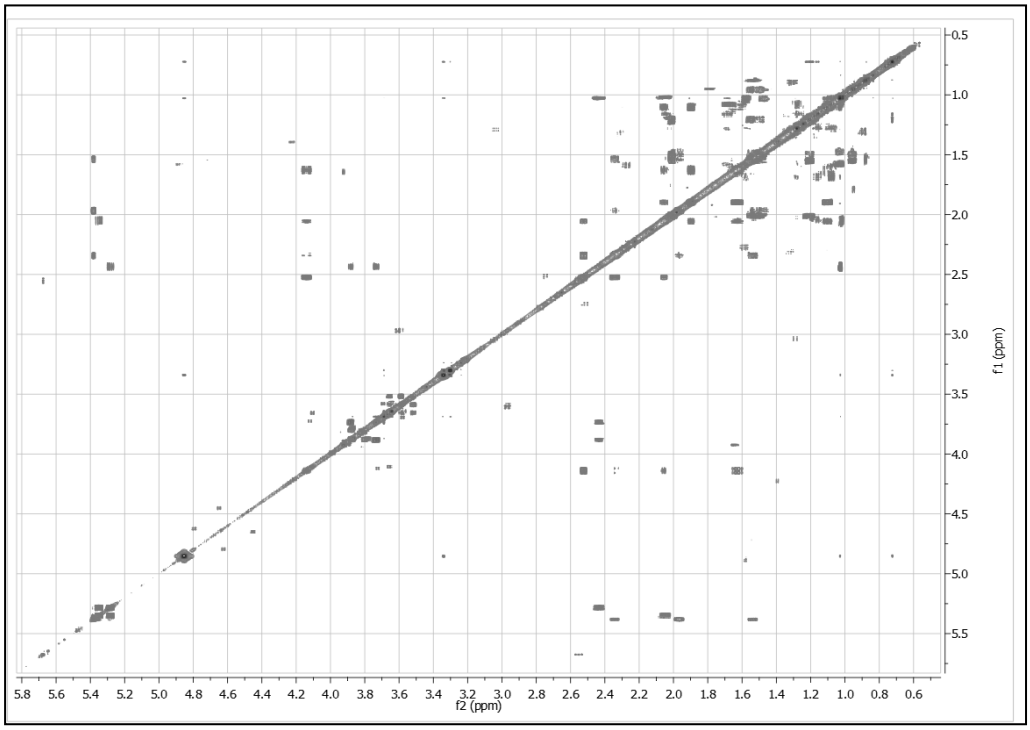

HMBC of compound **6** (CD_3OD

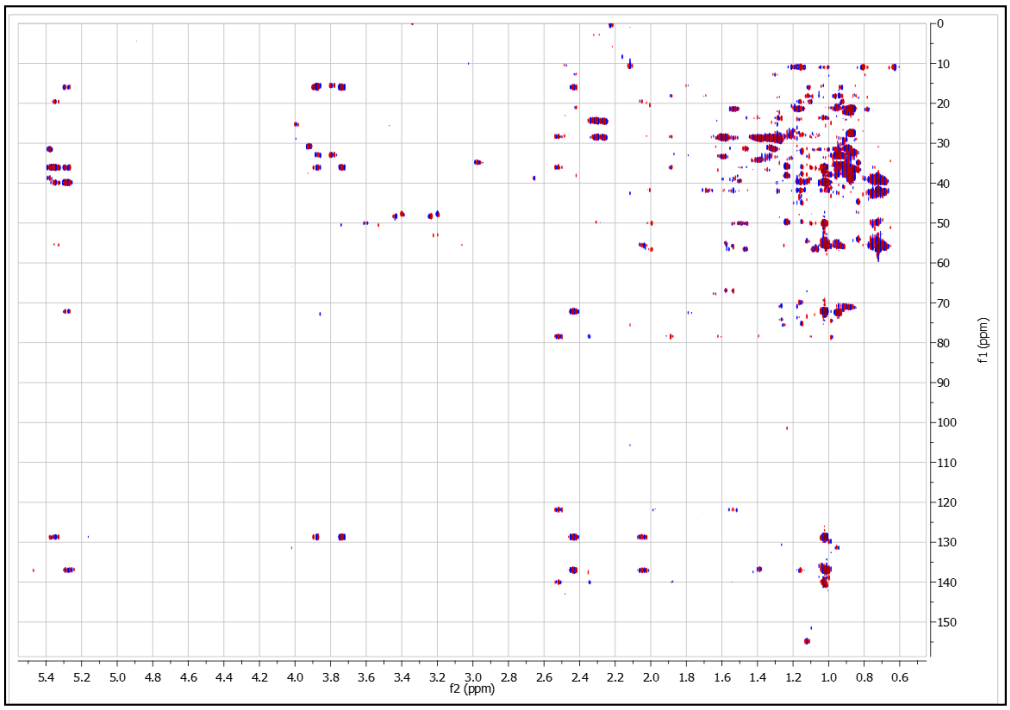

ROESY of compound **6** (CD_3OD)

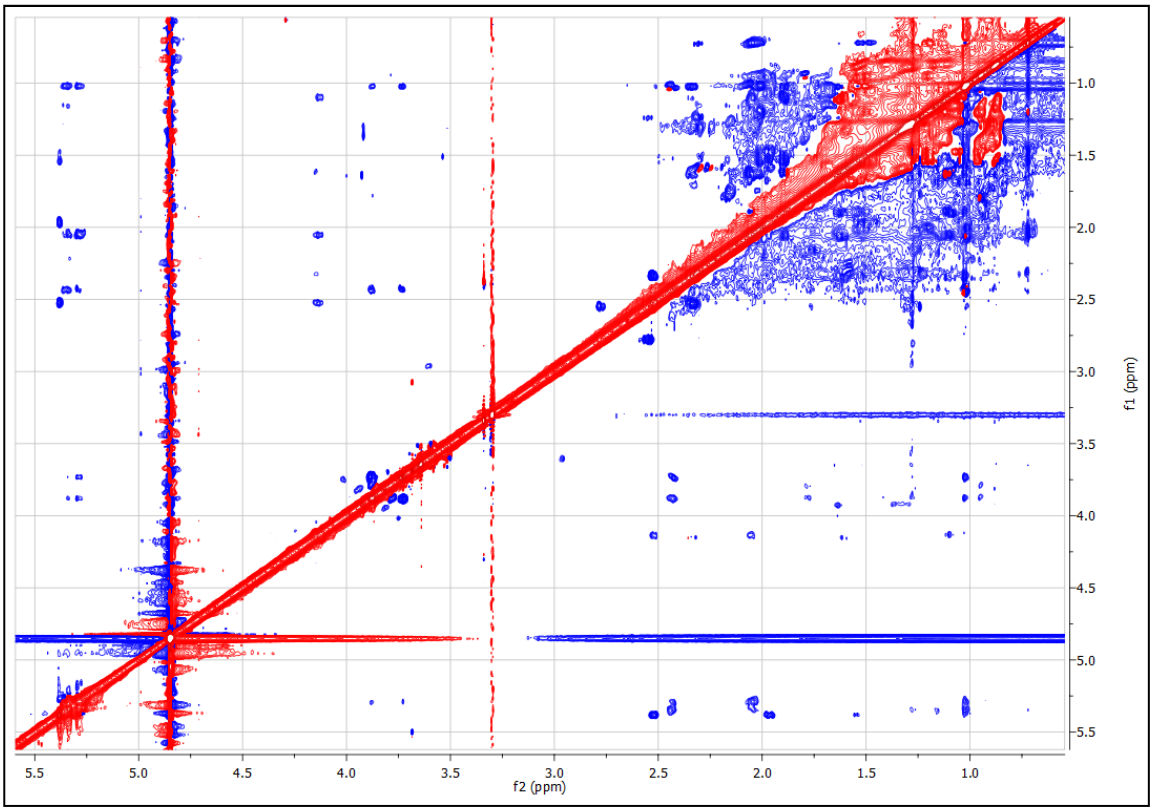

^{1}H NMR of compound (**18**) in $CDCl_3$

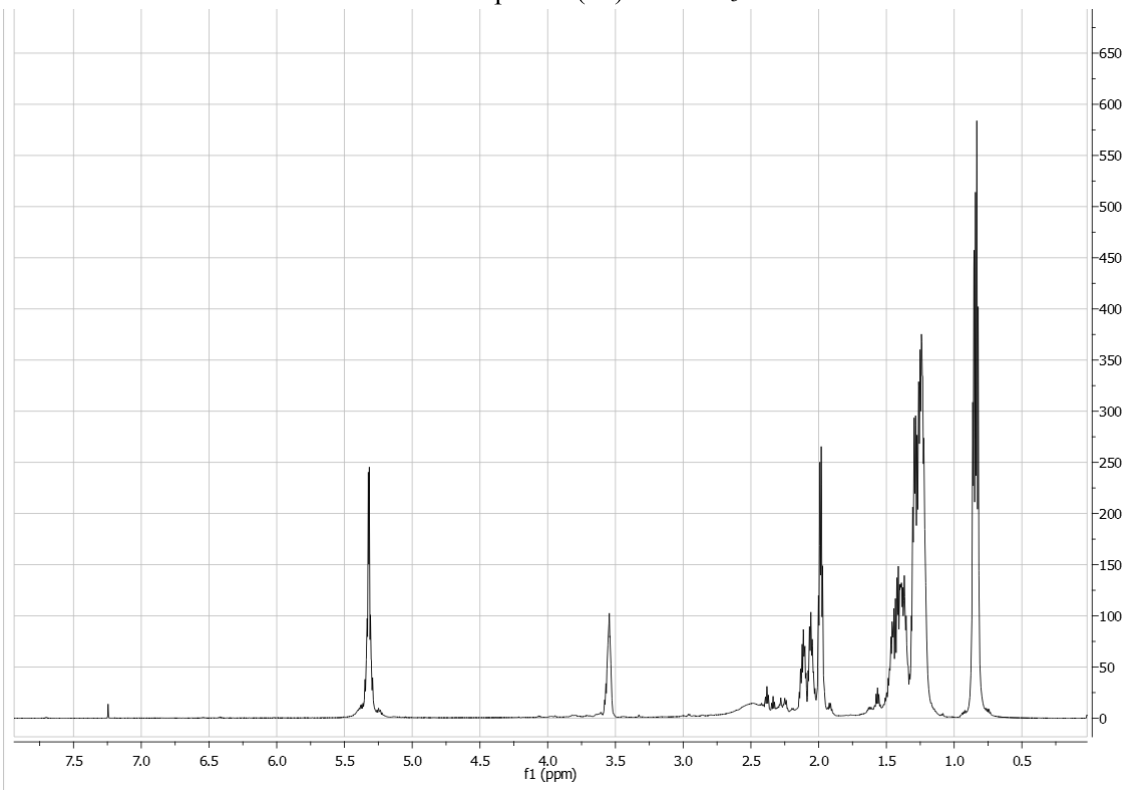

^{13}C NMR of compound (**18**) in $CDCl_3$

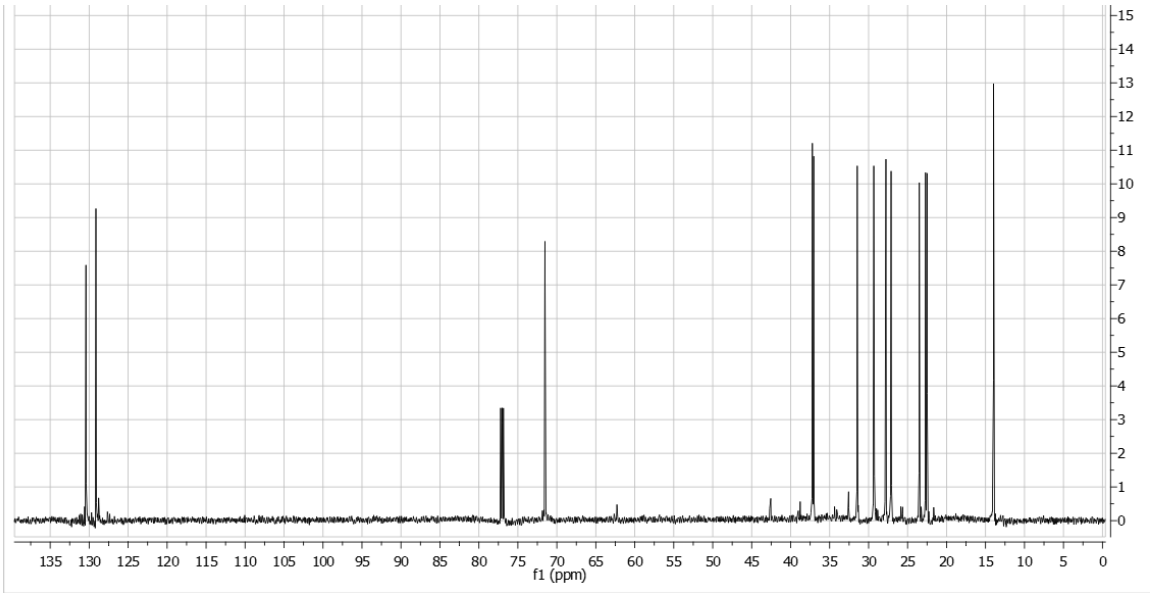

^{1}H NMR of compound (*rac*-**19**) in CD_3OD

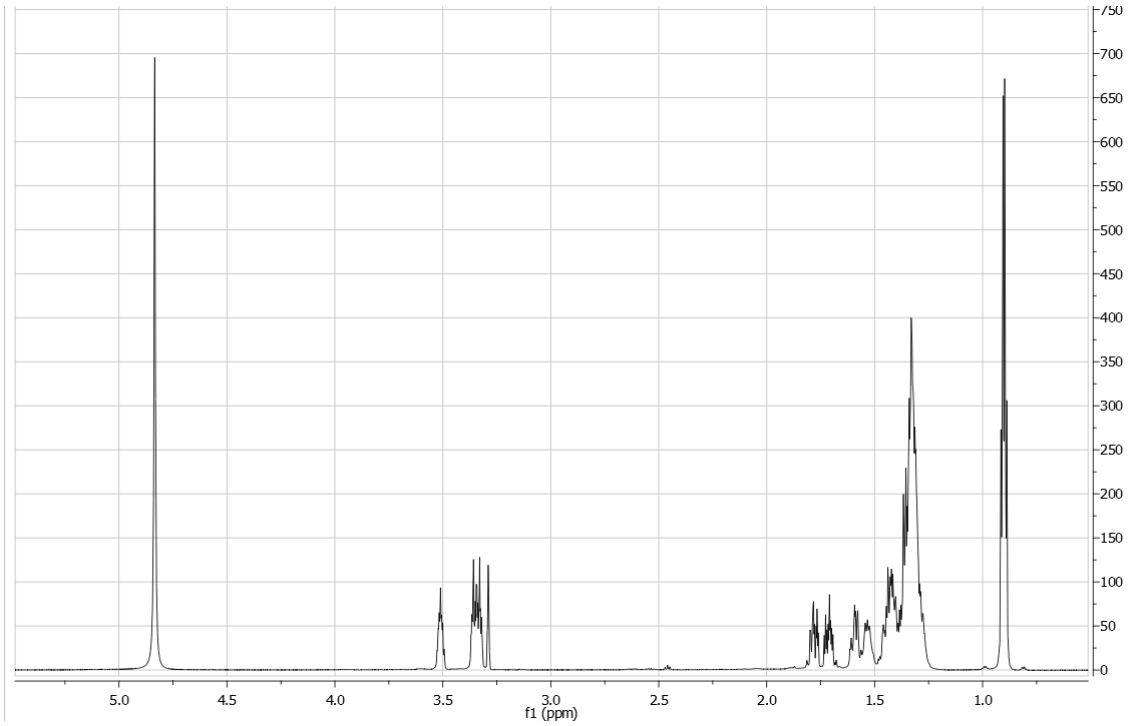

^{13}C NMR of compound (*rac*-**19**) in CD_3OD

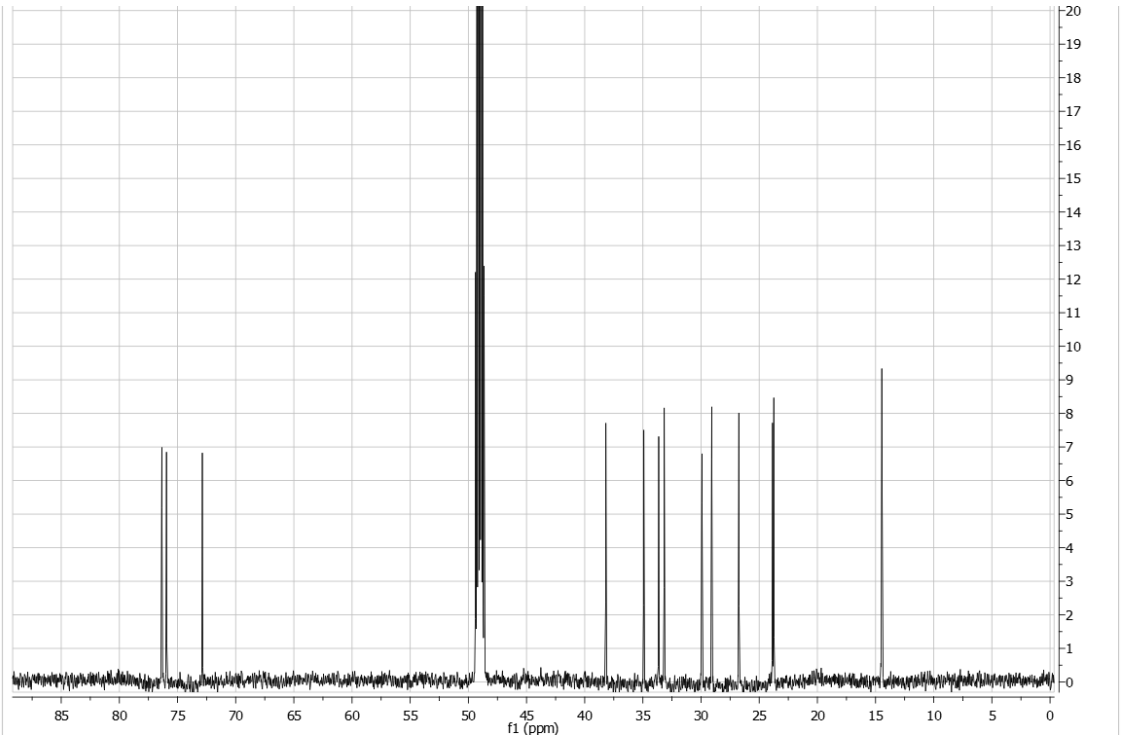

^{1}H NMR of compound (*rac*-**20**) in CD_3OD

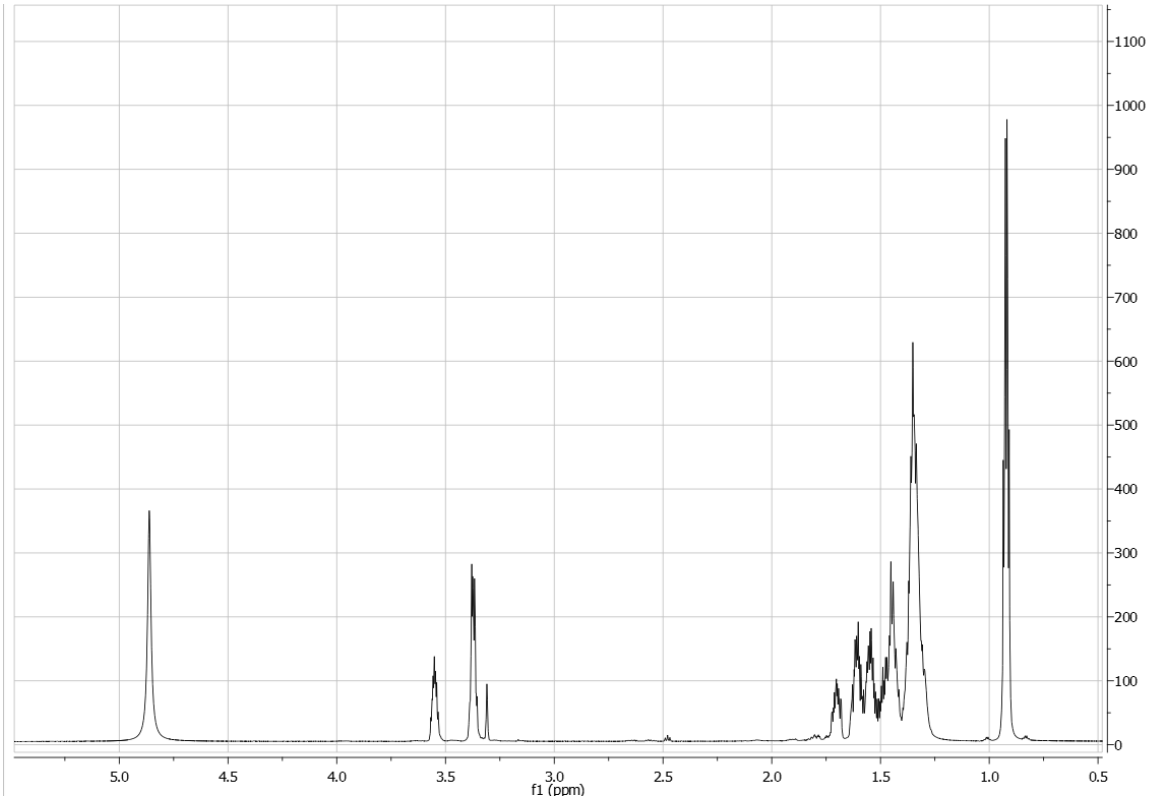

^{13}C NMR of compound (*rac*-**20**) in CD_3OD

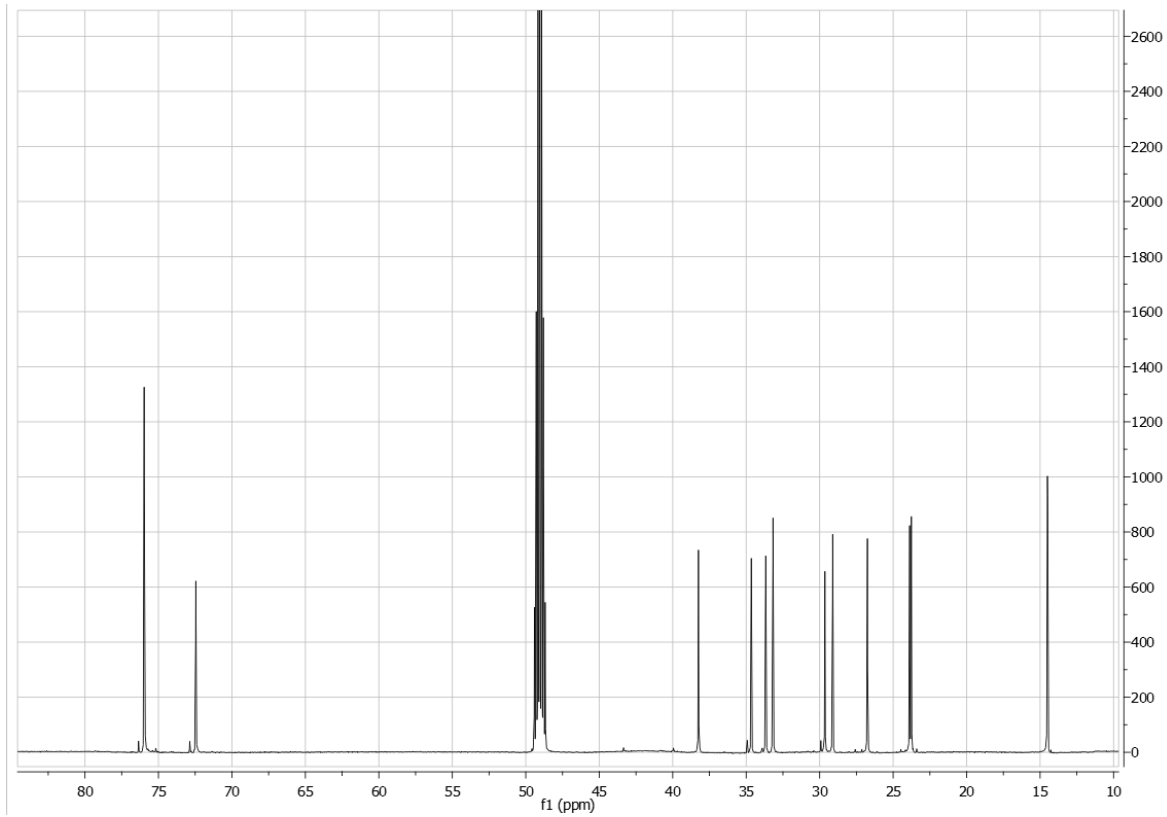

^{1}H NMR of compound (**21**) in $CDCl_3$

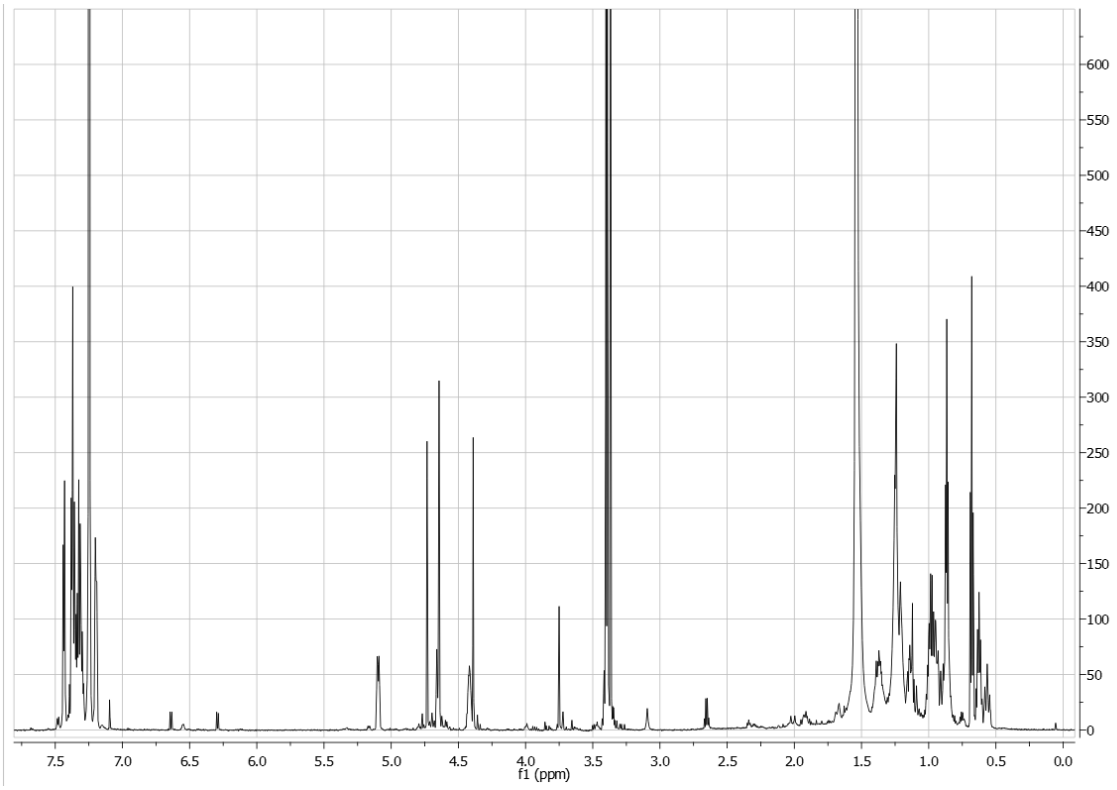

^{1}H NMR of compound (**22**) in $CDCl_3$

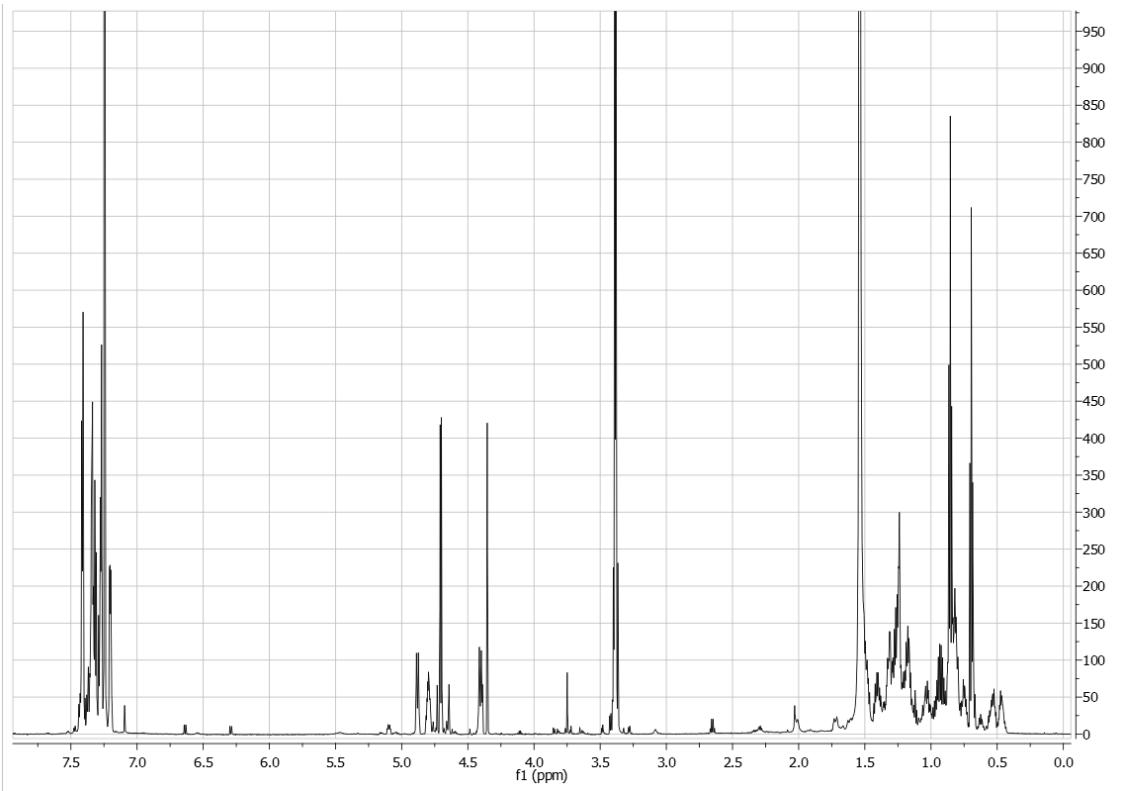

^{1}H NMR of compound (**23**) in $CDCl_3$

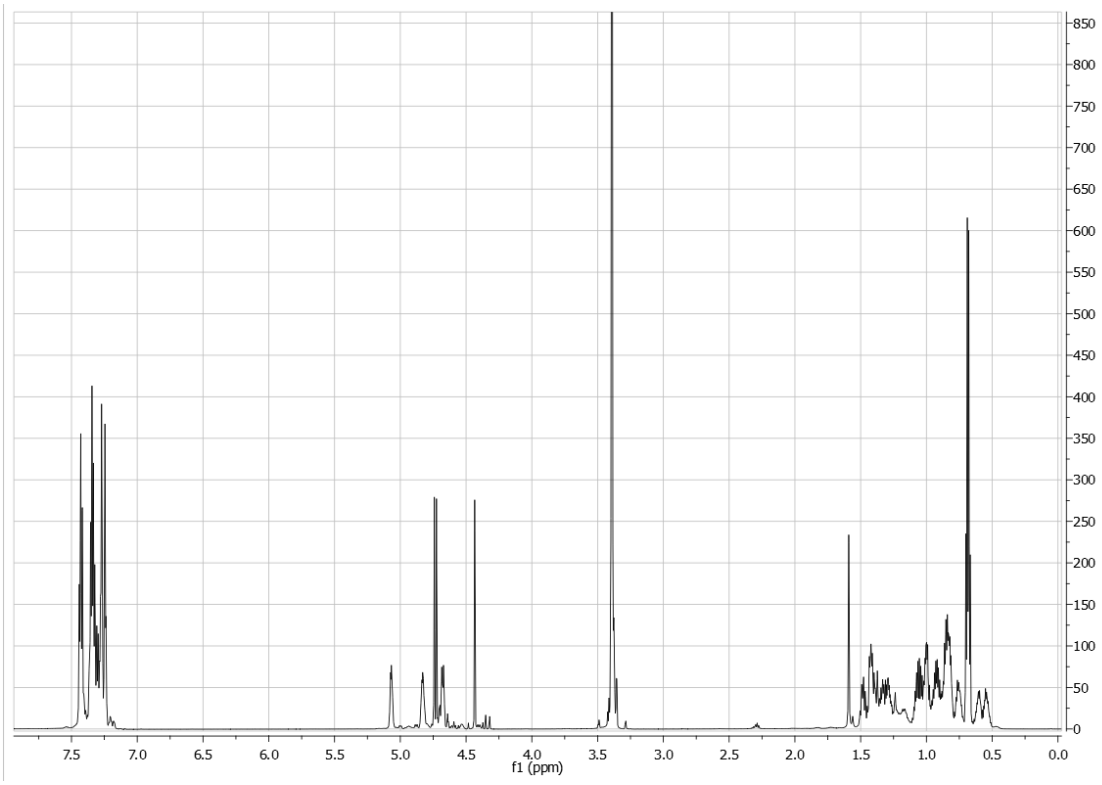

^{1}H NMR of compound (**24**) in $CDCl_3$

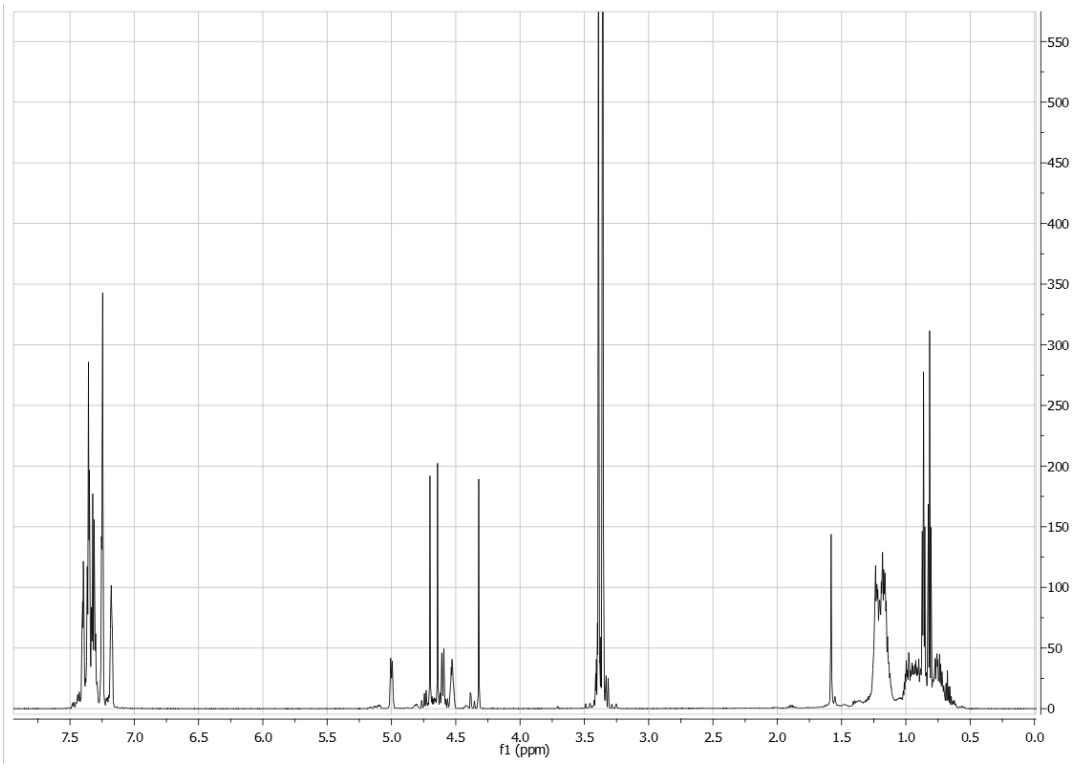

^{1}H NMR of compound (**25**) in $CDCl_3$

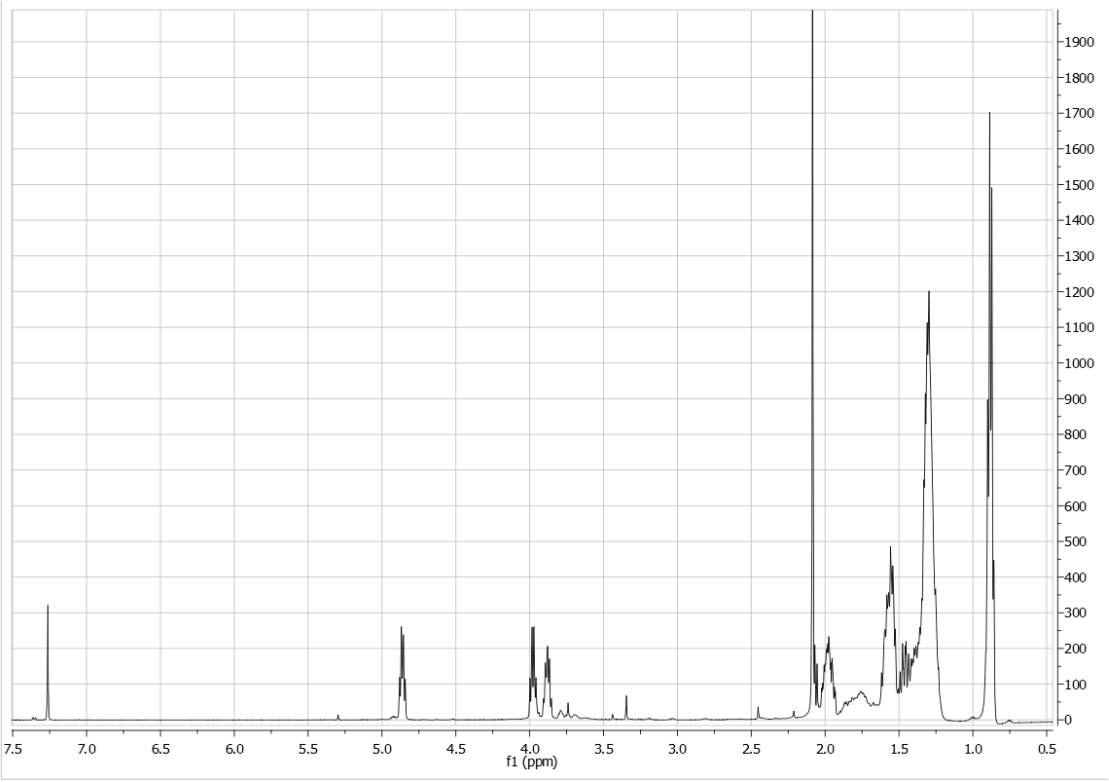

HSQC of compound **25** in $CDCl_3$

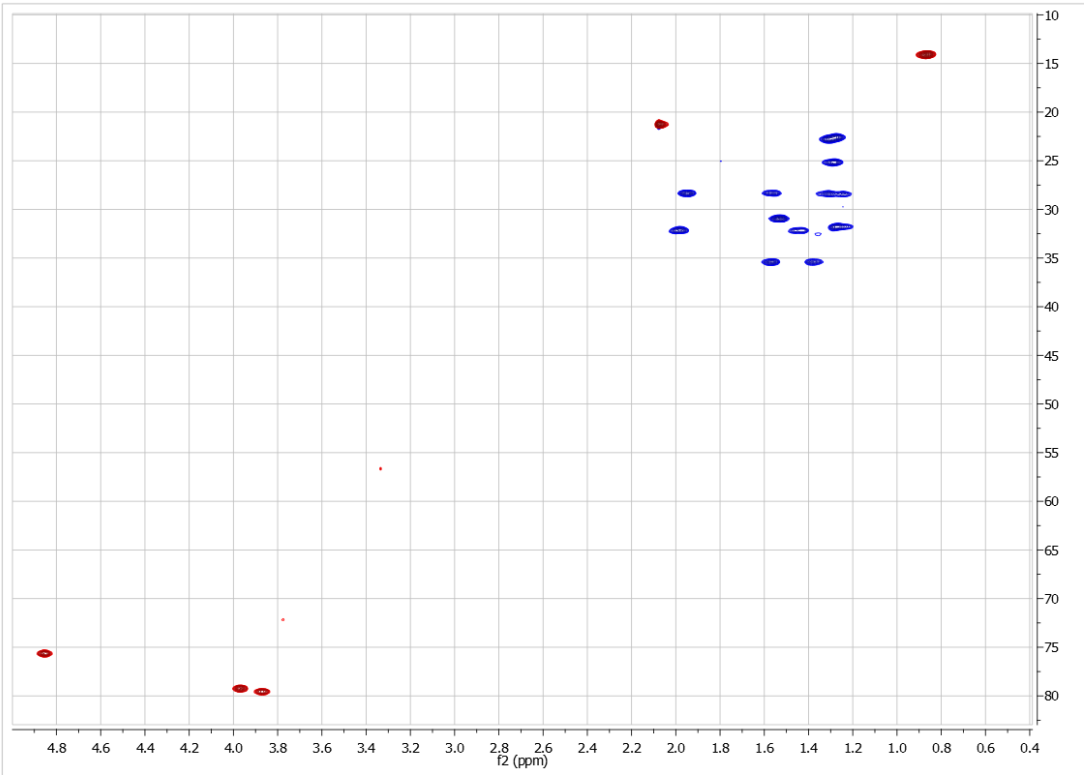

ROESY of compound **25** in $CDCl_3$

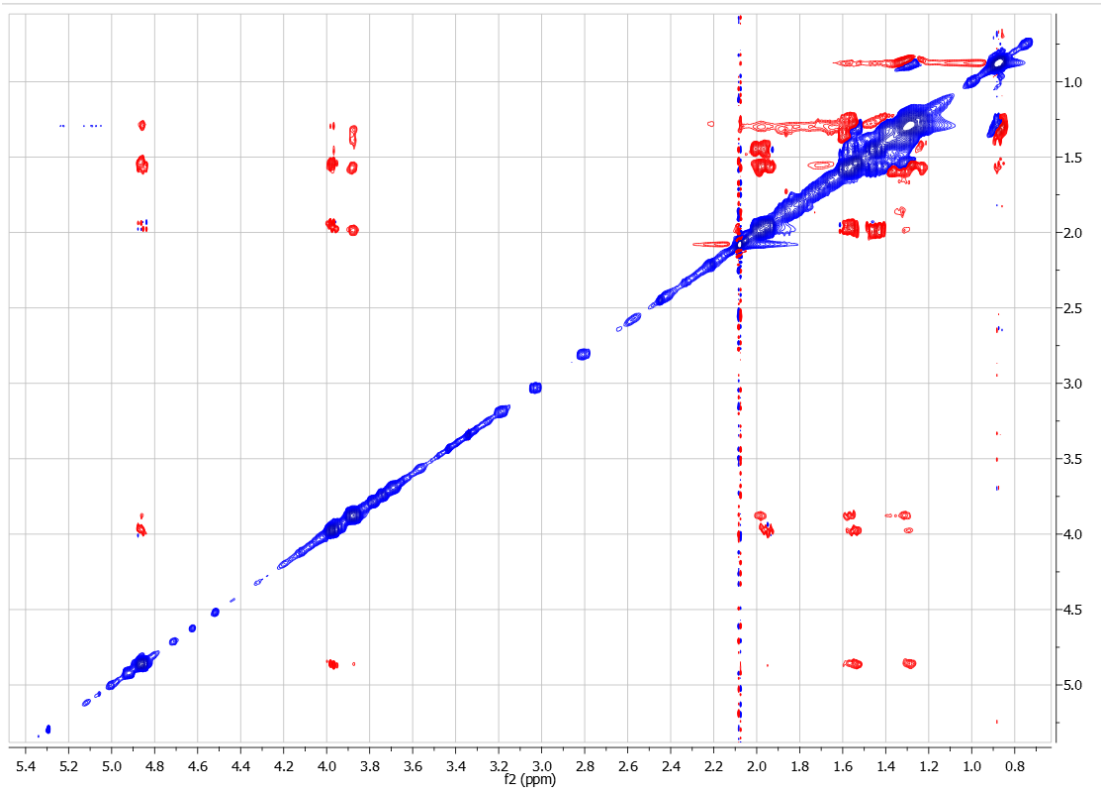

^{1}H NMR of compound **26** in $CDCl_3$

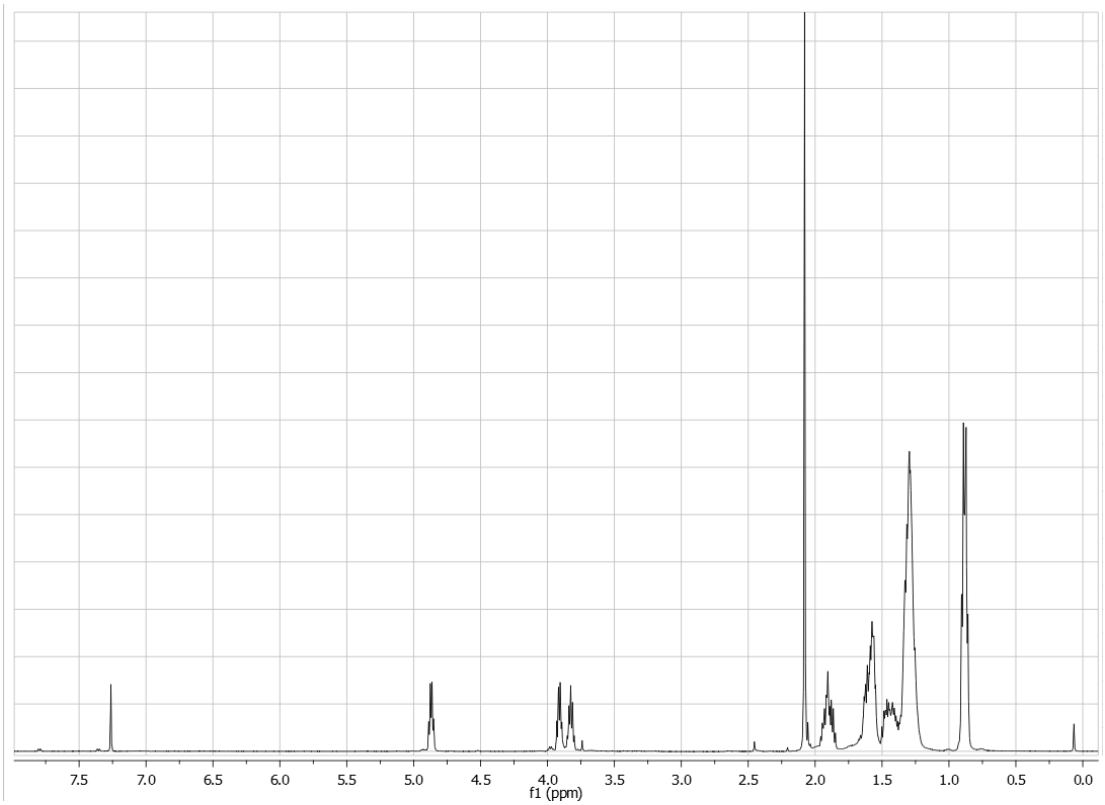

HSQC of compound **26** in $CDCl_3$

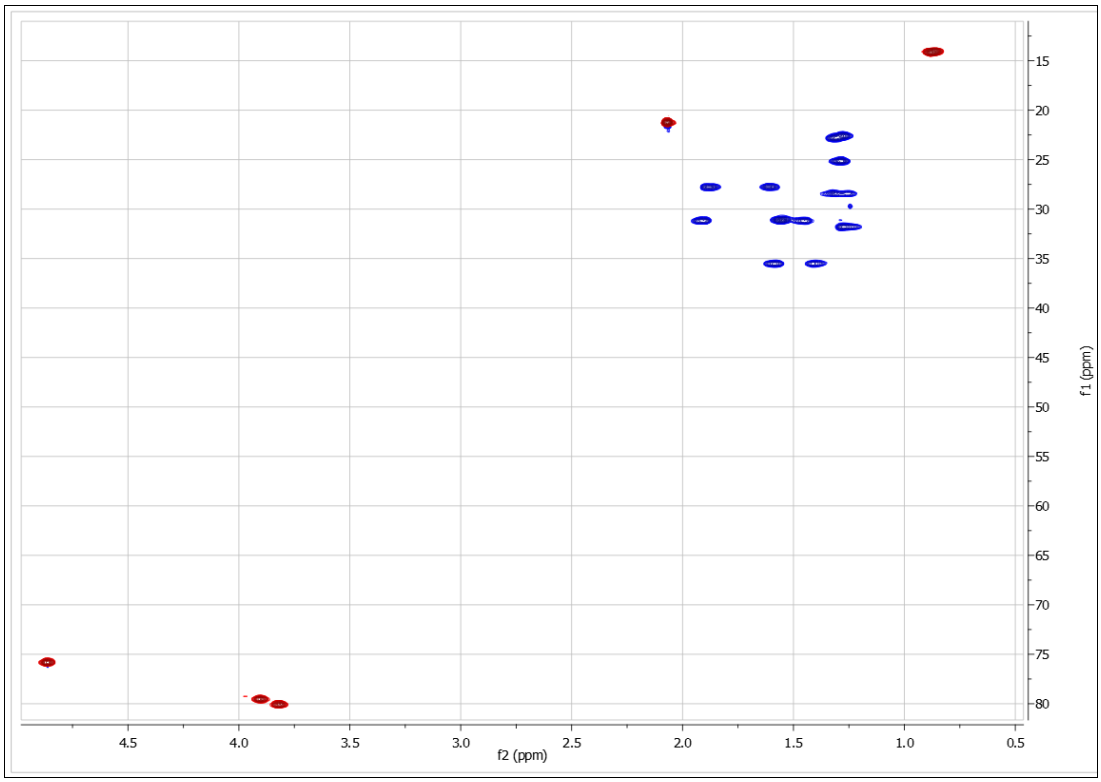

ROESY of compound **26** in $CDCl_3$

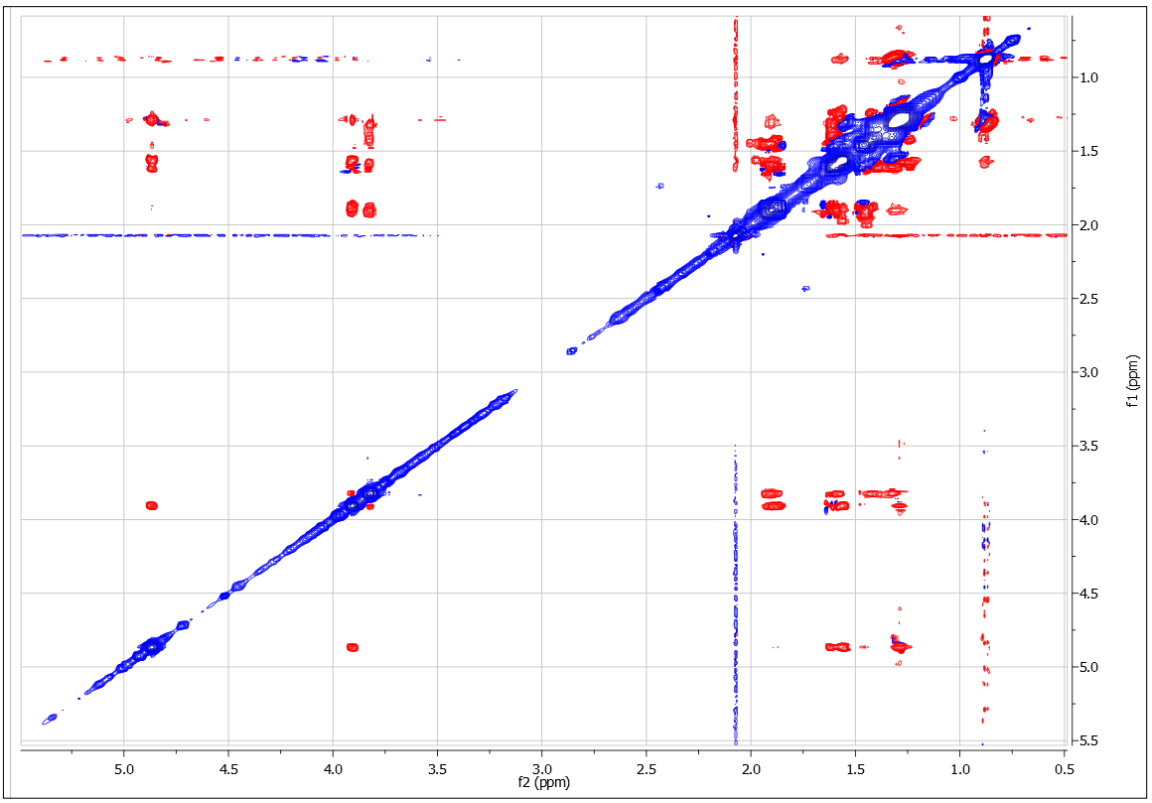

^{1}H NMR of compound **39**in CD_3OD

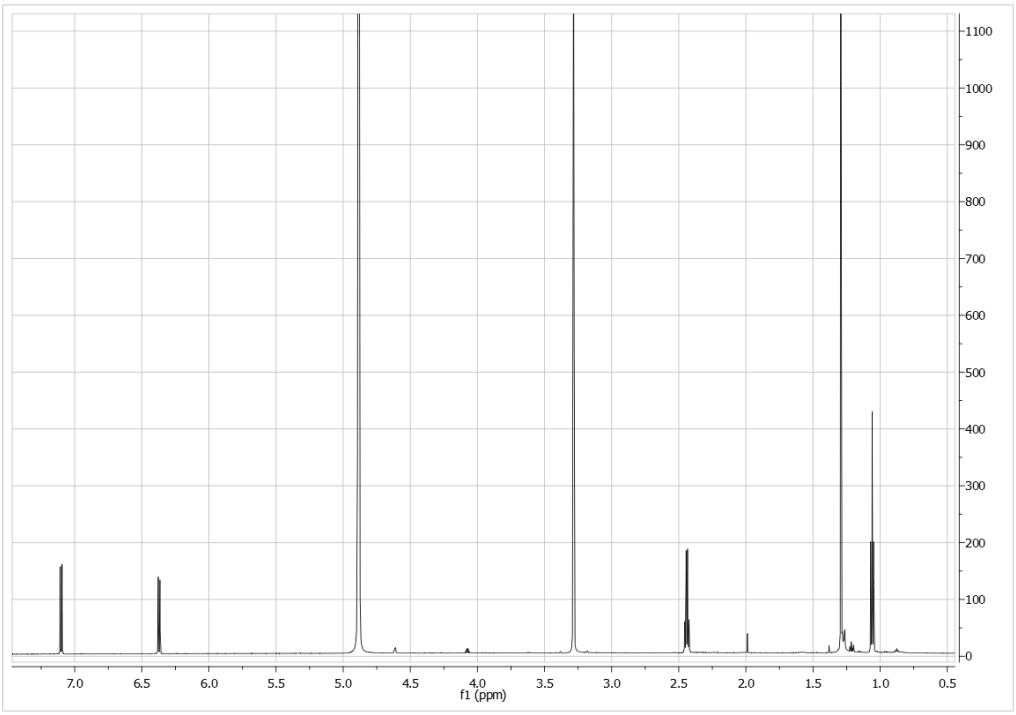

^{13}C NMR of compound **39** in CD_3OD

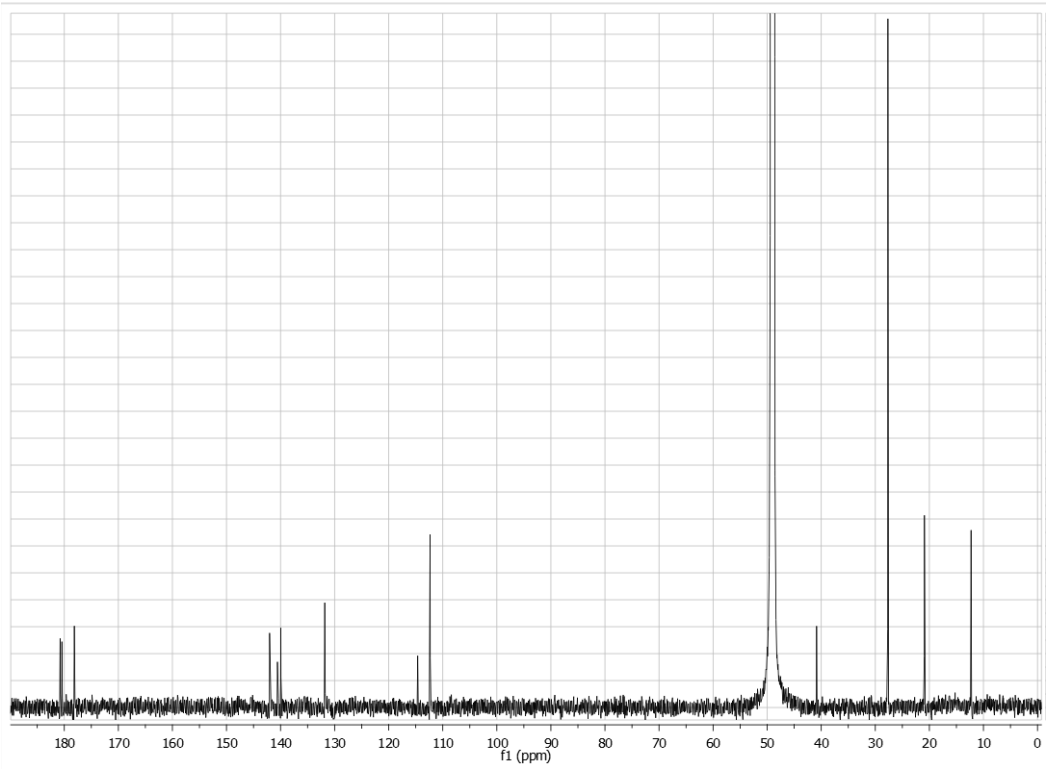

^{1}H NMR of compound **40** in CD_3OD

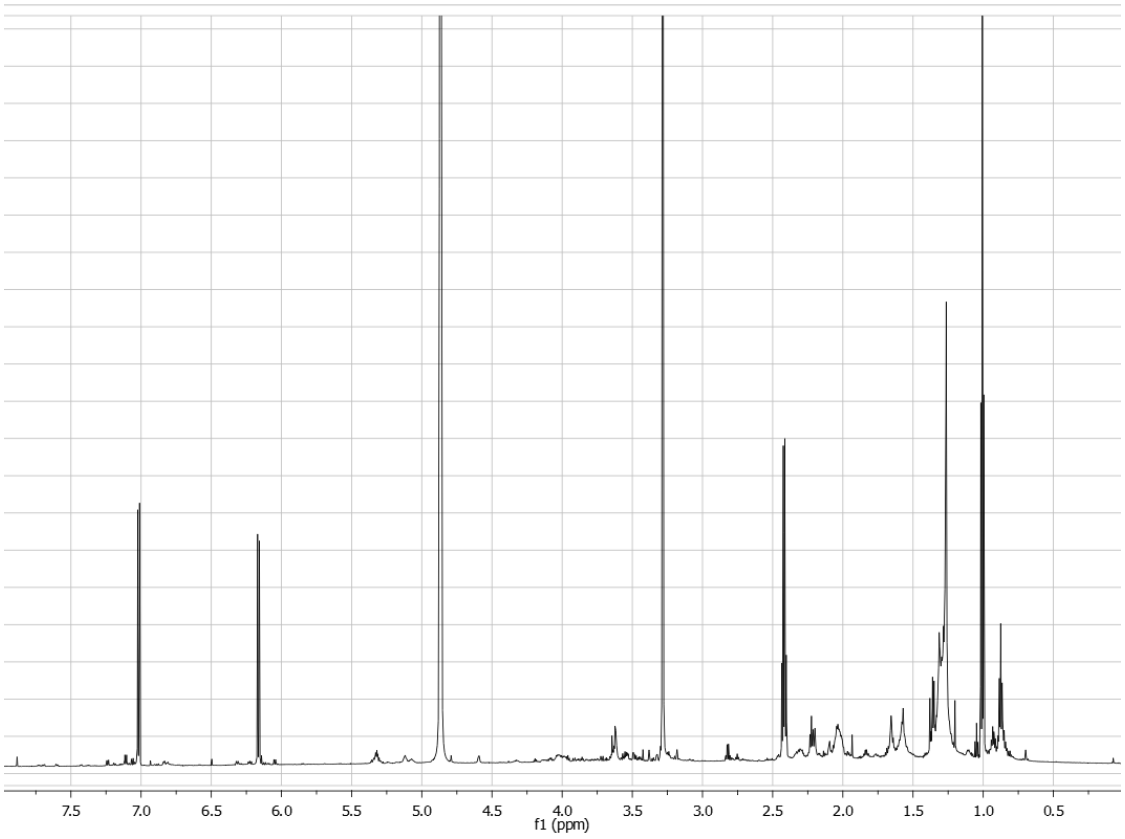

^{13}C NMR of compound **40** in CD_3OD

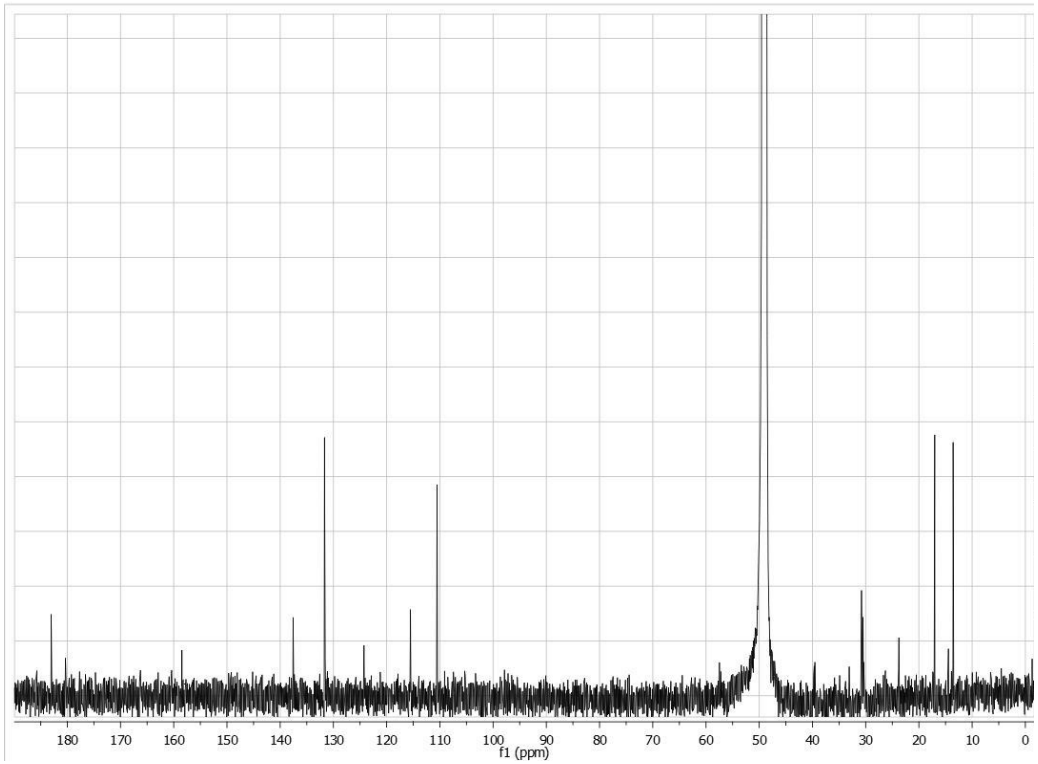

^{1}H NMR of compound **41** in DMSO-d6

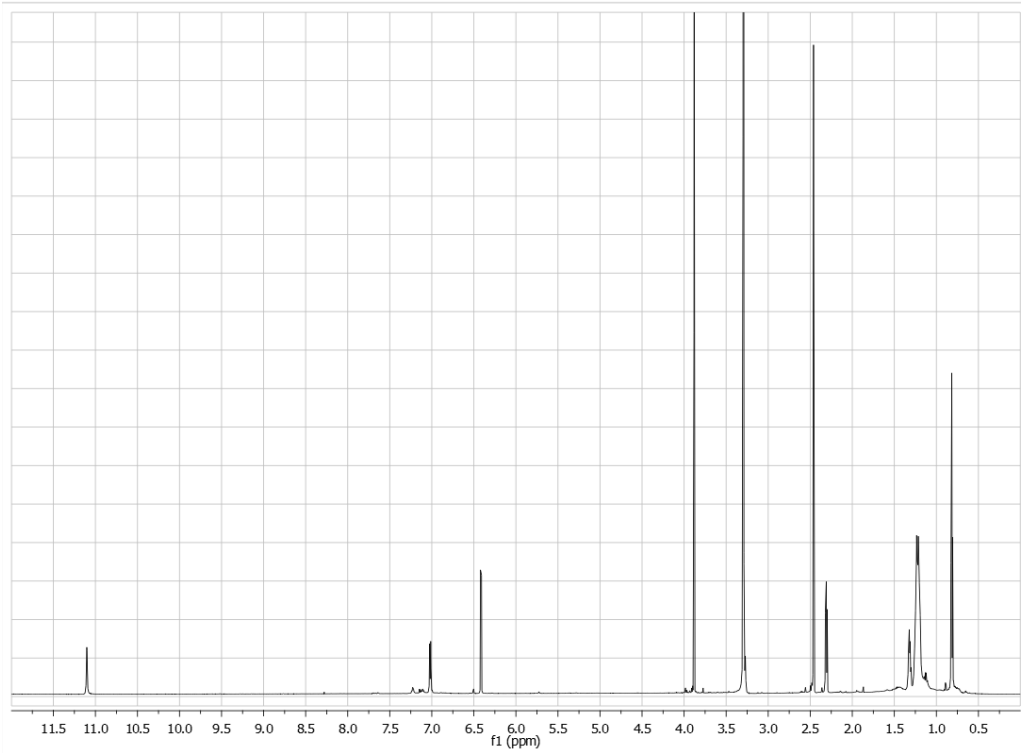

^{13}C NMR of compound **41** in DMSO-d6

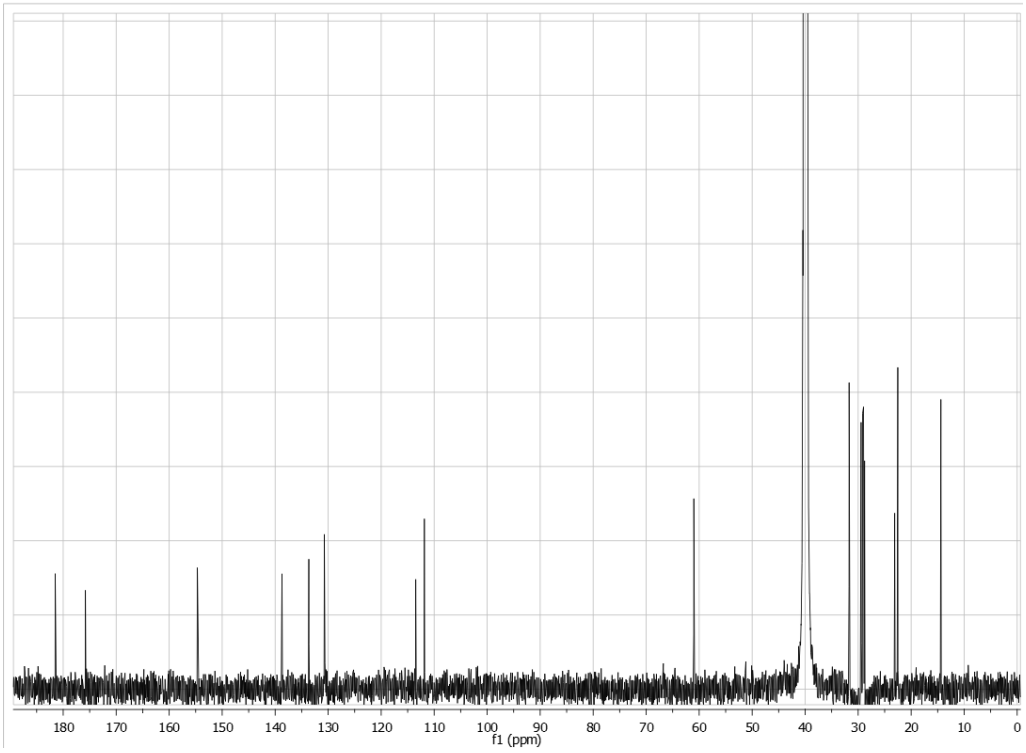

^{1}H NMR of compound **42** in CD_3OD

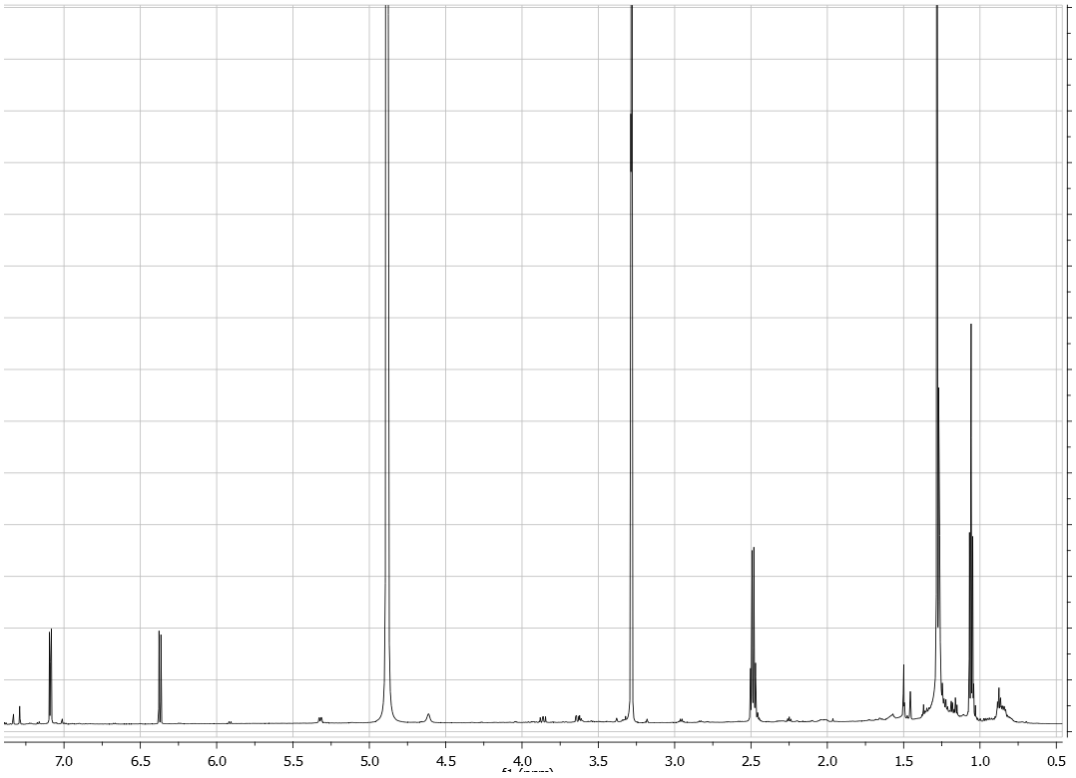

^{13}C NMR of compound **42** in CD_3OD

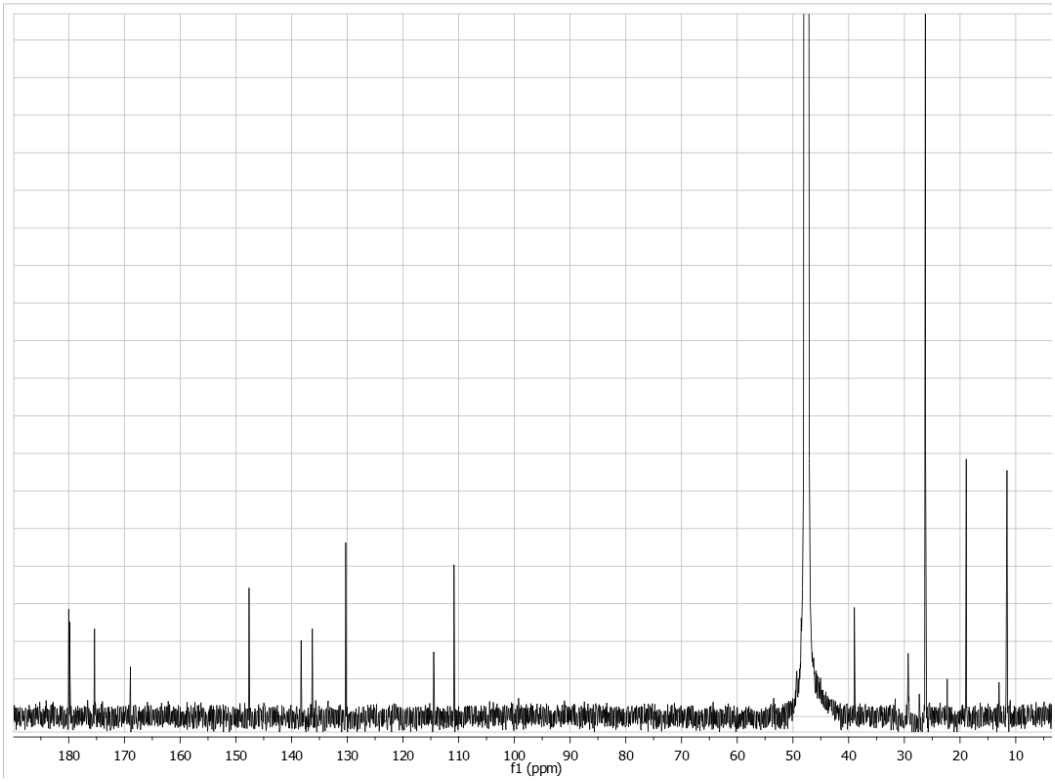

^{1}H NMR of compound **46** in $CDCl_3$

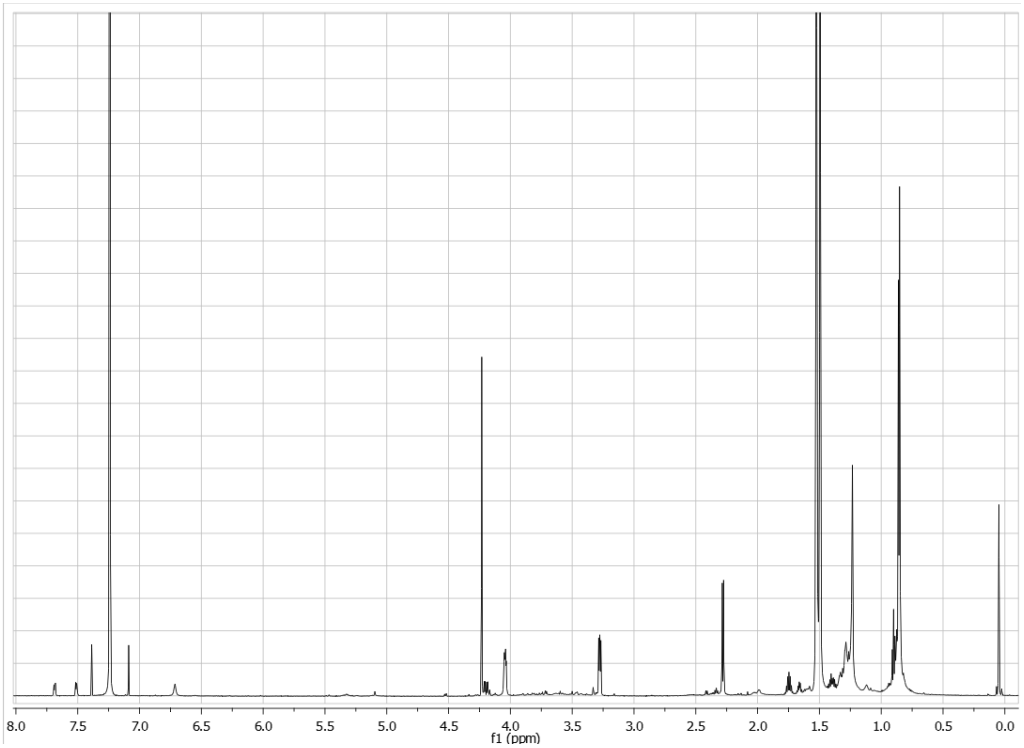

^{1}H NMR of compound **47** in $CDCl_3$

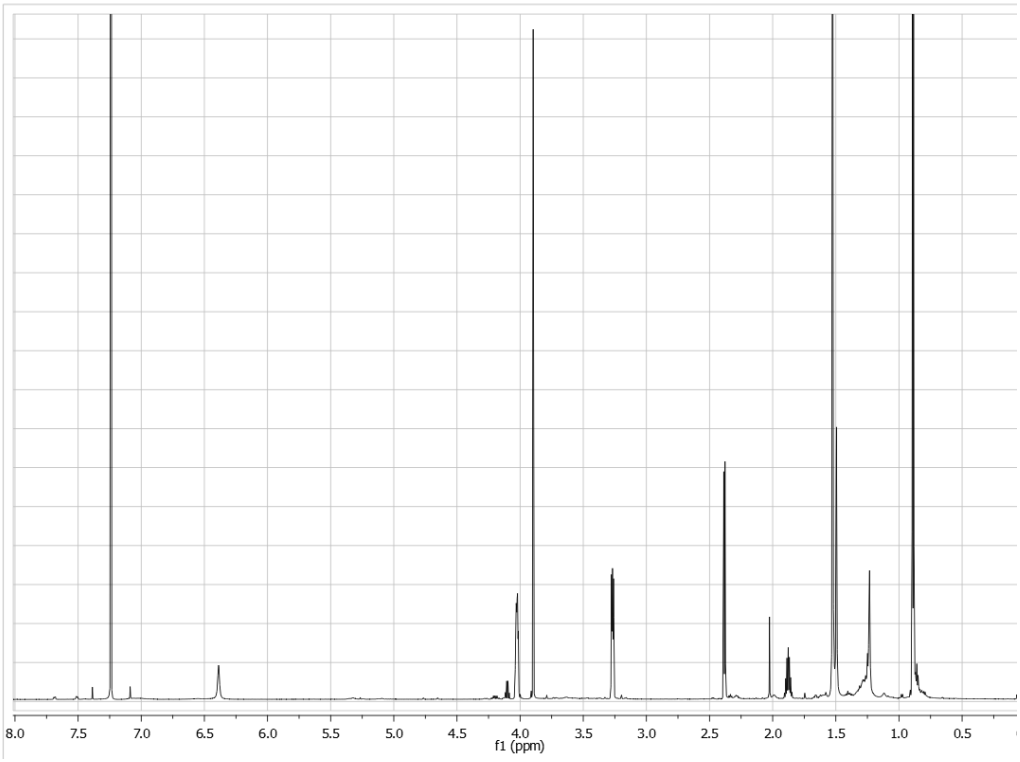

^{1}H NMR of compound **48** in $CDCl_3$

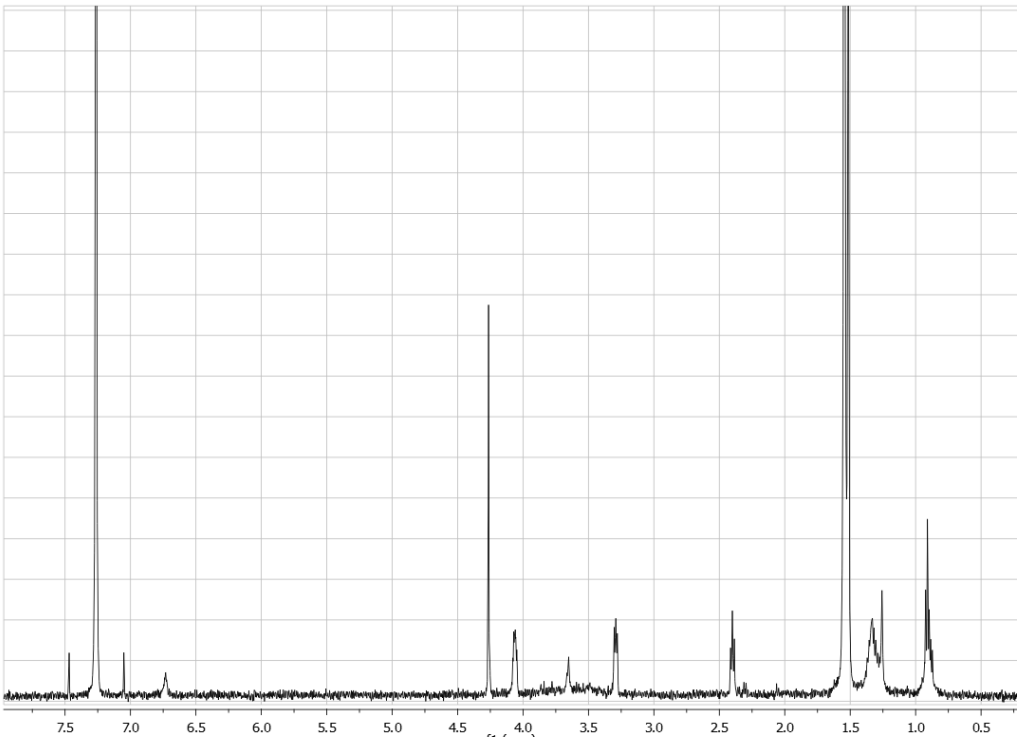

^{1}H NMR of compound **49** in $CDCl_3$

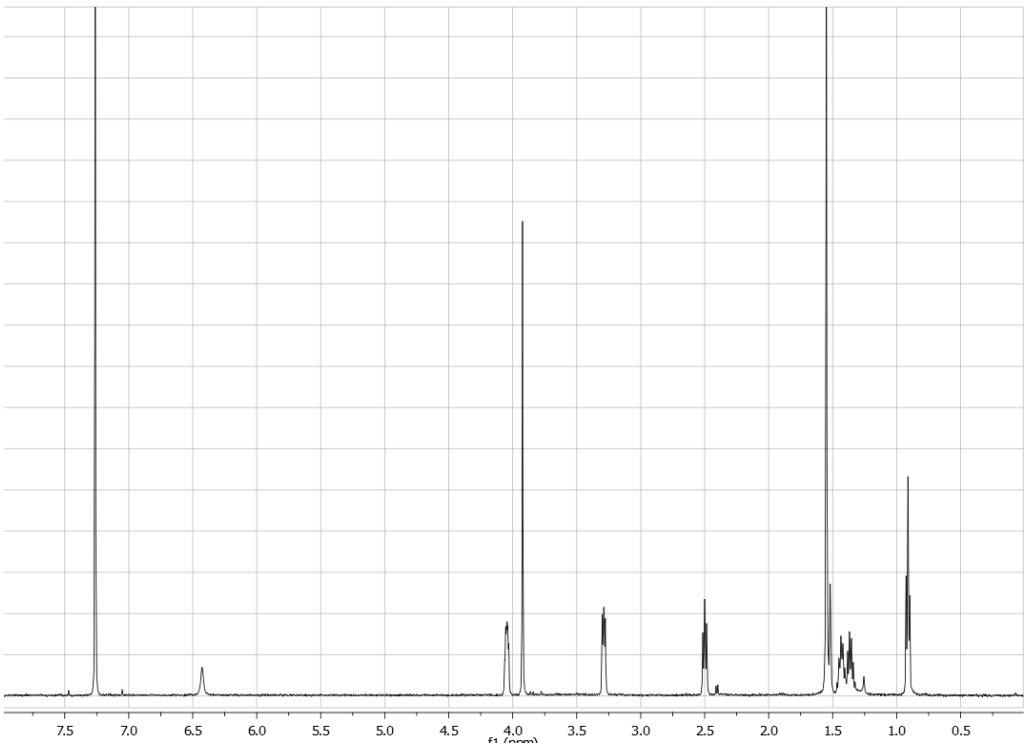

^{1}H NMR of compound **50** in $CDCl_3$

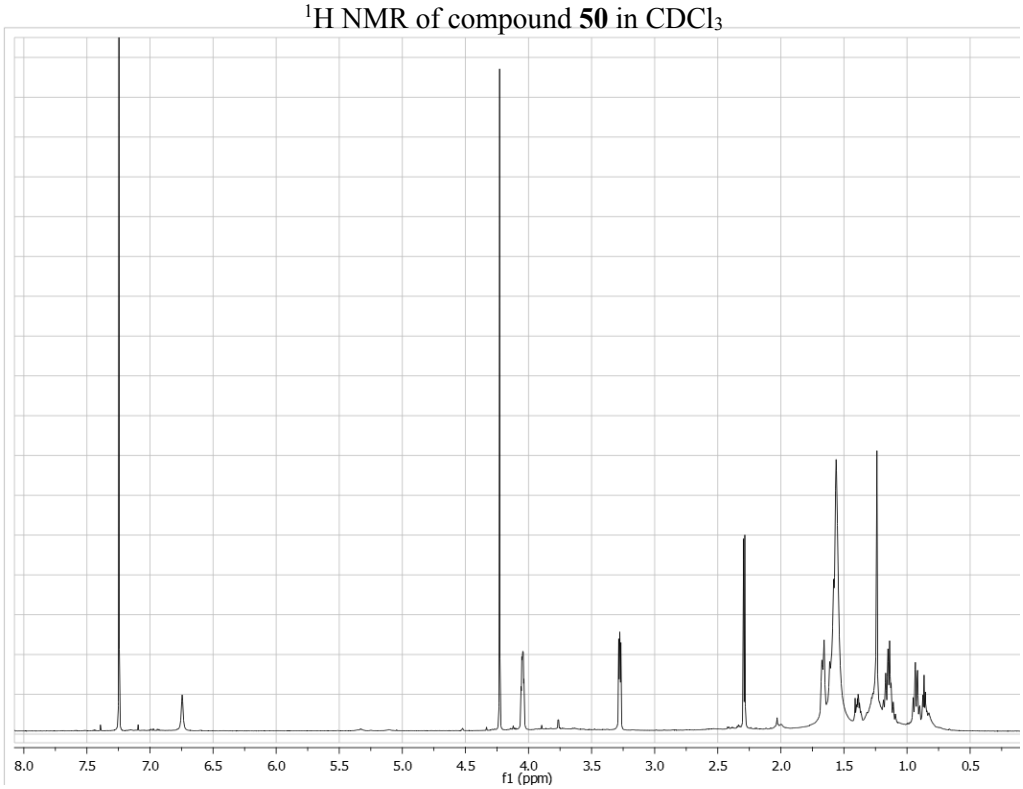

^{1}H NMR of compound **51** in $CDCl_3$

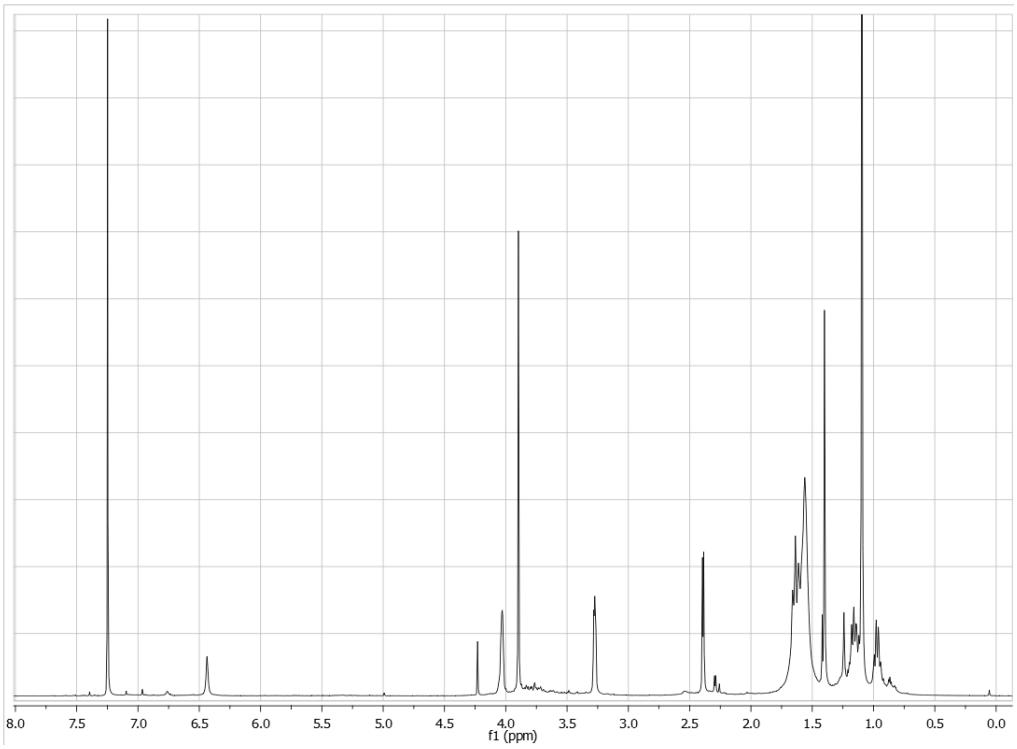

^{1}H NMR of compound **56** in $CDCl_3$

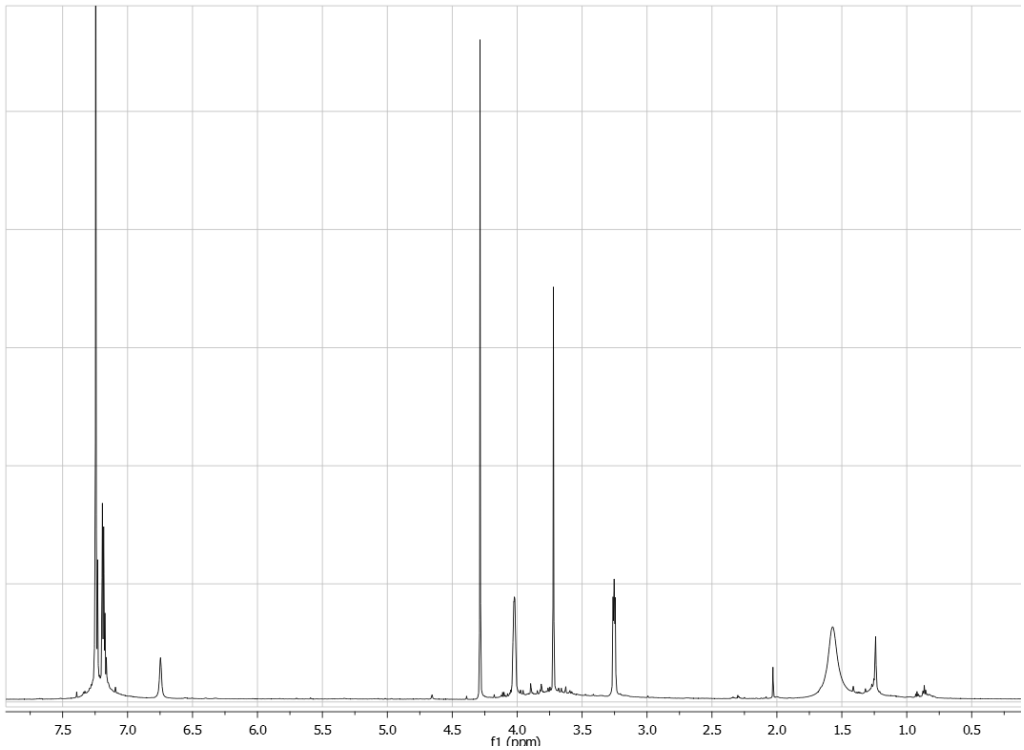

^{1}H NMR of compound **57** in $CDCl_3$

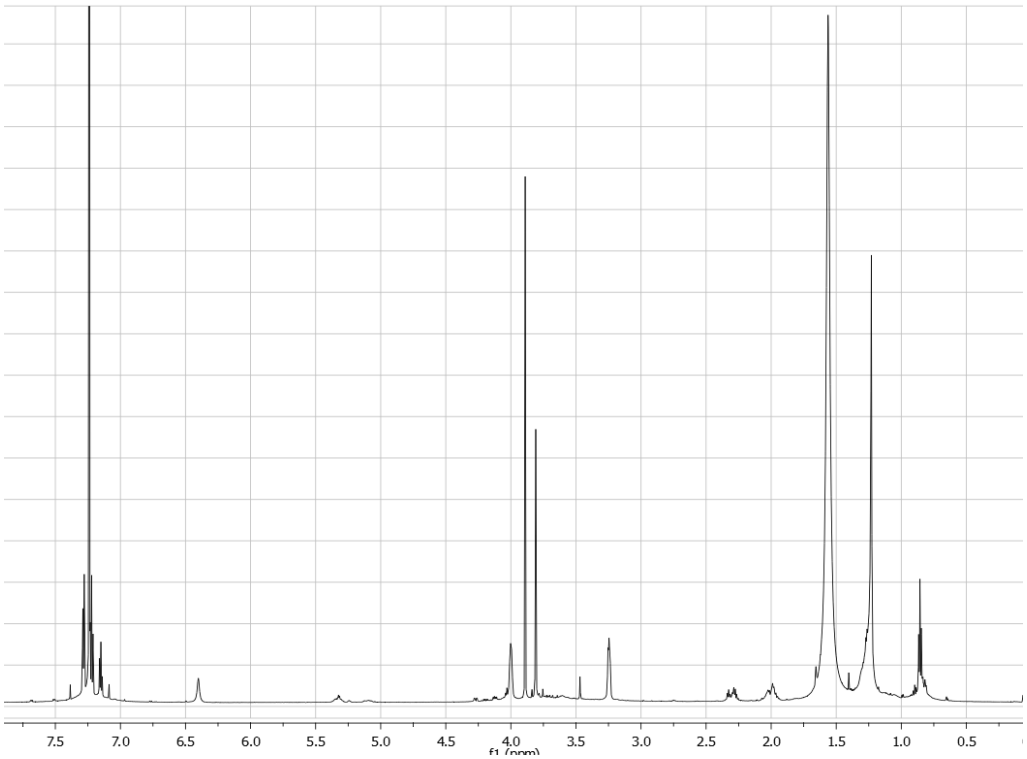

^{1}H NMR of compound **58** in $CDCl_3$

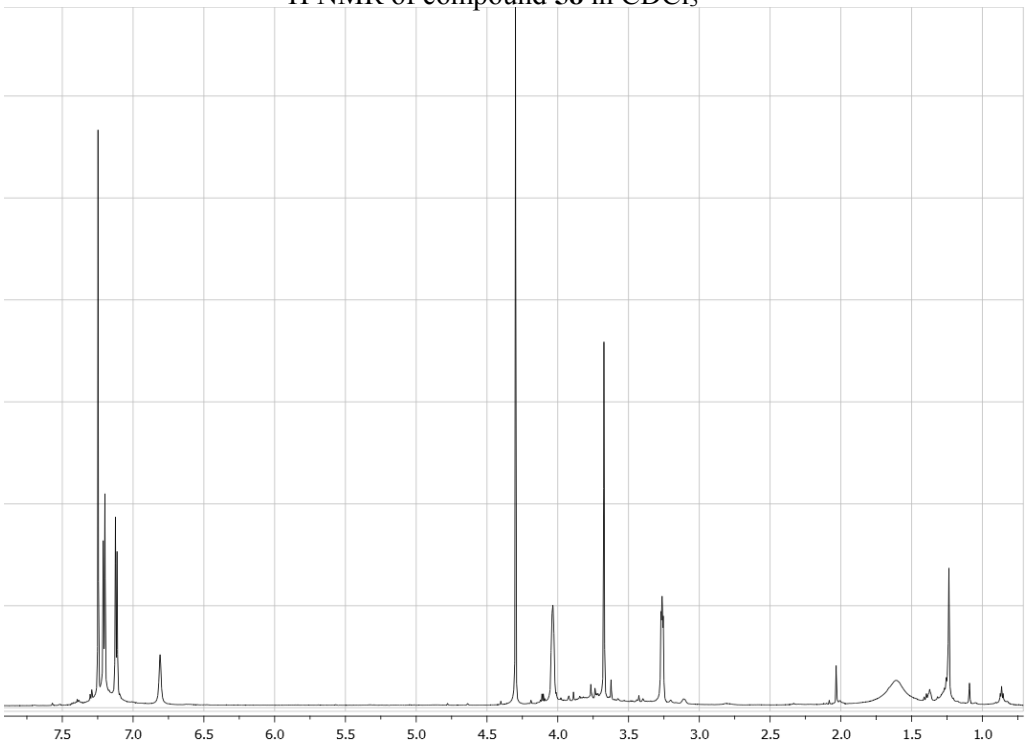

^{1}H NMR of compound **59** in $CDCl_3$

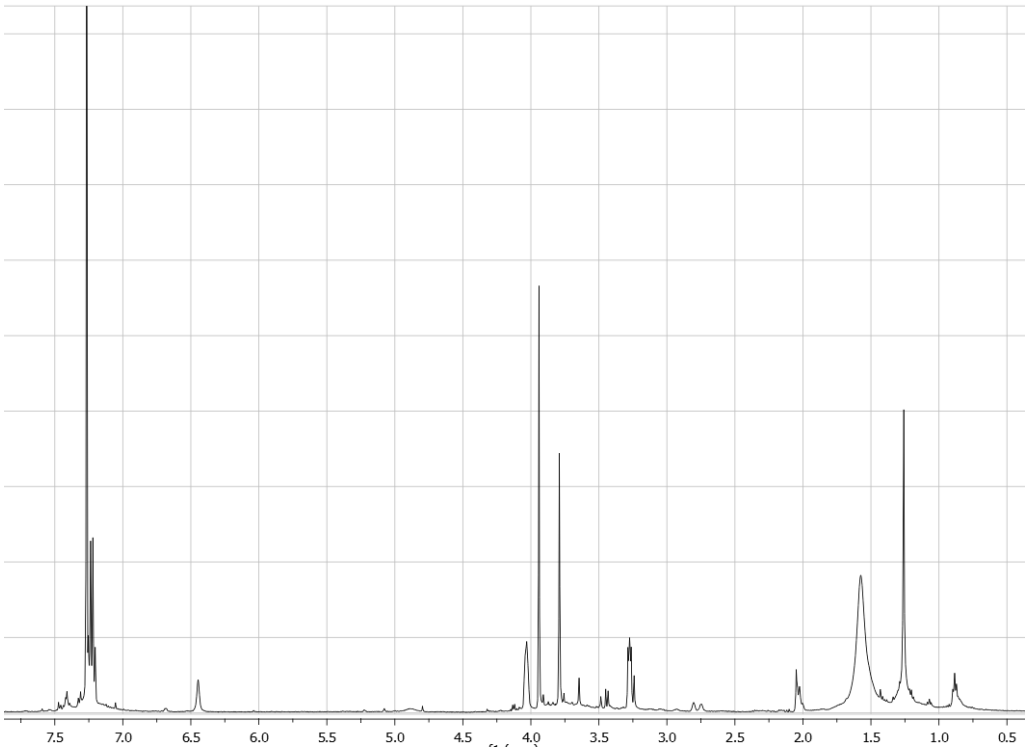

^{1}H NMR of compound **60** in $CDCl_3$

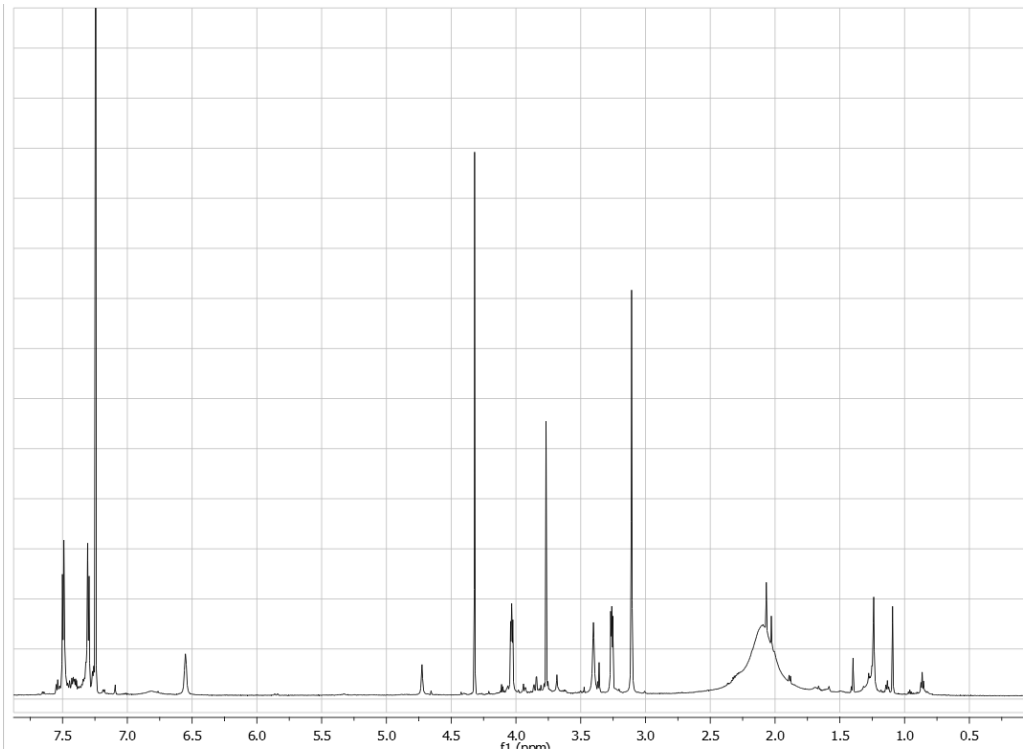

^{1}H NMR of compound **61** in $CDCl_3$

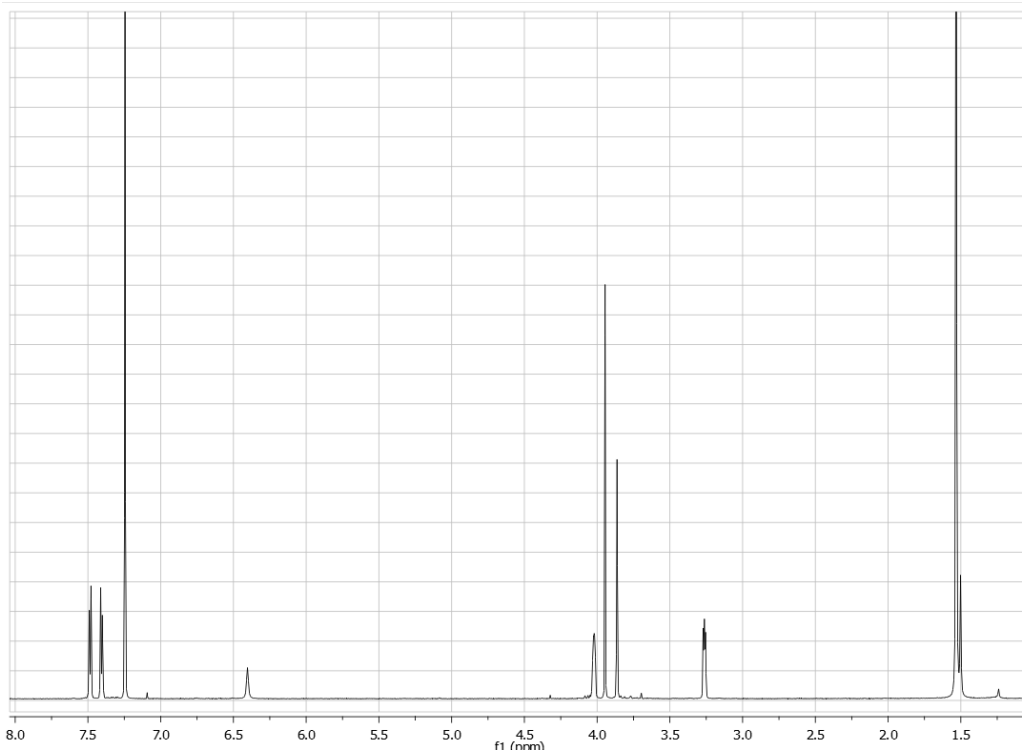

Acknowledgments

This work is the result of a multidisciplinary research project. The contribution of the following researchers from other Universities has been of key importance:

- Prof. Caterina Fattorusso (Department of Pharmacy, University of Naples "Federico II", Naples, Italy) for computational studies.
- Prof. Stefano Fiorucci (Department of Clinical and Experimental Medicine, Faculty of Medicine, University of Perugia, Peugia, Italy) for the evaluation of interactions on pregnane-X-receptor (PXR).
- Prof. A. Doménech-Carbó (Departament de Quimica Analitica, Universitat de Valencia, Spain) for electrochemical studies.
- Prof. Donatella Taramelli (Department of Biomedical, Surgical and Dental Sciences University of Milan, Milan, Italy) for *in vitro* antimalarial and cytotoxicity studies.

It is a pleasure to convey my gratitude to all of them in my humble acknowledgment.

This PhD research has been a life-changing adventure that I could not have experienced without a generous guidance and support.

I am grateful to my principal supervisor Prof. Anna Aiello and my second advisor Prof Marialuisa Menna whose immense expertise, understanding, patience, and motivation made it possible for me to work on this project and to become an independent researcher. Thanks to them I understood the power of critical reasoning. I simply could not have asked for better advisors and mentors.

I also would like to express my gratitude to the members of my thesis advisory: Professors Alberto Minassi and Claudio Trombini for finding time for me and for offering me valuable comments thanks to which I improved my work.

Besides my advisors, I would like to thank my dear colleague and friend Dr. Concetta Imperatore for her continuous interest in my work, for her precious advices, motivation, patience and for the nice moments spent together.

I am hugely indebted to my colleague and husband Dr. Paolo Luciano for his unlimited support and love. His technical knowledge has been essential to me. I want to thank him for pushing me throughout the research, for his brilliant opinions and for opening my mind. He has been a costant source of joy.

I am grateful to all students, who spent a period in laboratory 512, with love I will remember all of them.

Lastly, and most of all, I would like to thank my family for their continuous and unconditional love, for their help and support. I am grateful to my sister for her sincere friendship and encouragements during my studies.
I will always be highly indebted to my parents for giving me the best opportunities, the best experiences and the right advices at the right time. Putting their faith in me, they encouraged me to discover new paths and to do better. Thanks to them I am who I am today. They will always be my source of motivation; this is why I want to dedicate this milestone to them.

Thanks All
Maria Senese